



<https://theses.gla.ac.uk/>

Theses Digitisation:

<https://www.gla.ac.uk/myglasgow/research/enlighten/theses/digitisation/>

This is a digitised version of the original print thesis.

Copyright and moral rights for this work are retained by the author

A copy can be downloaded for personal non-commercial research or study,
without prior permission or charge

This work cannot be reproduced or quoted extensively from without first
obtaining permission in writing from the author

The content must not be changed in any way or sold commercially in any
format or medium without the formal permission of the author

When referring to this work, full bibliographic details including the author,
title, awarding institution and date of the thesis must be given

Enlighten: Theses

<https://theses.gla.ac.uk/>
research-enlighten@glasgow.ac.uk

A methanol only route to acetic acid and
methyl acetate



UNIVERSITY
of
GLASGOW

Graham Ormsby ©

A Thesis Presented to the University of Glasgow for the
Degree of Doctor of Philosophy

ProQuest Number: 10754022

All rights reserved

INFORMATION TO ALL USERS

The quality of this reproduction is dependent upon the quality of the copy submitted.

In the unlikely event that the author did not send a complete manuscript and there are missing pages, these will be noted. Also, if material had to be removed, a note will indicate the deletion.



ProQuest 10754022

Published by ProQuest LLC (2018). Copyright of the Dissertation is held by the Author.

All rights reserved.

This work is protected against unauthorized copying under Title 17, United States Code
Microform Edition © ProQuest LLC.

ProQuest LLC.
789 East Eisenhower Parkway
P.O. Box 1346
Ann Arbor, MI 48106 – 1346

GLASGOW
UNIVERSITY
LIBRARY

Abstract

Methanol carbonylation to produce acetic acid is a reaction of industrial interest and is currently performed via homogeneous catalytic routes in the Cativa and Monsanto processes using iridium and rhodium complexes respectively. Whilst these processes produce acetic acid with high selectivity, the use of halide promoters is required. Due to this corrosive nature, the development of a catalyst system without the need for promoters is of significant commercial interest. Studies demonstrate that copper mordenite is a potential candidate. The present project concerns the production of acetic acid and methyl acetate in the absence of a halide promoter via a methanol only route. The methanol is firstly partially decomposed to form CO and H₂ over a methanol decomposition catalyst and in a subsequent step the unconverted methanol is carbonylated using the copper mordenite catalyst to form acetic acid and methyl acetate. Both catalysts are contained within one reactor. The experimental work undertaken has focussed on three main objectives: (i) study of methanol decomposition over a range of materials under directly comparable conditions. (ii) methanol carbonylation using copper mordenite under various feed conditions containing H₂ and (iii) combination of methanol decomposition catalysts with the copper mordenite in a single reactor.

The behaviour of copper methanol synthesis catalysts and palladium based catalysts in methanol decomposition is consistent with the literature with palladium being the more selective for CO formation. The rate of CO formation over copper is lower due to the formation of methyl formate by-product. Raney nickel decomposed methanol with CH₄ being a side-product. The most active catalyst for CO production was a NiB alloy, formed from the reduction of nickel acetate with sodium borohydride. A series of molybdenum carbide and nitride catalysts were also investigated due to the literature reports that these materials often behave like noble metals. All carbide and nitride phases were active in methanol decomposition. CH₄ and CO₂ were observed by-products and in general it was found that they behaved like Ni based catalysts.

Methanol carbonylation studies over copper mordenite demonstrate that acetic acid is a minor product with methanol to olefin and methanol to gasoline chemistry occurring. In addition, DME is formed from the dehydration of methanol. The presence of H₂ in the

feedstream influences the rate of acetyl formation. A CO/H₂ feed ratio of 4 is optimal whilst a further increase in H₂ partial pressure lowers the acetyl formation rate. Acetic acid and methyl formate are produced when the copper mordenite catalyst is combined with methanol decomposition catalysts but the selectivity is low.

The choice of methanol decomposition catalyst combined with copper mordenite influences the formation of acetyls. In addition it was observed that physically mixed catalyst beds produce lower yields of acetyls whilst the acetyl yield is increased by separating the two catalyst components.

Table of contents

Abstract.....	1
Table of contents	3
List of tables.....	9
List of figures	10
Publications	13
Acknowledgements	14
Authors declaration.....	15
1 Introduction	16
1.1 Acetic acid.....	16
1.2 Methanol carbonylation.....	17
1.2.1 Methanol carbonylation using heterogeneous catalysts	20
1.2.2 Non- promoted heterogeneous methanol carbonylation.....	22
1.3 Alternative routes to acetic acid.....	27
1.3.1 Ethane oxidation.....	27
1.3.2 Acetic acid from synthesis gas.....	28
1.3.3 Acetic acid production from methane – non-synthesis gas routes.....	29
1.3.4 Acetic acid synthesis from methanol.....	32

1.3.5	Conclusion	33
1.3.6	Mordenite.....	34
2	Experimental.....	38
2.1	Catalyst synthesis.....	38
2.1.1	Synthesis of copper based methanol decomposition catalysts.....	38
2.1.2	Synthesis of palladium, ceria/zirconia methanol decomposition catalysts..	38
2.1.3	Synthesis of palladium based methanol decomposition catalysts supported on alumina	39
2.1.4	Synthesis of molybdenum carbide catalysts	39
2.1.5	Synthesis of molybdenum nitride catalysts	40
2.1.6	Synthesis of copper mordenite methanol carbonylation catalyst.....	41
2.1.7	Synthesis of doped copper mordenite catalysts	42
2.1.8	Preparation of Raney nickel catalysts.....	42
2.1.9	Preparation of nickel – boron catalyst	43
2.2	Catalyst testing.....	43
2.2.1	Methanol decomposition.....	43
2.2.2	Methanol decomposition reactions.....	46
2.2.3	Mixed methanol decomposition/methanol carbonylation experiments.....	46
2.2.4	GC calibration and analysis	47

2.2.5	Methanol carbonylation	47
2.3	Catalyst Characterization.....	50
2.3.1	Powder x-ray diffraction (XRD)	50
2.3.2	Surface area measurements.....	50
2.3.3	Elemental analysis.....	50
2.3.4	Thermal gravimetric analysis.....	50
2.3.5	²⁷ Al and ²⁹ Si MAS NMR	51
3	Methanol Decomposition	52
3.1	Methanol only route to acetic acid.....	52
3.2	Methanol decomposition	53
3.2.1	Mechanism of methanol decomposition.....	56
3.3	Results and discussion: Copper methanol decomposition catalysts	64
3.3.1	General background.....	64
3.3.2	Catalyst characterization- Copper based catalysts	67
3.3.3	Reaction data-Copper based catalysts	70
3.4	Results and discussion: Palladium methanol decomposition catalysts	77
3.4.1	General background.....	77
3.4.2	Catalyst characterization - Pd/CeO ₂ based catalysts	79
3.4.3	Reaction data - Palladium based catalysts	82

3.4.4	Palladium supported on γ -Al ₂ O ₃	86
3.4.5	PZC of γ -Al ₂ O ₃ support	87
3.4.6	Pd/ γ -Al ₂ O ₃ catalyst characterisation.....	88
3.4.7	Reaction data - Pd/ γ -Al ₂ O ₃ based catalysts.....	92
3.5	Results and discussion: Nickel methanol decomposition catalysts	97
3.5.1	General background.....	97
3.5.2	Reaction data: Ni based catalysts	99
3.6	Conclusions.....	106
4	Methanol decomposition over transition metal carbide and nitride materials	108
4.1	General introduction.....	108
4.1.1	Synthesis of transition metal carbides and nitrides	110
4.2	Results – Catalyst characterization	111
4.3	Methanol decomposition	116
4.3.1	Precursor materials	116
4.3.2	Methanol decomposition – Carbides	119
4.3.3	Methanol decomposition – Nitrides	122
4.3.4	Carbon and nitrogen analysis of nitride and carbide catalysts.....	129
4.3.5	Conclusions.....	130
5	Methanol carbonylation	132

5.1	Methanol Carbonylation.....	132
5.1.1	TGA analysis of spent copper mordenite	137
5.1.2	XRD analysis of copper mordenite	139
5.1.3	²⁷ Al and ²⁹ Si NMR study of mordenite samples	141
5.1.4	Methanol carbonylation summary.....	145
5.2	Methanol carbonylation studies under different feed conditions.....	145
5.3	Coupled methanol decomposition and carbonylation experiments	148
5.3.1	Coupled methanol decomposition and carbonylation experiments: Experimental results.....	149
5.4	Conversion of methanol with dual functional mordenite catalyst	156
5.5	Summary.....	162
6	Conclusions	164
6.1	Future work.....	168
7	Appendices.....	170
7.1	Methanol Decomposition	170
7.1.1	Methanol conversion	170
7.1.2	Space time yield calculations.....	170
7.1.3	Error values for duplicate reaction runs.....	170
7.1.4	Error values for comparison tables.....	170

7.1.5	Space time yield calculation for mixed bed methanol decomposition and carbonylation	171
7.2	Methanol carbonylation.....	171
7.2.1	Analysis of gas phase products	172
7.2.2	Analysis of liquid phase products	172
7.2.3	Methanol conversion	173
8	References	174

List of tables

Table 3-1: Thermodynamic data at 298K	55
Table 3-2: Space time yield data for methanol decomposition catalysts	63
Table 3-3: Elemental analysis for the Katalco catalyst	68
Table 3-4: Elemental analysis for the Cu/ZnO catalyst	68
Table 3-5: Catalyst data, ¹ coke content determined by CHN elemental analysis	76
Table 3-6: Elemental analysis for Pd based catalysts.....	80
Table 3-7: Catalyst data Pd/CeO ₂ based catalysts, ¹ coke content determined by CHN elemental analysis.....	85
Table 3-8 Catalyst data for Pd/ γ -Al ₂ O ₃ catalysts, ¹ coke content calculated using CHN elemental analysis.....	97
Table 3-9 Catalyst data for Ni catalysts, ¹ coke content calculated using CHN elemental analysis	105
Table 3-10: Methanol conversion and CO STY formation rate for all studied methanol decomposition catalysts. 0.15 g catalyst loaded. Methanol concentration = 40mol % in Ar, Total flow = 40ml/min. 0.3 g catalyst loaded ¹	107
Table 4-1: BET surface areas of nitride and carbide catalysts,.....	116
Table 4-2: CHN data for nitrogen content and coke content on spent catalysts. It was assumed that the fresh catalyst contains 5.9wt% carbon ¹	129
Table 4-3: STY data for CO production over molybdenum carbide and nitride catalysts	131
Table 5-2: Carbon content on spent copper mordenite catalysts after various times on stream	134
Table 5-2: Si/Al ratios for mordenite samples	144
Table 5-3: STY values for methanol carbonylation(g/kgcat/h). GHSV = 2400 h ⁻¹ , volume of catalyst = 5 ml, CO/methanol molar ratio = 10. ¹ CO/methanol molar ratio = 4.....	147
Table 5-4: Summary of selected methanol decomposition catalysts at 300°C.....	149
Table 5-5: STY values for acetyl formation at 300°C. GHSV = 2625 h ⁻¹ (calculated with respect to the Cu-MOR catalyst), methanol (39mol%) feed in argon 0.15g Cu-Mordenite catalyst. 0.15g decomposition catalyst.....	151
Table 5-6: Acetyl production and carbon content of Cu-Mor, MoO ₃ -Cu-mordenire and Pd-Cu-mordenite catalyst.....	161

List of figures

Figure 1-1: Use of acetic acid (adapted from reference [1]).....	16
Figure 1-2: Some preparative routes to acetic acid (adapted from reference [1]).....	17
Figure 1-3: Catalytic cycle for the Monsanto process	18
Figure 1-4: Catalytic cycle for the Cativa process	19
Figure 1-5: Product profile for methanol carbonylation over copper mordenite adapted from reference [19]. The squares represent the methanol conversion, the crosses represent the selectivity to hydrocarbons, the diamonds are the selectivity to acetyls (acetic acid + methyl acetate) and the triangles represent DME selectivity	24
Figure 1-6: Proposed mechanism for DME carbonylation over H-mordenite.....	26
Figure 1-7: CH ₃ Br carbonylation using a RhCl ₃ homogeneous catalyst (adapted from reference [33]) 30	
Figure 1-8: Proposed cycle for acetic acid production	32
Figure 1-9: Pore structure of mordenite viewed along the 001 plane. Adapted from reference [86]	35
Figure 1-10: 12 ring channel viewed normal to the 001 plane. Adapted from reference [86]	36
Figure 1-11: 8 ring channel viewed normal to the 001 plane. Adapted from reference [86]	36
Figure 3-1: Heterogeneous route to acetic acid with a methanol only feed	52
Figure 3-2: XRD pattern for calcined Katalco and Cu/ZnO catalysts	67
Figure 3-3: <i>In-situ</i> XRD patterns for Katalco catalyst.....	69
Figure 3-4: <i>In-situ</i> XRD patterns for Cu/ZnO catalyst.....	70
Figure 3-5: Methanol conversion, Katalco catalyst	71
Figure 3-6: STY data Katalco catalyst	71
Figure 3-7: Methanol conversion, Katalco catalyst.....	73
Figure 3-8: STY data Cu/ZnO catalyst.....	73
Figure 3-9: XRD patterns for spent Katalco and Cu/ZnO catalysts after 300° C reaction	76
Figure 3-10: Plot of H ₂ STY at 200°C vs Pd loading	79
Figure 3-11: XRD pattern of calcined and spent Pd/Ce _{0.8} Zr _{0.2} O ₂ catalyst at 300°C.....	81
Figure 3-12: XRD pattern of calcined and spent Pd/CeO ₂ catalyst at 300°C.....	81
Figure 3-13: Methanol conversion, Pd/ Ce _{0.8} Zr _{0.2} O ₂ catalyst.....	82
Figure 3-14: STY data Pd/ Ce _{0.8} Zr _{0.2} O ₂ catalyst.....	83
Figure 3-15: Methanol conversion, Pd/CeO ₂ catalyst at 300°C	84
Figure 3-16: STY data Pd/CeO ₂ catalyst at 300°C	84
Figure 3-17: Potentiometric titration of γ -Al ₂ O ₃	87
Figure 3-18: pH dependence of surface distribution of hydroxyl groups (a) and Pd species in solution (b) adapted from reference 93.	88
Figure 3-19: XRD pattern of calcined and spent Pd (1.5 wt%)/Al ₂ O ₃ catalyst at 300°C	89
Figure 3-20- XRD pattern of calcined and spent Pd (3 wt%)/Al ₂ O ₃ catalyst at 300°C	89
90	
Figure 3-21: XRD pattern of calcined and spent Pd (9 wt%)/Al ₂ O ₃ catalyst at 300°C	90
Figure 3-22: <i>In-situ</i> XRD experiment for Pd (1.5 wt%)/Al ₂ O ₃ catalyst.....	91
Figure 3-23: <i>In-situ</i> XRD experiment for Pd (3 wt%)/Al ₂ O ₃ catalyst.....	91
Figure 3-24: <i>In-situ</i> XRD experiment for Pd (9 wt%)/Al ₂ O ₃ catalyst.....	92

Figure 3-25: Methanol conversion for Pd (1.5wt%)/ γ -Al ₂ O ₃ catalysts at 300°C.....	92
Figure 3-26: Methanol conversion for Pd (3wt%)/ γ -Al ₂ O ₃ catalysts at 300°C.....	93
Figure 3-27: Methanol conversion for Pd (9wt%)/ γ -Al ₂ O ₃ catalysts at 300°C.....	93
Figure 3-28: STY data at 300°C, Pd (1.5 wt%)/ γ -Al ₂ O ₃ catalyst.....	94
Figure 3-29: STY data at 300°C, Pd (3 wt%)/ γ -Al ₂ O ₃ catalyst.....	95
Figure 3-30 STY data at 300°C, Pd (9 wt%)/ γ -Al ₂ O ₃ catalyst.....	95
Figure 3-31: Methanol conversion for NiAl catalysts.....	100
Figure 3-32: STY data NiAl catalyst at 250°C,	100
Figure 3-33: STY data, NiAl catalyst at 300°C	101
Figure 3-34: Mole percentage of CO ₂ and H ₂ produced at 300°C, NiAl catalyst,.....	101
Figure 3-35: XRD pattern of NiB material	103
Figure 3-36: Methanol conversion for NiB catalyst.....	104
Figure 3-37: STY data at 250°C, NiB catalyst	104
Figure 3-38: STY data at 300°C, NiB catalyst	105
Figure 4-1: Hexagonal close packed β - Mo ₂ C Figure 4-2: Face centred cubic γ -Mo ₂ N.....	109
Figure 4-3: Effect of carburisation agent on the structure of Mo carbides.....	111
Figure 4-4: XRD pattern of MoS ₂ and MoO ₃ precursor materials	112
Figure 4-5: XRD of pure phase β -Mo ₂ C and mixed phase carbide. (a) 4 hour dwell time and (b) 1hour dwell time.....	113
Figure 4-6: XRD of pure phase β -Mo ₂ N _{0.78}	114
Figure 4-7: XRD of pure phase γ -Mo ₂ N	114
Figure 4-8: XRD of pure phase δ - MoN	115
Figure 4-9: Methanol conversion for MoO ₃ at 400°C.....	117
Figure 4-10: Methanol decomposition for MoO ₃ at 400°C	118
Figure 4-11: XRD pattern of spent MoO ₃ catalyst	118
Figure 4-12: Methanol conversion for β -Mo ₂ C/MoO ₂ and β -Mo ₂ C at 300°C.....	120
Figure 4-13: Methanol decomposition β -Mo ₂ C/MoO ₂ at 300°C	120
Figure 4-14: Methanol decomposition β -Mo ₂ C at 300°C	121
Figure 4-15: Methanol conversion for β -Mo ₂ N _{0.78} at 300°C/350°C and 400°C	122
Figure 4-16: Methanol decomposition for β -Mo ₂ N _{0.78} at 300°C/350°C and 400°C.....	123
Figure 4-17: Methanol conversion for γ -Mo ₂ N at 250°C and 300°C	124
Figure 4-18: Methanol decomposition for γ -Mo ₂ N at 250°C and 300°C.....	124
Figure 4-19: Methanol conversion for δ - MoN at 250°C, 300°C and 400°C	125
Figure 4-20: Methanol decomposition for δ -MoN at 250°C and 300°C	126
Figure 4-21: Methanol decomposition for δ -MoN 400°C.....	126
Figure 4-22: Methanol conversion at 300°C for molybdenum nitride and carbide catalyst sas a function of BET surface area	128
Figure 5-1: Methanol carbonylation over copper mordenite. Reaction temperature = 300 °C, GHSV = 2421 h ⁻¹ , volume of catalyst = 5 ml, CO/methanol molar ratio = 12	134
Figure 5-2: N ₂ isotherm for fresh copper mordenite.....	135
Figure 5-3: N ₂ physisorption pattern of Spent copper mordenite after 60 minutes on stream	136
Figure 5-4: N ₂ physisorption pattern of Spent copper mordenite after 330 minutes on stream	136

Figure 5-5: TGA derivatives of copper mordenite performed under air. (a) fresh copper mordenite (b) Spent mordenite 60 minutes on stream (c) Spent mordenite 180 minutes on stream (d) Spent mordenite 330 minutes on stream (e) Spent mordenite 330 minutes on stream under argon.....	138
Figure 5-6: XRD pattern of fresh and spent copper mordenite catalyst	140
Figure 5-7: Simulated XRD pattern for mordenite adapted from reference [124].....	140
Figure 5-8: ²⁷ Al MAS NMR spectra for (a) NH4-Mor (b) H-Mor (c) Cu-Mor (d) Spent Cu-Mor.....	142
Figure 5-9: ²⁹ Si MAS NMR spectra for (a) NH4-Mor (b) H-Mor (c) Cu-Mor (d) Spent Cu-Mor.....	144
Figure 5-10: STY DME and methanol conversion for the Katalco catalyst.....	152
Figure 5-11: H ₂ and CH ₄ STY data for the Katalco catalyst (mixed bed configuration)	152
Figure 5-12: CO, H ₂ and CH ₄ STY data for the Katalco catalyst (stacked bed configuration).....	153
Figure 5-13: STY DME and methanol conversion for the Pd /CeO ₂ catalyst	154
Figure 5-15: CO, H ₂ and CH ₄ STY data for the Palladium catalyst (mixed bed configuration).....	155
Figure 5-16: CO, H ₂ and CH ₄ STY data for the Palladium catalyst (stacked bed configuration)	155
Figure 5-16: XRD pattern of spent palladium-copper mordenite catalyst.....	157
Figure 5-17: Methanol conversion and DME production over Pd-Cu-mordenite catalyst at 300°C	158
Figure 5-18: STY production of CO, H ₂ and CH ₄ over Pd-Cu-mordenite catalyst at 300°C.....	159
Figure 5-19: STY production for H ₂ and CH ₄ and DME for methanol reaction with copper mordenite at 300°C.....	160
Figure 5-20: Methanol conversion and DME production over MoO ₃ -Cu-mordenite catalyst at 300°C	161

Publications

- J.S.J Hargreaves and G Ormsby “A CO and H₂ space time yield comparison of recent literature on methanol decomposition” , Specialist Periodical Reports in Catalysis, RSC Cambridge ,20, 107-121 (2007).

Acknowledgements

There are many people who I would like to thank for contributing in some way or other to this thesis. I should first thank Dr Justin Hargreaves for being a very good supervisor over the past 3 years. It was a pleasure to work with him and I would like to thank him for his support and enthusiasm especially at the beginning of this project. I feel that my PhD was a rounded experience from which I gained many experiences and I thank you for that Justin. Thank you very much and it is very much appreciated!

Secondly I would like to thank Dr Evert Ditzel and the guys from BP Hull who supported me during my short placement. I would especially like to thank Evert for his help understanding and enthusiasm throughout the whole project, even during the tougher times! It was a pleasure to work with you.

I would like to thank the technical staff for all of their support at the University of Glasgow. Thanks to Kim Wilson who provided CHN analysis Stephen Wimperis for providing solid state NMR support and Ron (finger tight) Spence for his wealth of Swagelok experience. However, I would especially like to thank Andy Monaghan for his friendship, wisdom on current affairs and of course his technical support throughout the project.

I would finally like to thank all of the guys who made working in the lab enjoyable if not unproductive at times! You know who you are and al the best to you!

Finally I would like to thank my family.

Authors declaration

The work contained in this thesis submitted for the degree of Doctor of Philosophy, is my own original work, except where due reference is made to others. No material within has been previously submitted for a degree at this or any other university.

1 Introduction

1.1 Acetic acid

Acetic acid is important for the chemical industry as it is used in a broad range of applications. Most acetic acid produced is used a chemical feedstock for further chemical processes and the main uses are displayed in Figure 1-1. These include vinyl acetate monomer synthesis, acetic anhydride synthesis and as a solvent for terephthalic acid production. The final products of such processes include polymers, paints and inks. The World capacity of acetic acid was 7.8 million tonnes in 1998 with BP- Amoco and Celanese reported to account for 50% of the world's total production capacity.

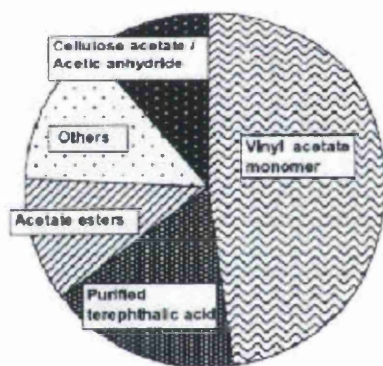


Figure 1-1: Use of acetic acid (adapted from reference [1])

Since the first commercial processes for acetic acid production were introduced, there has been a wide range of novel processes which have been developed and improved continuously in order for the main producers to protect and grow their share of the market. Ultimately the aim has been to reduce raw material consumption, energy requirements and investment costs [1]. There are many processes by which it can be produced and some of these are displayed in Figure 1-2.

	Catalyst	Reaction condition (°C, atm)	Yield	By-product
Methanol carbonylation	Rhodium complex	180-220, 30-40	MeOH: 99%, CO: 85%	None
Acetaldehyde oxidation	Manganese acetate or cobalt acetate	50-60, atmospheric pressure	CH ₃ CHO: 95%	None
Ethylene direct oxidation	Palladium/heteropolyacid/ methyl	150-160, 80	Ethylene: 87%	Acetaldehyde, CO ₂
Hydrocarbon oxidation (n-butane, naphtha)	Cobalt acetate or manganese acetate	150-230, 50-60	n-Butane: 50%, naphtha: 40%	Formic acid, propionic acid, etc

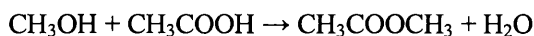
Figure 1-2: Some preparative routes to acetic acid (adapted from reference [1])

Originally acetic acid was produced by the aerobic fermentation of ethanol, used for the production of vinegar. It can also be synthesised by the direct oxidation of ethanol using a V₂O₅/TiO₂ heterogeneous catalyst [2]. The first commercial synthesis was based on the oxidation of acetaldehyde in 1916. Acetaldehyde was produced from acetylene in a process which involved a toxic mercury catalyst. As a result acetylene was phased out and replaced with ethylene as the feedstock for acetaldehyde production. Throughout the 1950s and 1960s, processes involving the oxidation of n-butane and naphtha to acetic acid were developed by Celanese and BP respectively along with the oxidation of ethylene. As observed in Figure 1-2, these routes produce a range of by products including formic acid and propionic acid [1]. Further developments in the production of acetic acid were made by the direct homogeneous carbonylation of methanol with the Monsanto and Cativa processes. By the year 2000, methanol carbonylation accounted for approximately 60% of the World production capacity [3].

1.2 Methanol carbonylation

The first homogeneous methanol carbonylation process was commercialised by BASF in 1960. This process used a CoH(CO)₄ catalyst and methyl iodide co-catalyst [4]. The selectivity of this process was 90% based on methanol. This was improved in 1966 when Monsanto discovered that a rhodium based catalyst could achieve a selectivity of >99% (based on methanol). The Monsanto process was run under milder conditions (150-200°C and 30-60 bar) compared with the BASF process (250°C and 680 bar) [3]. Figure 1-3 is a simplified catalytic cycle for the Monsanto process. The mechanism has been studied and the active species was identified as [RhI₂(CO)₂]⁻ with methyl iodide acting as a co-catalyst [5]. The first step involves the addition of methyl iodide to the active species via oxidative addition in the rate-determining step. The methyl group then migrates to an adjacent

carbonyl forming a rhodium-acyl species in the second step. CO insertion followed by reductive elimination forms acetyl iodide and regenerates the active rhodium species. Acetic acid is then produced by the reaction of acetyl iodide with water to form acetic acid and hydrogen iodide. Methyl acetate is also produced either by the esterification of methanol and acetic acid via the following:



CO₂ production is also observed in the homogeneous carbonylation of methanol. It is formed via the water gas shift (WGS) reaction:

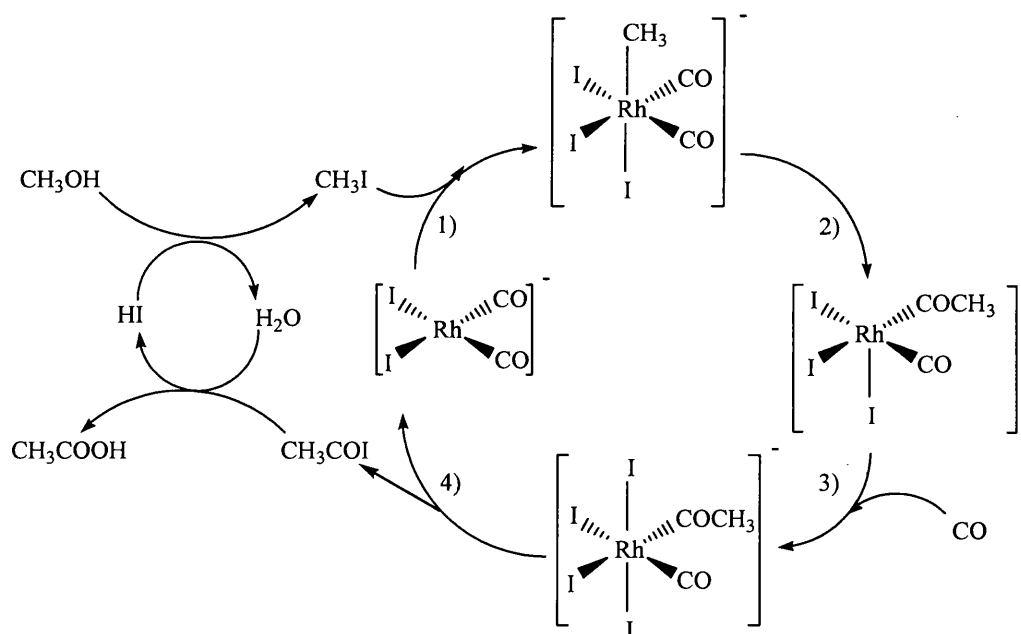
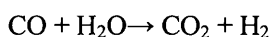


Figure 1-3: Catalytic cycle for the Monsanto process

To maintain high reaction rates, a high concentration of methyl iodide is required. The reaction is first order in both methyl iodide and rhodium but the reaction rate is independent of the methanol concentration. BP Chemicals acquired the licensing rights to the Monsanto process in 1986. In 1996 BP Chemicals announced the Cativa Process which is based on homogeneous carbonylation of methanol using an iridium catalyst and

methyl iodide co-catalyst. The Cativa process offers several advantages over the Monsanto process. The selectivity is improved with reduced formation of acetaldehyde and propionic acid by-products. In the Monsanto process, the expensive rhodium can be lost downstream by precipitation and this is avoided by using high water concentrations, and a minimum CO partial pressure. The iridium catalyst remains stable down to low water concentrations and thus a distillation column, necessary for removing the acetic acid from the water can be taken away reducing the processing and capital costs in the Cativa process. In addition the low water concentration limits CO₂ formation via the WGS reaction. The net effect and commercial advantage of the Cativa process over the Monsanto process are improvements in reactor productivity and lower costs. The Cativa process is now operated commercially [3]. Figure 1-4 is a simplified illustration for the Cativa process catalytic cycle.

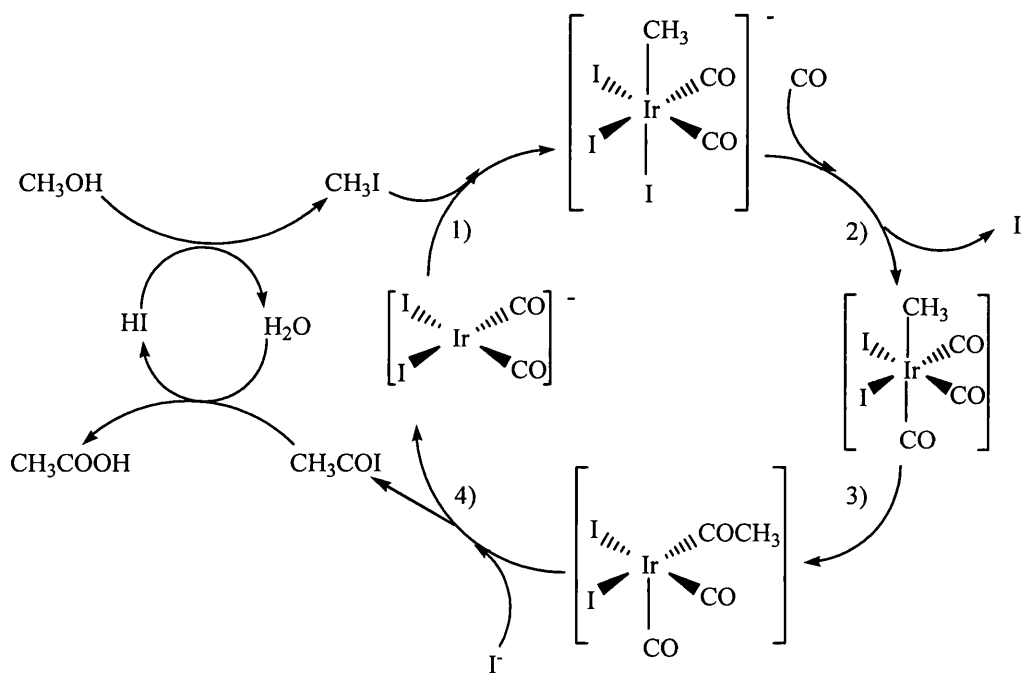


Figure 1-4: Catalytic cycle for the Cativa process

The rate-determining step of the Monsanto process is the oxidative addition of methyl iodide to the active [Rh (CO)₂ I₂]⁻ species but in the Cativa process this occurs 160 times faster so there is a reduced dependence on the reaction rate on methyl iodide

concentration. The rate-determining step of the Cativa process is believed to be the dissociation of the ionic iodide and the co-ordination of CO in step 2). Metal iodide and metal carbonyl promoters are used to increase the reaction rate. Although there is a lower concentration of methyl iodide required to achieve high reaction rates in the Cativa process compared with the Monsanto process, methyl iodide is corrosive and may also poison the downstream processes. This is the case in vinyl acetate monomer synthesis where there are steps to reduce the concentration of the methyl iodide in the acetic acid feedstream [6]. As a result, the complete removal of any need for halide promoters would be desirable and of commercial interest.

1.2.1 Methanol carbonylation using heterogeneous catalysts

The homogeneous carbonylation of methanol is a very successful commercialized route to acetic acid. However, the need for product and catalyst separation has meant that the development of a heterogeneous catalyst has attracted much interest. Not surprisingly rhodium has been widely studied, along with cheaper alternatives like iron and cobalt [7-9].

In a study by Chateau *et al.* [10], supported rhodium catalysts were used to form acetyls in the presence of methyl iodide at moderate pressures (21 bar). Synthesis gas mixtures were used (CO:H₂ = 60:40) and the reaction temperature was 230°C. La₂O₃, Pr₆O₁₁, CeO₂ and SiO₂ were used as supports and typical rhodium loadings were 3 and 5wt%. La₂O₃ was found to be the best support for acetic acid production in steady state activity tests with an STY value of 1200 g/kg/h reported. The formation of higher acetyls occurred and this was thought to be as a consequence of acid hydrogenation. Two different mechanisms for acetic acid formation were proposed to occur. On the rhodium metal, the mechanism was thought to proceed through CO insertion in the presence of methyl iodide analogous to that of the homogeneous reaction. This was supported by the formation of surface acetyl and acetate species, confirmed in a trapping experiment with methyl iodide. On the support, it was proposed that acetic acid was formed via methyl formate isomerization [10].

Various supports have been used for rhodium and tested for methanol carbonylation. Rhodium supported on Zeolite Y has been studied at atmospheric pressure, and methyl acetate was reported to be the only product [11]. In that study, the carbonylation reaction was reported to be first order in methyl iodide and zero order with respect to methanol and CO. The reaction mechanism for carbonylation was proposed to be similar to the

homogeneous route involving oxidative addition of methyl iodide to an active rhodium site followed by the insertion of the CO into the acetyl-rhodium bond. Whilst these studies have focussed on rhodium metal, other heterogeneous rhodium based systems have been based on the immobilization of rhodium complexes onto solid supports. In a study by Jarrel *et al.* [26], $\text{RhCl}(\text{CO})(\text{PPh}_3)_2$ was bound to styrene – divinylbenzene polymers via ligand exchange. Methyl acetate was the observed acetyl product with dimethyl ether (DME) also observed as a by-product. Stability tests found that the catalyst became inactive due to the formation of a coordinatively saturated rhodium (III) complex.

Nickel supported on activated carbon has also been investigated for the methyl iodide promoted vapour phase carbonylation of methanol [8]. In a study by Merenov *et al.* [8], an optimal nickel loading of 3.5wt% was found to be an effective catalyst forming methyl acetate and acetic acid. Methyl acetate was the major product with a maximum yield of 21% reported at 225°C. However the catalyst stability was lower at elevated temperatures with irreversible catalyst deactivation occurring. The deactivation was attributed to poisoning with acetic acid. Nickel carbide formation was also proposed as a cause for catalyst deactivation, although no direct experimental evidence for this claim was presented in the study. In a subsequent study by the same group, the deactivation of nickel supported on activated carbon was attributed to strong adsorption of reactant methanol, and reaction products blocking the catalyst pores causing diffusion limitation [9]. Nickel supported on activated carbon has also been shown to be active for the vapour phase carbonylation of dimethyl ether (DME) to yield methyl acetate [12]. In a study by Fujimoto *et al.* [12], a Ni/C catalyst with a metal loading of 10 wt% produced methyl acetate at a yield of 15 % with a selectivity of 90% at 11 atmospheres and 250° C. Acetaldehyde, CH_4 and CO_2 were the detected by-products.

In order to overcome the problems of stability with activated carbons as supports, the use of polymer- derived carbon has been reported to lead to greater stability compared with activated carbon [13]. Nickel was found to be more active than cobalt, with iron showing the lowest catalytic activity. Porous carbon beads formed from poly (vinylidene chloride) have also been used to support rhodium. This catalyst exhibited high methanol conversion value of 84% and a 99% selectivity to methyl acetate [14].

It should be noted that all of the above heterogeneous catalyst systems still require a methyl iodide co-catalyst.

1.2.2 Non- promoted heterogeneous methanol carbonylation

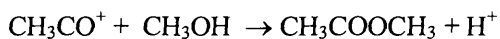
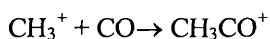
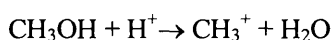
In addition to the advantages of a heterogeneous catalytic system for methanol carbonylation, the complete removal of the corrosive halide promoter would be desirable. As a result, the direct vapour phase carbonylation of methanol without a methyl iodide co-catalyst is of significant interest. In the homogeneous system, the iodide species is used to cleave the strong carbon oxygen bond of methanol to form methyl iodide as illustrated in Figure 1-3. An alternative approach to activating the carbon oxygen bond is to protonate the oxygen using an acid.

Successful vapour phase carbonylation in the absence of halide promoters has been reported using several different catalysts at atmospheric pressure. Sulfided bi-metallic cobalt-molybdenum supported on activated carbon is active for the formation of methyl acetate with no co-formation of acetic acid [15]. DME, CH₄, CO₂ were observed by products along with trace amounts of C₂-C₃ hydrocarbons. The production of methyl acetate increased with time on stream and H₂S was lost from the surface of the catalyst over 5 hour reaction runs. The effect of synthesis gas composition was investigated. It was found that having H₂ in the feedstream reduced the formation of methyl acetate. Ethanol, formed by the hydrogenation of methyl acetate was also observed. The methanol conversion was around 22% and the methyl acetate selectivity 53% at the optimal temperature of 250°C. The optimum catalyst composition contained cobalt-molybdenum loadings of 3wt%-10wt% and 3wt%-1wt%. In order to study the role of each metal in the bimetallic catalyst, Co/C and Mo/C catalysts were tested separately. It was found that Co/C was active for methanol carbonylation whilst Mo/C produced CO₂ and CH₄ only. On the basis of these observations, it was postulated the molybdenum decomposed the methanol to form methyl species which migrated to active carbonylation sites containing cobalt atoms. To support this mechanism, methanol decomposition experiments were performed in the absence of CO over the Mo/C catalyst which resulted in the formation of CO₂ and CH₄. The type of carbon support was of importance with methyl acetate selectivity higher in carbon supports with a lower surface pH. It should be noted that although no co-catalyst is used in this study, the loss of H₂S is a major disadvantage, not considered by the authors.

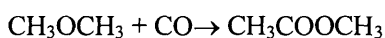
Activated carbon supported NiCl₂-CuCl₂ catalysts have been reported to be active for the production of methyl acetate at atmospheric pressure and 300 °C [16]. CH₄ and DME were by-products. The optimum catalyst composition contained 5wt% NiCl₂ and 15wt% CuCl₂ resulting in a methanol conversion of 46.9% and methyl acetate selectivity of 70.9%. 22

The production of methyl acetate increased with time on stream similar to the sulfided Co-Mo catalysts [15]. No catalyst deactivation occurred until after 18 hours on stream, after which methyl acetate production remained high. XRD analysis of the spent catalyst showed reflections corresponding to copper metal. However, experiments using a copper and nickel metal bimetallic catalyst supported on activated carbon yielded no carbonylation activity. Peng *et al.* noted that the decrease in the Cl(Ni+Cu) atomic ratio was due to the aggregation of small particles, however the loss of chlorine from the catalyst as HCl was not considered [16]. Although no halide promoter was used in this catalyst system, elimination of HCl would be a disadvantage.

Wegman *et al.* [17] has shown that the atmospheric, vapour phase carbonylation of methanol with ion exchanged heteropoly acids (HPAs) supported on SiO₂ materials results in the formation of methyl acetate and DME at 225 °C. A catalyst of composition IrW₁₂PO₄₀ gave the highest yield of methyl acetate (40%) and a 52% yield of DME. Wegman postulated that the acidic nature of these materials was responsible for their catalytic properties analogous to Koch type chemistry as follows:



It was also suggested that DME formed by the condensation of methanol on the acid catalyst can be directly carbonylated to methyl acetate:



A major disadvantage with HPAs is lifetime, as these materials quickly deactivate [18].

Copper supported on mordenite, has been shown to be active for the carbonylation of methanol under moderate conditions without the use of a halide promoter [19]. The typical reaction conditions employed in the study were 10 bar pressure, 350 °C and a CO:MeOH ratio of 10:1. In a typical reaction run, a characteristic product profile was observed. In

the first 6 hours on stream, the formation of polymethyl benzenes indicative of methanol to gasoline (MTG) chemistry was observed. Acetic acid then becomes the major product as the formation of MTG products declined. The selectivity to acetyls (acetic acid and methyl acetate) remained greater than 70% for the next 12 hours on stream before giving way to the formation of DME. MTG and CO₂ products were calculated to account for less than 15% of the total methanol converted. After 25 hours on stream the conversion of methanol remained above 90%, however the selectivity to acetyls rapidly declined.

This characteristic reaction profile is illustrated in Figure 1-5, which has been adapted from reference [19].

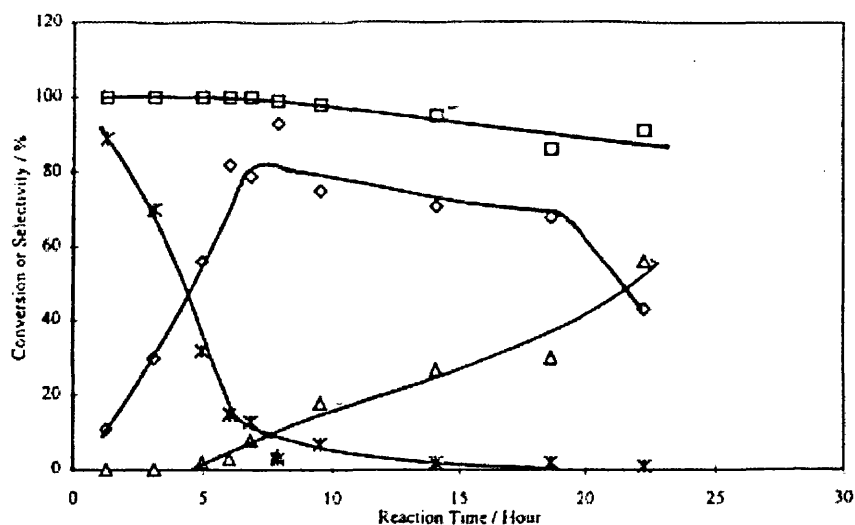


Figure 1-5: Product profile for methanol carbonylation over copper mordenite adapted from reference [19]. The squares represent the methanol conversion, the crosses represent the selectivity to hydrocarbons, the diamonds are the selectivity to acetyls (acetic acid + methyl acetate) and the triangles represent DME selectivity

It was found that Cu- mordenite performed better than H- mordenite. Lower yields of MTG products and an increased selectivity to acetyls were observed. The optimum catalyst composition consisted of a 3.4 wt% loading of copper with a SiO₂:Al₂O₃ ratio 20. A promotional effect of adding 1 wt% palladium was reported to reduce the selectivity for hexamethylbenzene and pentamethylbenzene MTG products. N₂ physisorption analysis indicated that the pores of the mordenite had become completely blocked as a result of

the formation of high boiling aromatics in the MTG chemistry. The fresh catalyst contained copper (II) species which were observed by XANES and temperature programmed reduction (TPR) studies, however XRD analysis of the spent catalyst samples showed that copper metal had formed rapidly as large metal particles of 120 Å diameter. FTIR studies using CO as a probe molecule confirmed that Cu(I) and Cu(II) ions still existed on the spent catalyst. On the basis of these findings, it was postulated by Ellis *et al.* [19] that only a small amount of the copper present in the catalyst was responsible for acetyl production.

Very recently, it has been demonstrated that using DME as a feed instead of methanol offered several advantages in the production of acetyls [20]. Methyl acetate was produced with selectivities in excess of 99% using a H-mordenite catalyst at low temperatures [20]. At temperatures of 150- 190 °C, methyl acetate was produced at a much higher rate than acetyls formed by methanol carbonylation. It was found that the rate of the carbonylation increased linearly with CO partial pressure and was independent of the DME partial pressure. Iglesia *et al.* [20] reported reversible kinetic inhibition. The addition of water into the feed resulted in lower methyl acetate synthesis rates and the removal of the water led to activity regeneration. These findings, together with the CO partial pressure dependence on the rate of methyl acetate, suggest that the water competes competitively for CO binding sites reducing the rate of methyl acetate formation. It was suggested that DME carbonylation is more effective than methanol carbonylation because DME carbonylation results in anhydrous conditions whereas methanol, used as a reactant readily forms DME and water under acidic conditions, which inhibits CO adsorption and ultimately acetyl formation. In a subsequent study by Iglesia *et al.* [21], the mechanism of DME carbonylation over H-mordenite was investigated by using adsorption/desorption studies, isotopic exchange studies and FTIR spectroscopy. Figure 1-6 shows the proposed catalytic cycle for the synthesis of methyl acetate. DME initially reacts with acidic protons to form methyl groups and methanol. This was confirmed by FTIR studies where the intensities of bands associated with hydroxyl stretches decrease, while those associated with methyl stretches increase. Methyl acetate synthesis rate increased initially with time on stream and the methanol synthesis rate decreased concurrently during an induction period. The steady state selectivity to methanol remained below 1% and the induction period for the reaction was removed by exposing the mordenite to DME prior to carbonylation. This behaviour was reported to be consistent with a saturation coverage of methyl groups on the catalyst and zero order dependence on reaction rate with respect to DME reported by Iglesia *et al.*

[21]. The CO, adsorbed on a site denoted *, reacts with the methyl group to form an acetyl intermediate in the rate step. This surface acetyl species finally reacts with DME to produce methyl acetate, completing the catalytic cycle with the regeneration of the surface methyl species. Although the surface acetyl groups were not directly observed, in order to support this hypothesis, Iglesia and co-workers performed an experiment using acetic anhydride dissociative adsorption to form surface acetyl species, which were observed by FTIR. Subsequent reaction of these acetyl species with DME led to the formation of methyl acetate and methyl species. Interestingly, there was a difference in carbonylation activity among mordenites with the same Si/Al ratios obtained from different sources, and no correlation with methyl acetate formation rates was observed with respect to the number of extra-framework aluminium species. There was also no reported dependence of carbonylation activity on the total number of Lewis acid sites. The DME carbonylation rates have been shown to be proportional to the number of acidic hydroxyl groups within the 8 membered ring zeolite channels of mordenite [22]. In the same study it was found that no carbonylation activity occurred with zeolites without these 8 membered ring channels and as a result carbonylation occurred exclusively on mordenite and ferrierite [22].

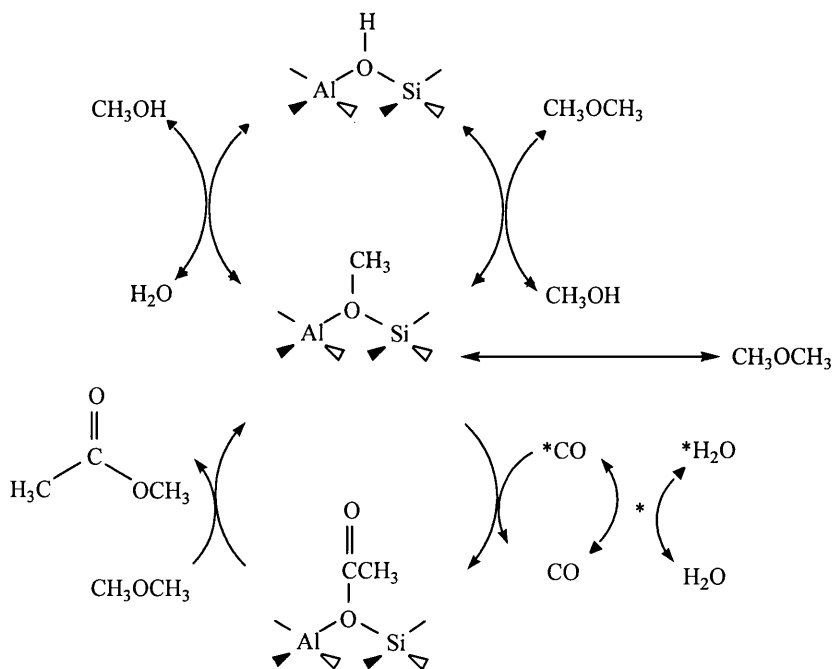


Figure 1-6: Proposed mechanism for DME carbonylation over H-mordenite

1.3 Alternative routes to acetic acid

1.3.1 Ethane oxidation

The heterogeneous catalysed gas phase oxidation of ethane to acetic acid occurs via the following route:



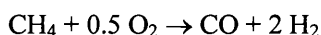
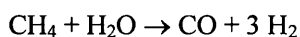
This is seen as an attractive route to acetic acid due to the low cost and availability of ethane feedstocks from natural gas and it is catalysed using mixed metal oxide catalysts [23]. Ethane dehydrogenation to ethene also occurs on these mixed metal oxide materials and the relative selectivity to acetic acid is dependent on catalyst composition and reaction conditions [23]. Burch *et al.* [23], have reported that a large number of various mixed metal oxide catalysts in the literature are active for the oxidative dehydrogenation of ethane to ethene and only metal oxides based on Mo-V, W-V, V and V-P are active for the selective oxidation of ethane to acetic acid. They synthesised, characterized and tested a Mo-V-Nb mixed metal oxide catalyst with the composition Mo(73)V(18)Nb(9)O(x) along with pure model oxide phases in order to relate the structure and composition of the oxide catalyst to their catalytic properties. The multiphase catalyst, analysed by XRD, showed only three crystalline phases. These were Mo₆V₉O₄₀, Mo₃Nb₂O₁₁ and MoO₃. There was a high surface area amorphous component. These individual phases were tested and compared with the active multiphase catalyst for ethane oxidation using air as the feed gas [24]. All of the pure crystalline phases catalysed the formation of ethene whilst the Mo₆V₉O₄₀ phase was the only crystalline phase found to catalyze the formation of acetic acid [24]. Optimal conditions for acetic acid production were 240°C and 20 bar pressure. The total oxidation to CO and CO₂ was observed at 400°C. Trace amounts of acetaldehyde and ethanol were produced at optimal conditions. On the basis that the multiphase catalyst was more active than the Mo₆V₉O₄₀ phase when normalised to BET surface area, it was concluded that the high surface area amorphous phase may be responsible for catalytic behaviour of these materials. TPR measurements made indicate that the multi-component catalyst and the single Mo₆V₉O₄₀ phase are more easily reducible compared to the other crystalline phases observed in the multi component catalyst. These are the only two phases reported to make acetic acid and it was postulated that both phases provided lattice oxide sites which can participate in a Mars van Krevelen mechanism where the acetic acid is

formed from ethane by hydrogen abstraction and then oxygen insertion.

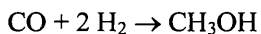
It should be noted that any ethene by-product formed in the dehydrogenation of ethane may be oxidised to acetic acid in the presence of a heterogeneous catalyst. It has been shown that Pd/SiO₂ and Pd/TiP₂O₇ promoted with alkali metals and alkaline earth metals are active for the oxidation of ethane to acetic acid at various temperatures and pressures [25].

1.3.2 Acetic acid from synthesis gas

Synthesis gas is formed by the steam reforming or partial oxidation of methane via the following reactions [26]:



Acetic acid is also indirectly synthesised from synthesis gas. In methanol carbonylation for example, the methanol can be synthesised from synthesis gas using a heterogeneous copper based catalyst [27]:



The methanol produced can then be transported and carbonylated using the Monsanto or Cativa processes or by directly integrating the methanol synthesis and carbonylation processes in series [28]. It has been shown however that the one pot synthesis of acetic acid is possible by integrating a methanol synthesis catalyst into the acetic acid process [29].

It is possible to synthesise acetic acid directly from synthesis gas using a rhodium based heterogeneous catalyst as follows:

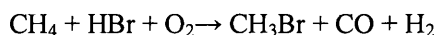


Rhodium does not selectively catalyze the formation of acetic acid. Methane, ethanol, and hydrocarbons are observed as significant by-products [30]. In a study using Rh/ γ -

Al₂O₃, a maximum CO conversion of 7.6% was observed and the selectivity to C₂ oxygenates was 43% at 260°C and 20 bar. In the same study it was found that the formation of oxygenates was suppressed by the sintering of the rhodium metal with selectivity lost to hydrocarbon formation [30]. However in that study, no specific selectivity to acetic acid was reported. The activity and selectivity to C₂ oxygenates can be improved by the addition of promoters such as manganese, magnesium and alkali metal promoters to the monometallic rhodium catalyst [31]. In a study by Luo *et al.* [32], it was found that manganese and lithium exhibited promotional effects for acetic acid production using a Rh-Mn-Li/SiO₂ catalyst. The selectivity profile was very sensitive to metal doping. For example, it was shown that the Rh/SiO₂ catalyst doped with vanadium produced ethanol as the only product. The enhanced selectivity using manganese and lithium dopants was attributed to a suppression of rhodium reduction and preservation of Rh⁺ species on the surface of the catalyst which are believed to be responsible for acetic acid and acetaldehyde production. Selectivity to acetic acid remained low, with methane, acetaldehyde and ethanol all major by-products along with smaller quantities of propanol, methyl acetate and ethyl acetate. At 300°C and 30 bar, the CO conversion was 4.8% and the selectivity to C₂ oxygenates was 67%. However the C₂ oxygenate fraction contained 31.6 wt% acetic acid and 0.6wt% methyl acetate.

1.3.3 Acetic acid production from methane – non-synthesis gas routes

The direct conversion of CH₄ to C₁ acetyls via non-synthesis gas routes is an attractive pathway. Xin and co-workers [33], synthesised acetic acid in a multi-step process. The first step involved the oxidative bromination of CH₄ to form the precursor CH₃Br compound using a heterogeneous Ru/SiO₂ catalyst at 530°C as illustrated by the following equation:



A CH₄ conversion of 30.1% with a CH₃Br selectivity of 72.4% was reported. Selectivity loss was due to the formation of CH₂Br₂. In the subsequent step, the CH₃Br was carbonylated with CO using a RhCl₃ catalyst and KI co-catalyst in a homogeneous batch reaction at 175 °C using water as a solvent. The simplified catalytic scheme adapted from reference [33] is illustrated in Figure 1-7. It can be observed that the reaction proceeds by the oxidative addition of CH₃Br to the RhCl₃ catalyst forming Rh(CH₃)BrCl₃. Subsequent CO insertion to the rhodium – methyl bond followed by hydrolysis forms acetic acid and regenerates the active catalyst. The reaction was found to proceed more slowly without

the KI co-catalyst. It was proposed that under reaction conditions, the methyl bromide was converted into methyl iodide and the increased rate was due to the faster oxidative addition of methyl iodide, analogous to the rate-determining step of the Monsanto process.

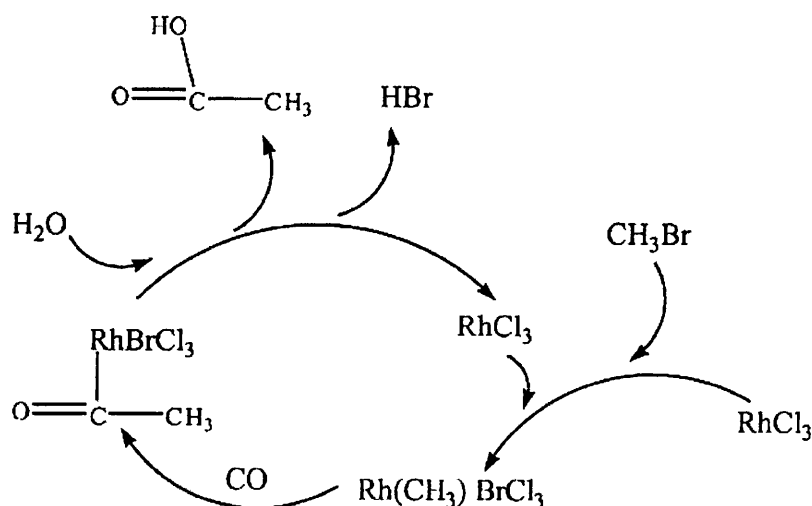


Figure 1-7: CH_3Br carbonylation using a RhCl_3 homogeneous catalyst (adapted from reference [33])

For the carbonylation step, a CH_4 conversion of 99% was achieved after a 20 hour reaction and acetic acid was produced with a selectivity of 99%. CH_3Br , CH_2Br_2 , CHBr_3 , CO , methyl acetate and CO_2 were the detected by-products.

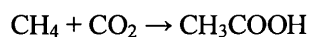
The direct conversion of CH_3Br to acetic acid using a RhCl_3 homogeneous catalyst with a KI co-catalyst in a water solvent has also been reported in a study by Sen *et al.* [34]. In that study a reaction mixture of CH_4 , CO and O_2 also yielded formic acid and methanol by-products. The following reaction scheme was proposed:



A maximum concentration of 0.275M (determined by ^1H NMR spectroscopy) was achieved after a 352 hour reaction at 95°C and 73 bar. The role of the iodide promoter was not determined. A mechanism analogous to homogeneous carbonylation of methanol was discounted because isotopic labelling studies confirmed that the acetic acid was formed

through CH₄ and not methanol, which may have been formed as an intermediate.

Acetic acid can be synthesised by the reaction of CH₄ and CO₂. This is an appealing reaction pathway because it utilizes the greenhouse gases CH₄ and CO₂ as a feedstock in the synthesis.



The problem is that this is thermodynamically unfavourable with a large Gibbs free energy change. ($\Delta G^\circ_{298\text{K}} = 16.98\text{kJ/mol}$, [35]). Spivey *et al.* performed Gibbs free energy minimization calculations and found the maximum fractional conversion of CH₄ to be 1.6×10^{-6} at a temperature of 727°C, pressure of 100 bar and inlet composition of 95% CO₂ and 5% CH₄. In the same study, the formation of acetic acid was studied over a 5wt%Pt/Al₂O₃ and 5wt% Pd/C catalysts using temperature-programmed reaction. The production level of acetic acid was so small that it was not detected by the thermal conductivity detector (TCD) and was only observed using mass spectrometry. The peak maximum for 60 amu and 43 amu corresponding to acetic acid was observed at a reaction temperature of 375°C, and the Pt catalyst performed better than the Pd catalyst. The authors of this study reported no by-product formation.

Some groups have taken approaches to overcome the thermodynamic limitations. Huang *et al.* [36] report the formation of acetic acid using a Co-Cu catalyst. In that study a cyclic method is used whereby the catalyst is first exposed to CH₄, forming a CH_x species on the surface. The gas flow was then changed to CO₂ and this cyclic process was repeated. The optimum catalyst contained a Cu/Co weight ratio of 5 and the maximum rate of acetic acid formation (2.4g/kgcat/h) occurred at 250°C. Formic acid was detected as the main by-product but it was not formed at 250°C. Other by-products reported were methanol, formaldehyde, butanone, methyl furan and cyclopentane derivatives.

A similar approach was taken by Ding *et al.* [37] who also studied acetic acid formation using a cyclic method using Pd/SiO₂ and Rh/SiO₂ catalysts at low temperatures. The palladium catalyst was found to be the most active and the optimal temperature and palladium loading was 200°C and 2wt% respectively. The maximum rate of acetic acid formation was 2.5g/kgcat/h. Formic acid was the only reported by-product in this study and it only occurred with the palladium based catalyst.

The following reaction cycle was proposed [36]:

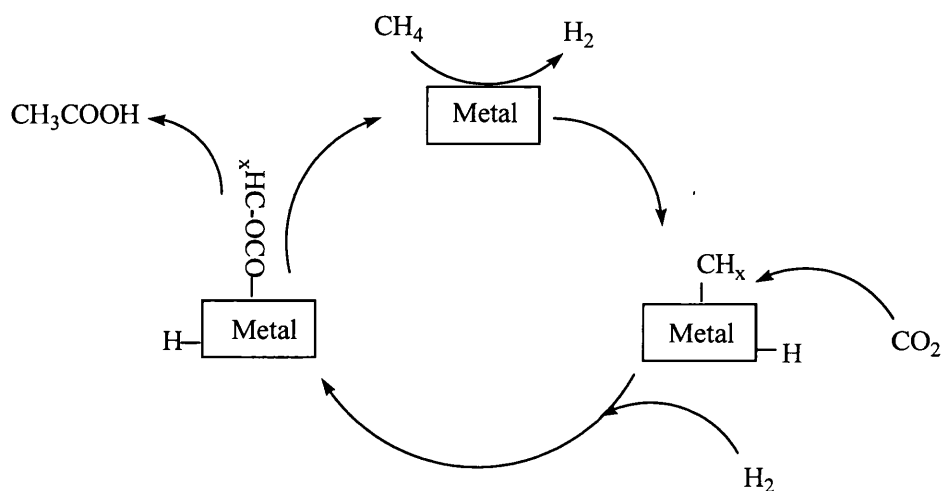


Figure 1-8: Proposed cycle for acetic acid production

In the first step, CH_4 was adsorbed and dissociated to generate the surface CH_x species with the evolution of H_2 . In the second step the CH_4 feed is switched off and CO_2 introduced resulting in the formation of an adsorbed $x\text{HCOCO}$ species, which desorbs as acetic acid. In that study however no evidence of this proposed intermediate was given. Although a possible route to acetic acid, this is unlikely to be commercially viable due to the very low formation rates of acetic acid.

1.3.4 Acetic acid synthesis from methanol

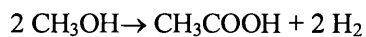
Acetic acid can be synthesised directly from methanol without the need for carbon monoxide feedstocks. Yamakawa *et al.* [38] have synthesised methyl acetate directly from methanol in a one pot homogeneous reaction using $\text{Ru}^{\text{II}}\text{-Sn}^{\text{II}}$ cluster complexes ($\text{Ru}(\text{SnCl}_3)_5\text{L}$) where $\text{L} = \text{MeCN}$ or PPh_3 . The products observed were methyl acetate and a small amount of methyl formate. The reactions were carried out in a methanol/solvent mixture with the volumetric ratio of 1:1. The maximum turnover reported for methyl acetate formation at 65°C was 9.2 over a 120 hour reaction time using methyl cyanide as the solvent. A dual functionality where the reactant methanol is dehydrogenated to

methyl formate (via formaldehyde) which was then isomerised to form acetic acid was postulated. In that study formaldehyde was also used as the reactant and on the basis of product spectrum the following reaction sequence was suggested to support methyl formate as an intermediate:



It should be noted that yields of product in this study were low. However Yamakawa *et al.* have tested heterogeneous catalysts for the same reaction using methanol in the gas-phase [39]. Ru^{II}-Sn^{II} cluster complexes were supported on inorganic supports. The supports employed were CuO/ZnO/SiO₂ and Cu/Cr₂O₃/SiO₂ known to catalyse the dehydrogenation of methanol to methyl formate [40]. Tests were carried out at 200°C and atmospheric pressure and the methanol conversions remained low. In the same study, activated carbon when used as a support was found to be less active for the formation of acetic acid and methyl acetate. Mechanical mixtures of CuO-ZnO/SiO₂ and (NEt₄)₄ [Ru(SnCl₃)₆] yielded methyl formate as the only product.

In a study by the same group, Ru-Sn supported on Zeolite Y was reported to produce acetic acid and methyl acetate from methanol [41]. At atmospheric pressure and 200°C a yield of 10.9% methyl acetate was achieved with optimal catalyst preparation using Cl₂ catalyst pre-treatment. The Cl₂ gas was introduced at the preparation stage after the ruthenium metal particles were formed on the zeolite cavities. This was reported to form RuCl_n species, which upon subsequent reaction with gaseous SnCl₂, formed the active catalyst. The quantitative analysis of methyl acetate and hydrogen in the product spectrum confirmed that acetic acid was being produced by the direct dehydrogenation of methanol via the following reaction scheme:



1.3.5 Conclusion

There have been many different reaction routes employed to synthesise acetic acid and methyl acetate. It has been evident that the current homogeneous routes to acetic acid dominate, however the disadvantages of a homogeneous system has meant there have been attempts to create a successful heterogeneous system. The present work is concerned with the halide free heterogeneous carbonylation of methanol to acetic acid and methyl

acetate from a feed containing only methanol, which involves an investigation into methanol decomposition covered in Chapter 3.

1.3.6 Mordenite

This section has been included in this Chapter to give an introduction to mordenite. Mordenite is the catalyst used in this study for the methanol carbonylation study and therefore it is appropriate that some background information is provided. Mordenite is a zeolite. Zeolites are microporous crystalline aluminosilicate solids with well defined structures, comprising of 3 dimensionally linked AlO_4 and SiO_4 tetrahedra, linked by oxygen atoms. The acidic properties, and well defined pore structures of zeolites mean that they are used in a wide range of catalytic reactions. These include fluid catalytic cracking, hydrocracking, dewaxing, alkylation, isomerisation as well as the conversion of methanol to hydrocarbons. Such processes are reviewed in more detail elsewhere [143]. Each AlO_4 unit has a net negative charge balanced by a cation, and zeolites can be further classified in terms of their Si/Al ratio, which affects both zeolite stability and acidic behaviour of the zeolite. In addition to their acid properties, zeolites also exhibit ion exchange capacity. The synthesis of zeolites results normally in the formation of Na^+ ions to balance the framework charge. The Na^+ ions can be exchanged for other metal ions or NH_4 , which upon heating results in the proton form of the zeolite with the evolution of ammonia. Whilst metals can be doped onto zeolites with simple impregnation techniques, the ion exchange capability provides another method of preparation which can result in a greater degree of metal dispersion throughout the zeolite pore structure. Typically Cu^{2+} zeolites can be formed by ion exchange from CuCl_2 or $\text{Cu}(\text{acetate})$ from the parent Na^+ zeolite [144]. It has been demonstrated that the resulting coordination of the exchanged ion influences the redox properties and catalytic behaviour of the zeolite [144]. In a study by Wichterlova et al [144], the coordination environment of Cu ions, planted in MFI, erionite and mordenite were studied using IR spectroscopy and Cu^+ luminescence. The catalytic activity of the systems was investigated using NO decomposition to molecular nitrogen and oxygen and NO reduction. It was found that Cu^+ ions adjacent to one framework were responsible high activity in NO decomposition whilst Cu^{2+} ions neighbouring two framework Al atoms were active in NO reduction.

The structure of mordenite comprises of 2-dimensional, straight 12 ring channels (7.0×6.5 Å) connected by short alternating 8-ring channels (3 Å), via side channels [86]. Figure 1-9

illustrates this pore structure, where the 8 and 12 membered rings are observed. Figures 1-10 and 1-11 illustrate the 12 and 8 membered channels respectively.

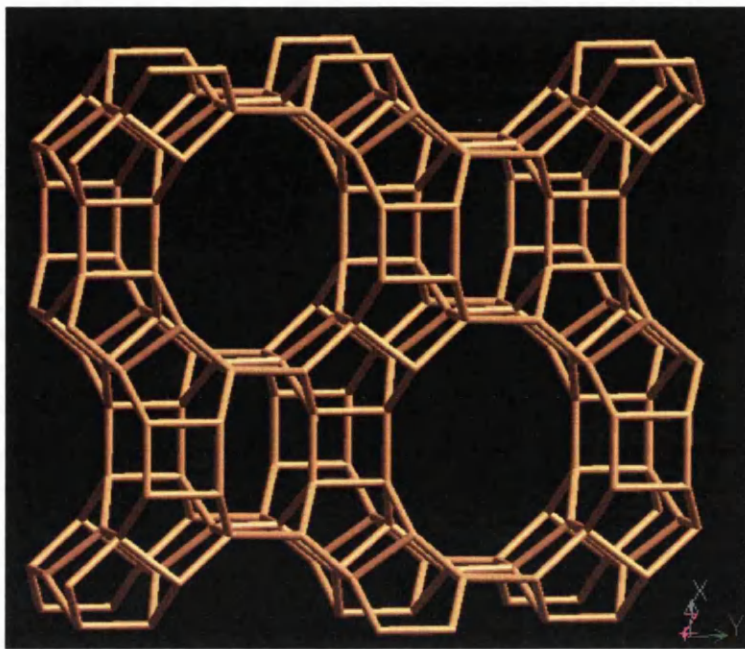


Figure 1-9: Pore structure of mordenite viewed along the 001 plane. Adapted from reference [86]

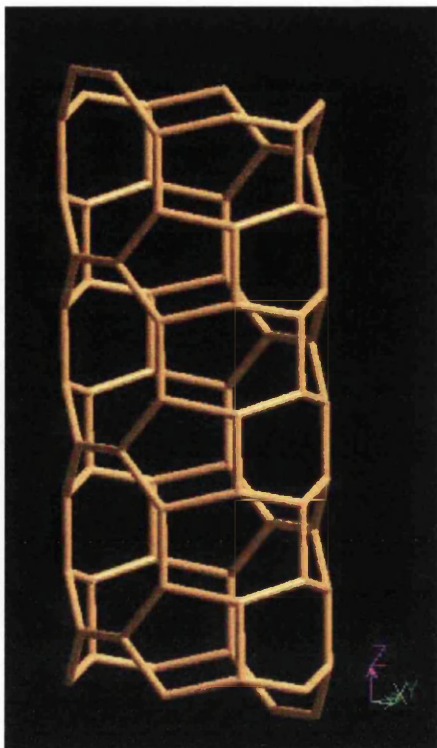


Figure 1-10: 12 ring channel viewed normal to the 001 plane. Adapted from reference [86]

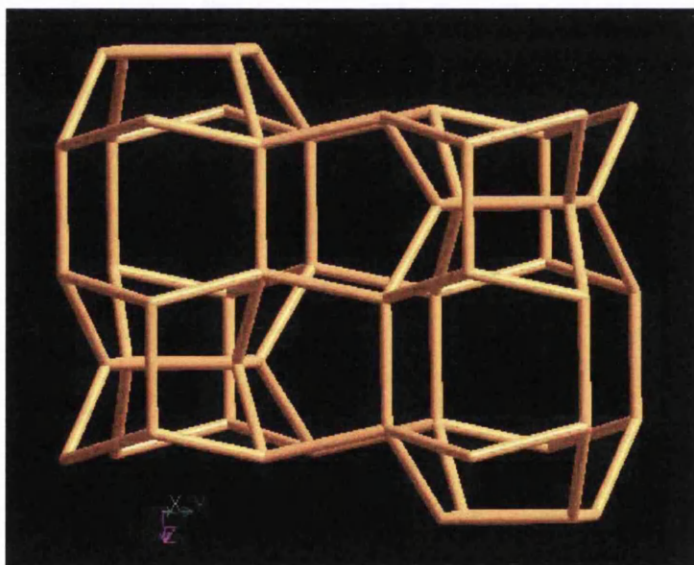


Figure 1-11: 8 ring channel viewed normal to the 001 plane. Adapted from reference [86]

In a study by Sobalik and co-workers [145], the environment of Cu ion of various loadings was investigated over various zeolites including mordenite. In that study the Cu^+

photoluminescence spectrum showed 4 peaks at 450nm, 480nm, 510nm and 540nm. The peaks at 450nm and 480nm were due to Cu sites balanced by pairs of framework Al atoms with the Cu ion exhibiting square pyramidal coordination. The latter peaks were assigned to Cu ions adjacent to single framework Al atoms with the Cu ions square planar environment. It was reported that these latter sites were more reducible compared to the other sites in NO decomposition, and these sites which were dominant in Cu-ZSM-5 and are responsible for its unique activity in NO decomposition.

The Si/Al ratio was found to influence the nature and abundance of the Cu ion sites in the zeolite structure. Increasing the Si/Al ratio from 17 to 630 resulted in a relative increase intensity of the 540 nm band with respect to the band at 480nm. This indicates that at higher Si/Al ratios, there is an increase in the number of Cu ions adjacent to single Al framework atoms and this is also reflected in the increase in activity for NO decomposition at higher Si/Al ratios. It was also noted that in addition to the Si/Al ratio, the loading of Cu affected the nature of the resulting Cu ion coordination in the zeolite structure. During the first ion exchange and at low Cu loadings, the Cu ions occupy sites in large cavities as single Cu²⁺ ions adjacent to two framework Al atoms, corresponding to peaks at 450nm and 480nm in the photoluminescence spectra. At higher Cu loadings, sites in smaller cavities are also occupied. It was observed that at low Cu loadings, with Cu mordenite, there was an equal distribution of Cu ions in all sites, however at higher loadings, there was a substantial increase in the band at 450nm. This is in contrast to the other zeolite materials studied, whereby the Cu sites at 450nm were readily saturated at relatively low Cu loadings. It is clear that even at higher loadings, copper ions can still be placed into the larger cavities and pores of the mordenite.

Whilst it has been shown that the environment and nature of Cu ions within the framework structure can influence the catalytic behaviour with respect to NO decomposition for example, there is limited literature regarding these issues with respect to copper mordenite and methanol carbonylation.

2 Experimental

2.1 Catalyst synthesis

2.1.1 Synthesis of copper based methanol decomposition catalysts

The synthesis of copper methanol decomposition catalysts was based on the formulation of a methanol synthesis catalyst containing CuO, Al₂O₃, ZnO, and MgO components [85].

The catalysts were prepared using co-precipitation. Solutions of copper (II) acetate (Fluka, >99% purity), zinc acetate (Riedel, 99% purity), aluminium lactate (Riedel, 99%purity) and magnesium nitrate (Fluka, >99% purity) were separately dissolved in 100ml of deionised water and then mixed together in a total volume of 600ml. Typically a target yield was to obtain 10g of catalyst with a composition of 64wt% CuO, 24wt% ZnO, 10wt% Al₂O₃, and 2wt% MgO. The reagent mixture was stirred and co-precipitated using a 2M potassium carbonate (Aldrich ACS Reagent) solution which was added dropwise into the mixture at a temperature of 80°C using a burette. The resulting precipitate was aged in the mother liquor at a pH of 9 for 1 hour and then washed 3 times with 100ml water and dried for 24 hours at 100°C. The dried solid was then ground into a fine powder and sieved to obtain a particle size less than 250 microns. The catalyst was calcined in static air at 450°C for 18 hours. Prior to each reaction run, a 0.15g portion of the calcined catalyst was charged onto a quartz tube reactor and reduced at 250°C in a 20% H₂ 80% Ar (BOC, 99.999% purity) mixture for 3 hours at a total flow rate of 47ml/min.

2.1.2 Synthesis of palladium, ceria/zirconia methanol decomposition catalysts

Co-precipitation was used for the synthesis of supported palladium methanol decomposition catalysts. A target yield was to obtain 2g of catalyst with various palladium loadings supported on CeO₂ and Ce_{1-x}Zr_xO₂ mixed supports. Cerium (III) nitrate (Aldrich, 99% purity), zirconyl nitrate hydrate (Aldrich, 99.99% purity) and palladium (II) nitrate (Aldrich, 99% purity) were separately dissolved in 100ml of deionised water and then mixed together to give a total volume of 700ml. The reagent mixture was stirred and co-precipitated using a 2M ammonium carbonate base (ACS Reagent, 99.995% purity) added dropwise into the mixture at a temperature of 90°C using a burette. The resulting precipitate was aged in the mother liquor at pH 10 for 1 hour and then filtered and washed three times with 100ml water and dried for 24 hours at 100°C. The dried solid was then

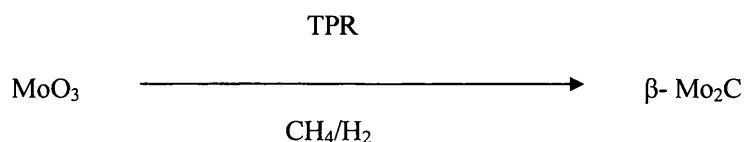
ground to a fine powder and sieved to obtain a particle size less than 250 microns. The catalyst was then calcined in air at 450°C for 3 hours. Prior to each reaction run, a 0.15g portion of the calcined catalyst was charged onto a quartz tube reactor and reduced at 450°C for 1.5 hours in a 20% H₂/ 80% Ar mix at a total flow rate of 47ml/min.

2.1.3 Synthesis of palladium based methanol decomposition catalysts supported on alumina

Catalysts were prepared by loading palladium onto γ -Al₂O₃ (Alfa Aesar, 99.97% purity). Typically a 2g batch of catalyst was prepared. Sodium tetrachloropalladate (II) (Alfa Aesar, 99.95% purity) was dissolved in deionised water to create a stock solution. The concentration of the solution was varied from 0.057M, 0.011M and 0.34 M to result in palladium metal loadings of 1.5, 3 and 9 weight percent respectively. Using incipient wetness, a 5ml aliquot of the stock solution was added dropwise onto 2g of γ -Al₂O₃ to obtain a targeted loading of the palladium metal. The precursor was then dried at 100°C for 24 hours. Once dried and sieved to obtain a particle size less than 250 microns, the catalyst precursor was calcined in static air at 450°C for 3 hours. Prior to each reaction run, a 0.15g portion of the calcined catalyst was charged onto a quartz tube reactor and reduced at 450°C for 1.5 hours in a 20% H₂/ 80%Ar mix at a total flow rate of 47ml/min.

2.1.4 Synthesis of molybdenum carbide catalysts

The synthesis of beta- phase molybdenum carbide occurs via the following simplified reaction.



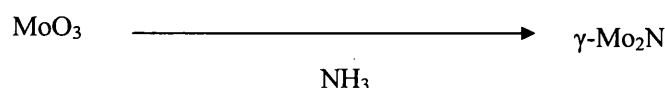
Molybdenum carbide catalysts were synthesised by passing mixtures of CH₄ (BOC, 99.999 % purity) and H₂ (BOC, 99.999% purity) over molybdenum trioxide loaded onto a fixed bed quartz tube reactor in a TPR. Typically 0.21g molybdenum trioxide was charged

and the temperature ramped to 650°C at 2°C/min. The gas flow conditions applied were a 33% CH₄ in H₂ mixture at a total flow of 21 ml/min. The reaction was held for 4 hours at the final temperature and then cooled to room temperature under the reaction atmosphere. Once at room temperature, Ar gas was flowed over the catalyst prior to reaction.

2.1.5 Synthesis of molybdenum nitride catalysts

The synthesis of metal nitrides is possible via many routes, which ultimately produce a variety of different metal nitride phases [123]. In the study of methanol decomposition γ -Mo₂N, δ -MoN and β -Mo₂N_{0.78} were synthesised.

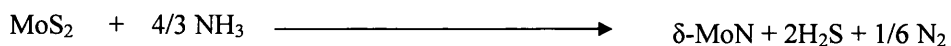
The method of preparing γ -Mo₂N involved the reduction of molybdenum trioxide using high flowrate NH₃ with controlled temperatures and ramp rates.



Molybdenum trioxide (Aldrich 99.5% purity) (1 g) was loaded into a quartz tube reactor and NH₃ (BOC) flowed at a rate of 94ml/min controlled by Brooks 5850 TR mass flow controllers. The furnace was programmed to heat the material in three separate steps. The temperature was first increased from ambient temperature to 375°C at a ramp rate of 5.6°C/min. Secondly the temperature was ramped to 447°C at 0.5°C/min and finally ramped to 785°C at 2.1°C/min where the temperature was held for 5 hours. The nitride material was cooled to ambient temperature under an NH₃ atmosphere and flushed through with 100ml/min nitrogen (BOC, 99.999% purity) to remove any residual NH₃.

Due to the pyrophoric nature of the nitride material, the final stage in the preparation of the molybdenum nitride involved the passivation of the nitride using a mixture of 2% O₂ in Ar (BOC, 99.999% purity) flowed at 5ml/min further diluted with a 95ml/min flow of N₂. This creates an oxide skin which protects the nitride preventing pyrolysis upon exposure to air. This oxide skin is removed by reduction prior to the reaction.

δ -MoN was synthesised directly from molybdenum sulfide. This is illustrated as follows:



Molybdenum sulfide (Aldrich, 99% purity) (1 g) was charged in to the quartz tube reactor and NH_3 (BOC) flowed at a rate of 94ml/min. The temperature ramps employed differ from those for the nitridation of molybdenum trioxide. The temperature was ramped from ambient to 785°C at a rate of 15 °C/min and held for 60 hours. The resulting material was cooled back to ambient temperature in flowing NH_3 . It should be noted that this is a crucial step as cooling δ -MoN under N_2 may result in the formation of the γ - Mo_2N [123].

β - $\text{Mo}_2\text{N}_{0.78}$ was synthesised by the TPR of molybdenum trioxide with mixtures of H_2 and N_2 . Typically 0.4g molybdenum trioxide (Aldrich 99.5% purity) was loaded into a quartz tube reactor and 3:1 mixtures of H_2 (BOC, 99.999% purity) and N_2 (BOC, 99.999% purity) were flowed at a total rate of 60ml/min. The furnace was programmed to heat the material in two separate steps. The temperature was first increased from ambient temperature to 700°C at a ramp rate of 10 °C /min and dwelled for 2 hours. Secondly the temperature was cooled to 400°C at 10°C/min and held for 5.5 hours to produce the β - phase nitride. The resulting nitride was finally cooled back to an ambient temperature under the synthesis mixture.

Prior to methanol decomposition runs, 0.15g of γ - Mo_2N was loaded and reduced at 450°C for 1.5 hours in a 20% H_2 / 80% Ar mix at a total flow of 47ml/min. δ -MoN and β - $\text{Mo}_2\text{N}_{0.78}$ were not pre-reduced as these materials were not passivated with O_2 after the nitriding process.

2.1.6 Synthesis of copper mordenite methanol carbonylation catalyst

A 100g batch of a mordenite catalyst was loaded with 5wt% copper as follows. Copper (II) nitrate hemipentahydrate (Aldrich,>98% purity) was dissolved in 100ml water and added to 100g H-mordenite(Süd Chemie) with a $\text{SiO}_2 / \text{Al}_2\text{O}_3$ ratio of 20 and mixed for 16 hours at room temperature using a rotary evaporator. Prior to calcination, the slurry was dried at 110 °C for 7 hours. Calcination was carried out in a static atmosphere of air in a muffle furnace (oven volume = 18 L). The temperature was increased from room temperature to

110 °C at a ramp rate of 5°C/min and then held at this temperature for 0.5 hours. The temperature was then increased to 550 °C at a ramp rate of 10°C/min and held at this temperature for 4 hours. The zeolite was then compacted at 12 tonnes in a 33 mm die set using a Specac Press, and then crushed and sieved to a particle size fraction of 500 to 1000 microns. Prior to methanol carbonylation reactions, the copper mordenite catalyst was heated up to reaction temperature under 140ml/min CO (BOC, 99.995% purity).

2.1.7 Synthesis of doped copper mordenite catalysts

Palladium and molybdenum trioxide were doped onto the copper mordenite catalyst in order to obtain a loading of 5wt%. To dope palladium onto the catalyst, the required amount of palladium nitrate was dissolved in 2 ml water and this solution was used to impregnate a 2g portion of the copper mordenite catalyst which was prepared as above. The slurry was dried in an oven at 110 °C for 24 hours. The resulting dried solid was then ground into a fine powder and sieved to obtain a particle size which was less than 250 microns and calcined at 400 °C in air for 16 hours. Prior to each reaction run, a 0.65g portion of the calcined catalyst was charged onto a quartz tube reactor and reduced at 450°C for 1.5 hours in a 20% H₂/Ar mix at a total flow of 47ml/min.

Molybdenum trioxide was doped onto 2g of the copper mordenite using ammonium heptamolybdate (Alfa Aesar) which was dissolved in 2ml water. The resulting slurry was dried at 100 °C for 24 hours, ground into a fine powder and sieved to obtain a particle size which was less than 250 microns and calcined at 500 °C in air for 16 hours.

2.1.8 Preparation of Raney nickel catalysts

Raney nickel catalysts were prepared from a metal alloy precursor containing 50% nickel and 50% aluminium (Fluka, 100% purity). Typically a 0.88g portion of alloy was weighed out and left in 100ml, 4M sodium hydroxide (Fisher, 97% purity) for 18 hours to leach out the aluminium. The resulting powder was then washed with deionised water several times prior to the reaction. Due to the pyrophoric nature of the material, the active Raney nickel was loaded into the reactor tube using a filter funnel and water washings. The tube was immediately connected to the argon line whilst damp and kept under this inert atmosphere until the reaction was performed.

2.1.9 Preparation of nickel – boron catalyst

A nickel – boron alloy material [99] was prepared by the reduction of a nickel salt with an aqueous solution of sodium borohydride as described elsewhere [98]. 1 g of sodium borohydride (Aldrich, 98% purity) was dissolved in 50ml deionised water. A 5 ml, 0.1 molar solution of nickel (II) acetate tetrahydrate (Aldrich 99.99% purity) was added to the solution of sodium borohydride at room temperature. The resulting black precipitate was obtained by filtering off the water. The powder was dried in an oven at 100° C for 2 hours and ground to a powder. Typically 0.15g of this material was charged for the reaction.

2.2 Catalyst testing

2.2.1 Methanol decomposition

Reaction runs were carried out in a specially commissioned atmospheric pressure methanol decomposition reactor. The reactor was a fixed bed plug flow reactor with on-line GC analysis. The reactor was also configured for on-line catalyst reduction prior to reactions and the synthesis of metal carbide materials. The reactor tube was constructed from quartz and had an outer diameter of 12 mm and contained a frit to support the catalyst powder. All gas and liquid feed lines were built from stainless steel. The glass reactor tube was attached and sealed to the stainless steel gas lines via Ultra torr O-ring fittings. Each gas line contained a pressure regulator and a non-return valve. H₂ and Ar flows were regulated using rotameters and a needle valve was used to regulate the CH₄ flow. Gas flow rates were accurately measured using a digital flow meter. Liquid methanol (Anal R grade supplied by BDH, 99.8 % purity) was pumped using a Knauer K- 501 HPLC pump and vaporised using trace heated lines. The methanol gas was mixed with an argon diluent to provide a smooth flow of reactant over the catalyst bed. Typically 0.03ml/min liquid feed rates of methanol was used. The stainless steel lines were also trace heated from the reactor exit to the GC exhaust in order to keep any condensable exit stream compounds in the gas phase for GC analysis. The reactor tube was heated with a ceramic furnace and the temperature controlled with a West 4400 temperature control unit and a K-type thermocouple placed in a quartz thermocouple pocket situated above the catalyst bed. On – line analysis of gas phase products was conducted using a Chrompack CP 9001 gas chromatograph equipped with a TCD detector and argon used as the carrier gas. CO, H₂, CO₂ and CH₄ were separated on a mol sieve packed column. Methanol, DME and methyl

formate were separated using a Porapak Q column. Contamination of the molecular sieve column by the larger compounds was avoided by utilising a column switching technique. A diagram of the methanol decomposition reactor is presented in Figure 2-1. The knock out pot was utilised for off- line analysis for the formation of acetic acid and methyl acetate during mixed bed methanol decomposition and carbonylation reactions. There was a bursting disk safety device which ensured that in the event of reactor blockage and pressure regulator failure, the quartz tube would not be exposed to the pressures of the external gas cylinder supply under a potentially hazardous atmosphere. The quartz tube reactor was protected from over heating utilising a trip thermocouple attached to the temperature controller.

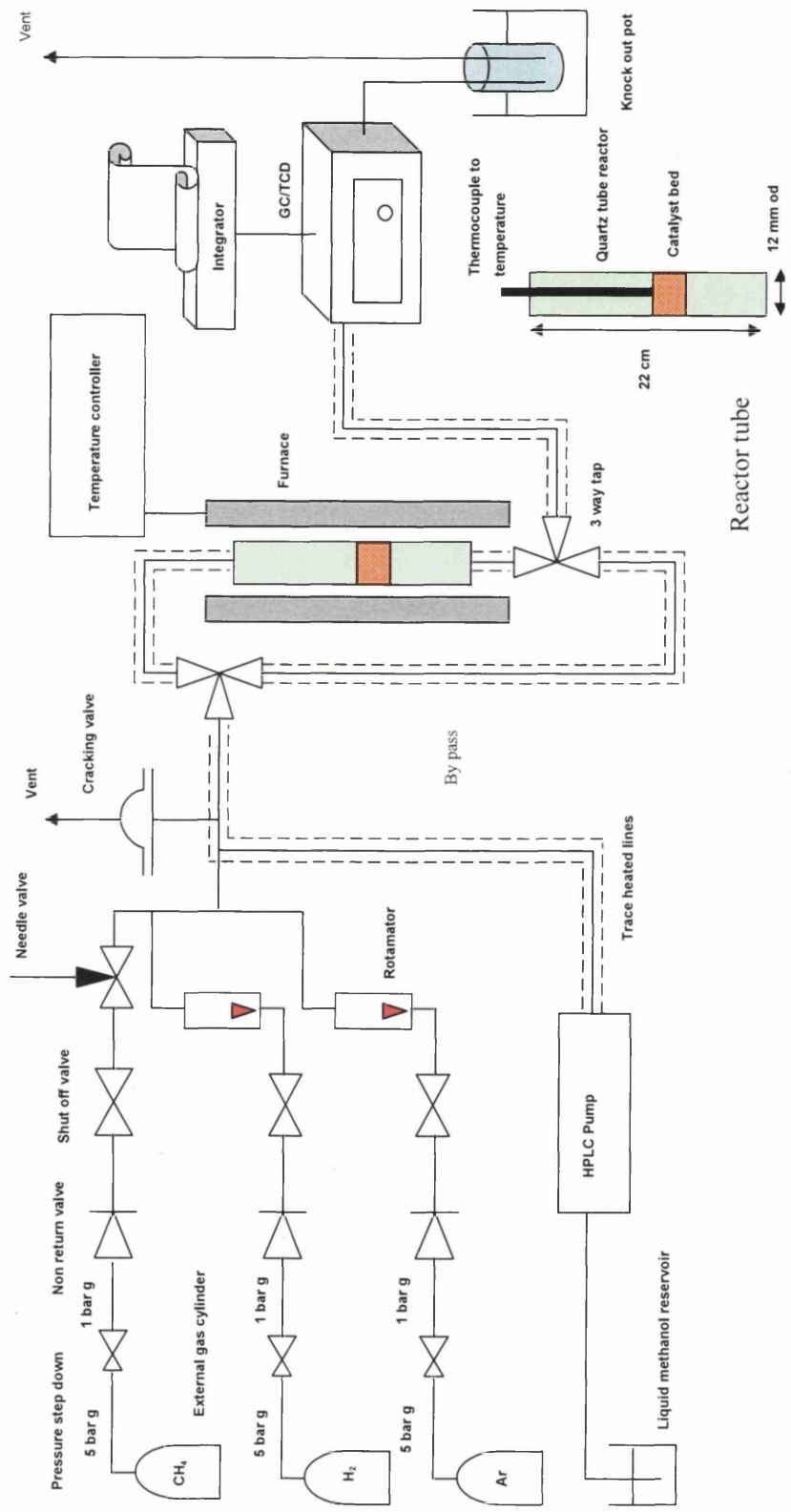


Figure 2-1: Methanol decomposition reactor

2.2.2 Methanol decomposition reactions

The catalysts were loaded and reduced in the reactor at the conditions described in the catalyst preparation section. Typically 0.15 g of catalyst was loaded. After reduction, the catalysts were exposed to a flow of argon prior to the reaction to prevent any chance of re-oxidation. The catalyst bed was ramped to the reaction temperature at a rate of 10 °C/min under the inert atmosphere and the heating tapes were ramped to 140 °C. Methanol was purged through from the liquid supply reservoir and pumped continuously at 0.03ml/min throughout the reaction. The argon gas carrier flow was set using the rotameter to approximately 25ml/min. The exact flow used was measured using a digital flow meter after the reaction. Typically a GC reading was taken after 10 minutes on stream and then at 30 minute intervals thereafter. The data collected from the integrator was processed from peak areas using calibrations.

2.2.3 Mixed methanol decomposition/methanol carbonylation experiments

Experiments were carried out to study methanol carbonylation using *in-situ* CO generated by methanol decomposition in a dual catalyst system containing both a methanol decomposition catalyst and copper mordenite methanol carbonylation catalyst. Unless otherwise stated, 0.65g copper mordenite and 0.15g of a methanol decomposition catalyst were charged to a quartz reactor tube after having been freshly reduced to the conditions described earlier. The catalysts were arranged in either a stacked bed or a mixed bed arrangement where the two powders were physically mixed. The catalyst bed was heated to 300 °C under a mixture of argon flowed at 30ml/min and H₂ flowed at 20ml/min. Once at temperature, the gas mixture was changed to one comprising 39 mole % methanol and 61 mole % argon at a total gas flow rate of 52 ml/min. Condensable products from the reactor were collected by passing the gas from the reactor through a knock-out pot cooled using an ice bath containing potassium chloride. Acetic acid and methyl acetate STYs were calculated from off-line GC analysis (Thermo Quest model KA00 gas chromatograph and HP-Plot Q capillary column) of the liquid collected in knock out pot at the end of 5 hour reaction runs. On-line GC analysis was carried out as described earlier to monitor the production of CO, H₂, CH₄, methanol, CO₂ and DME.

2.2.4 GC calibration and analysis

The GC responses to H₂, CO, CO₂ and CH₄ were calibrated using a calibration cylinder supplied by BOC (99.9% purity). The cylinder contained 10 mole % of each gas component in an argon diluent and the peak areas for each product were averaged to provide a one point calibration. This was deemed an acceptable method on the basis that a linear relationship was observed with a H₂ calibration at high concentrations demonstrating that the TCD response was in the linear range. DME was calibrated from a lecture bottle (Aldrich, 99.995% purity) which was purged through the sampling loop which was trace heated to avoid condensation. The products formed are quoted as space-time yields (g product produced/kg of catalyst loaded/hour). This is calculated using the total flow and percentage of product gas present from GC analysis assuming a molar volume of 22.4 litres at STP. The methanol conversion and space-time yield calculations are further explained in Appendices 1.1.1 and 1.1.2 respectively.

2.2.5 Methanol carbonylation

Methanol carbonylation runs were carried out using the fixed bed continuous flow reactor shown in Figure 2-2, which was designed to operate at atmospheric pressure. The reactor tube was made from quartz and contained a frit to which catalysts could be loaded. Typically 2.97g of the copper mordenite catalyst was charged between a pre and post-bed of 22.5ml and 18.5ml silicon carbide respectively. CO was supplied from an external cylinder (BOC, 99.9% purity) and the H₂ (BOC, 99.995% purity) from a lecture bottle. A total GHSV value of 2000h⁻¹ was used for the carbonylation reaction. The methanol (Aldrich-Chromasolv, 99.9% purity) was pumped steadily via an HPLC pump (Bio-tek Kontron 520) and fed directly into the reactor tube via a needle inserted through a rubber septum and vaporized by the heat from the reactor furnace (Carbolite) and mixed with the reactant gases in the pre- bed. CO and H₂ (BOC, 99.995% purity) flows were set using the needle valves and rotameters and measured using a bubble meter connected to the exit of the reactor prior to reaction runs. Gases were mixed in a gas mixer before entering the reactor tube. Connected to the end of the reactor tube was a knock out pot enclosed in an ice bath to condense out any products formed during the reaction. These products were analysed at the end of the reaction via an external gas chromatograph. Solid products were also produced, and these were collected in a large three necked flask attached to the exit stream to prevent blockage occurring. A three way tap connected to the exhaust line was

used to switch between venting and gas sampling. This allowed gas samples to be taken throughout the reaction and was performed using gas sampling bags. Prior to reaction the furnace was ramped to temperature under H_2 .

The gas sampling occurred periodically throughout the reaction and the products were analysed using a FID detector. CO and H_2 were not quantified for this reason and the conversion is calculated on the basis of methanol consumption. The products analysed by this method were CH_4 , C_2H_4 , C_3H_6 , DME, methyl acetate, methyl formate, acetaldehyde and acetone. The analysis of the gas samples was performed on a Chrompack CP9000, and the products were separated using a CP- Sil05CB column.

The products from the knock-out pot were analysed using a Chrompack 9000 gas chromatograph with an FID detector. The products quantified from this analysis were DME, acetaldehyde, methyl formate, acetone, methyl acetate, ethyl acetate, methanol, ethanol, acetic acid and propionic acid. These products were separated using a CP-Wax52CB column.

All of the above products are reported as space-time yields and the formulae applied are presented in Appendices 1.2.1 and 1.2.2. The conversion values for the carbonylation reactions were calculated on the basis of the methanol as discussed in Appendix 1.2.3.

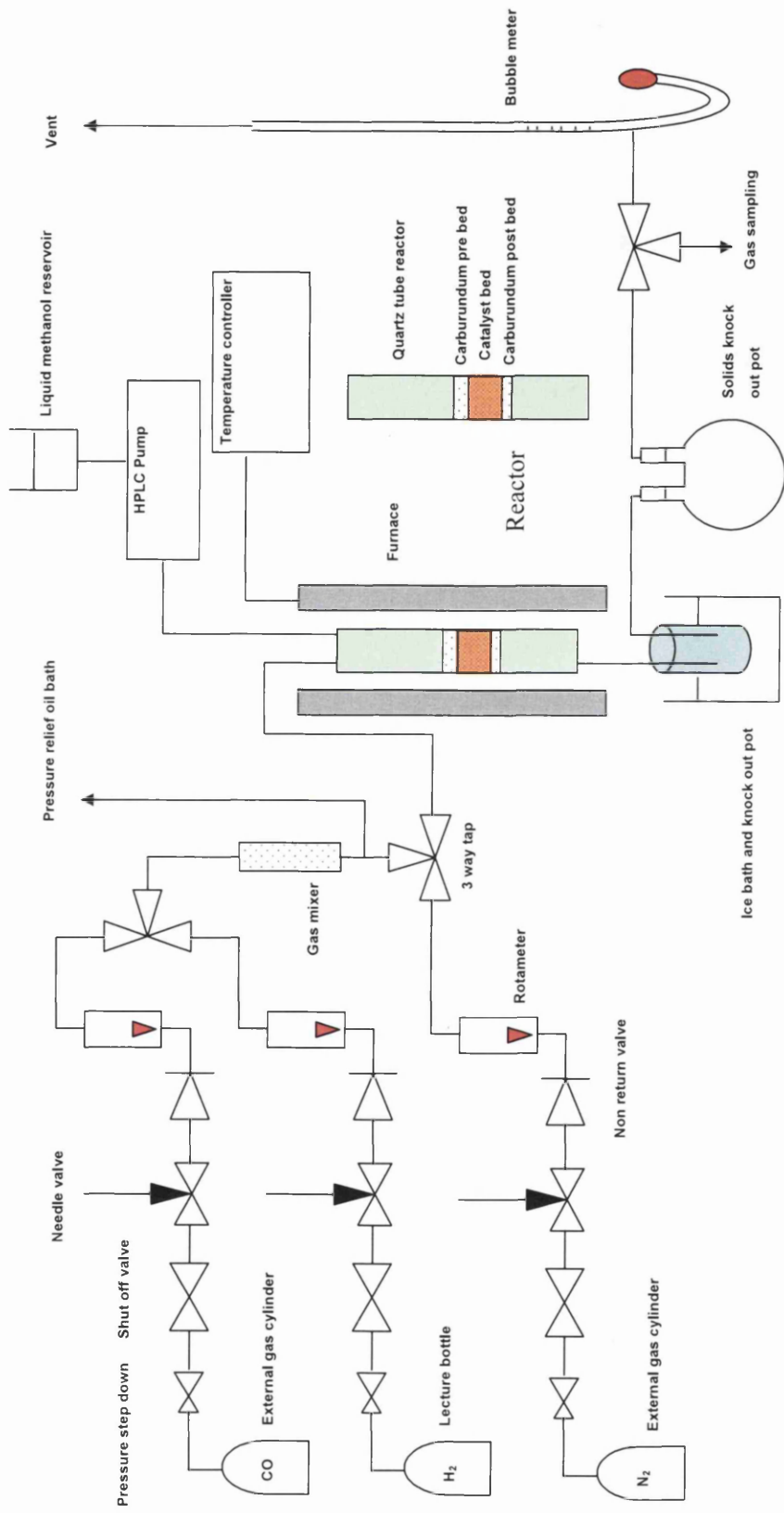


Figure 2-2: Methanol carbonylation reactor

2.3 Catalyst Characterization

2.3.1 Powder x-ray diffraction (XRD)

Powder x-ray diffraction patterns were obtained using a Siemens D5000 X-ray diffractometer (40 kV, 40mA, monochromatised) using a CuK α source (1.5418Å). The scanning range was typically 5- 85° 2 θ and the scanning rate 1 second/step with a step size of 0.02°. In order to be applicable, the BET method should only be applied to either BDDT type II or type IV isotherms within the P/P₀ limits of 0.05 - 0.3 and with a C constant below 300.

2.3.2 Surface area measurements

Where appropriate, the surface area of the catalysts was determined using the Brunauer, Emmett and Teller (BET) method using N₂ physisorption isotherms measured at liquid nitrogen temperature. The experiments were carried out using a Micromeritics Flow Prep 060 and Gemini BET machine. Prior to the measurements samples were degassed overnight using nitrogen at 110 °C to remove adsorbed moisture and gases. In the case of samples with low surface areas (i.e. <5 m²g⁻¹), Kr can be used as adsorbate at 77K, which offers a higher degree of precision in the actual measurement of the adsorption.

2.3.3 Elemental analysis

The amount of carbon, nitrogen and hydrogen was determined for fresh and spent materials by combustion analysis using an Exeter Analytical CE- 440 analyser. This technique was kindly performed by Mrs Kim Wilson at the University of Glasgow.

2.3.4 Thermal gravimetric analysis

Thermal gravimetric analysis was carried out using a Thermo Quest SDT Q 600 combined TGA/DSC analyser. The temperature was ramped from 30 to 1000 °C at 10° C/min under either a reducing or an inert atmosphere. Typically 10 mg of sample was loaded and the gas flow was 100ml/min. 2% H₂ (BOC, 99.999% purity) in balance Ar (BOC, 99.999% purity) was used for the reductive TGA experiments and argon for the inert (BOC,

99.999% purity).

2.3.5 ^{27}Al and ^{29}Si MAS NMR

^{27}Al and ^{29}Si MAS NMR experiments were carried out using a Bruker Avance 400 NMR spectrometer equipped with a widebore 9.4 T magnet. The ^{27}Al Larmor frequency was 104.3 MHz and the ^{29}Si operation resonance was 79.4 MHz. TMS (tetramethylsilane) and 1M $\text{Al}(\text{NO}_3)_3$ were used as the external standard references for the aluminium and the silicon chemical shifts respectively. These experiments were kindly performed by Prof Stephen Wimperis and Teresa Kurkiewicz at the University of Glasgow.

3 Methanol Decomposition

3.1 Methanol only route to acetic acid

In principle, the vapour phase heterogeneously catalyzed one-pot synthesis of acetic acid from methanol is possible via the decomposition of methanol to form CO. In such a system, the methanol would be partially decomposed over a heterogeneous catalyst to yield a mix of CO and methanol which would form acetic acid upon subsequent carbonylation. Such a system would preferably use a heterogeneous carbonylation catalyst without a halide promoter. This envisaged route to acetic acid is illustrated in Figure 3-1:

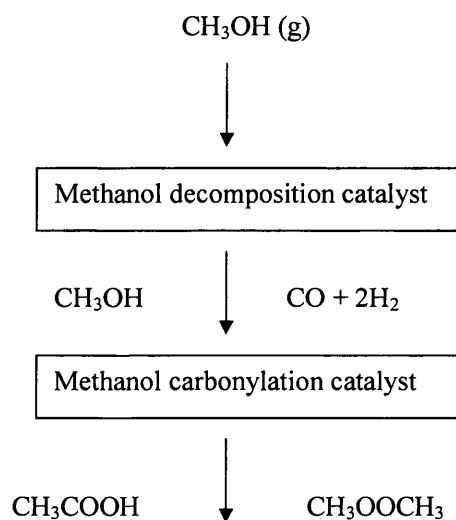


Figure 3-1: Heterogeneous route to acetic acid with a methanol only feed

The catalytic system would need to fulfil several requirements:

- Selective decomposition of the methanol to CO as the formation of any carbon-based by-products will result in an overall reduction in the product yield.
- Decomposition of only a portion of the methanol feed. Complete methanol

conversion to synthesis gas would result in a loss of the reactant methanol required in the carbonylation step.

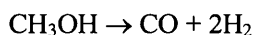
- High stability and lifetime.
- The methanol decomposition catalyst should have comparable activity to the methanol carbonylation catalyst.

The methanol carbonylation catalyst should:

- Selectively catalyse the formation of acetic acid and/or methyl acetate.
- Exhibit high lifetime and stability.
- Be hydrogen tolerant. The selective decomposition of methanol to synthesis gas yields two moles of H₂ for every mole of CO.

3.2 Methanol decomposition

The endothermic catalytic decomposition of methanol to CO and H₂ is a reaction of interest for the generation for fuel, thermal upgrading and the generation of chemical feedstocks [42]:



The decomposition of methanol to CO and H₂ does not always proceed with 100% selectivity to CO. The selectivity depends on the type of catalyst used and reaction conditions such as temperature and methanol contact time. In the current application, this is of importance as a drop in CO selectivity lowers the overall product yield and any lowering of CO partial pressure may affect the methanol carbonylation in the subsequent step.

In a strongly acidic environment, hydrocarbons and olefins are produced by the methanol to gasoline [43] and methanol to olefin [44] processes which can be catalysed using H-ZSM-5 and SAPO-34 catalysts respectively. With moderate acidity DME is formed by

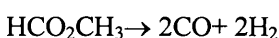
methanol dehydration, for example as seen with $\gamma\text{-Al}_2\text{O}_3$ [45]:



Methanol can also be partially dehydrogenated to form methyl formate:



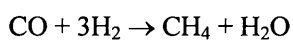
By increasing the reaction temperature and increasing the contact time methyl formate can be decomposed to yield synthesis gas. This is a commonly observed trend with copper based methanol decomposition catalysts [46]:



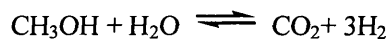
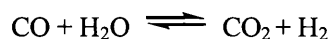
Lin and co-workers [46] investigated methyl formate decomposition to CO and H₂ studied at 167 °C and atmospheric pressure over a Cu/ZnO/Al₂O₃ catalyst. At low methyl formate concentrations (up to 1vol%) in helium, it was reported that methyl formate conversion increased with increasing contact time and the reaction followed first order kinetics. The conclusion of these experiments was that methyl formate decomposition to CO and H₂ can be suppressed by increasing the methyl formate partial pressure [46]. The synthesis of methyl formate from methanol was studied by Ruiz *et al.* [47]. In that study, the yield of methyl formate was increased using high space velocities and low temperatures. It was found that a Cu/ZnO catalyst behaved poorly compared with copper supported on SiO₂ and ZrO₂. A maximum methyl acetate yield of 29% was attained at 240°C. It was concluded that the catalyst activity was not influenced by the copper dispersion but by the acid/base properties of the support. Non-acidic SiO₂ and amphoteric ZrO₂ led to highly selective catalysts while the basic MgO and ZnO supports yielded poor selectivities due to the decomposition of methyl formate into CO and H₂ at basic sites.

Some of the other reaction pathways in methanol decomposition are shown below:

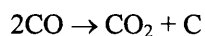
The hydrogenation of CO results in CH₄ formation which is commonly observed with nickel based catalysts [48]:



CO can be converted to CO₂ via the water-gas shift reaction and the steam reforming of methanol can also produce CO₂ via the following reactions respectively:



The low temperature water gas shift and methanol reforming reactions are most commonly observed over commercial Cu/ZnO/Al₂O₃ catalysts, which are used to produce hydrogen industrially [49]. CO₂ can also be formed by the Boudouard reaction:



The thermodynamic data for some of these reactions are shown in Table 3-1. It can be seen that direct methanol decomposition to synthesis gas is the only endothermic reaction and so high temperatures generally favour this reaction and limit the formation of side products.

Reaction	ΔG°_{298} (kJ/mol)	ΔH°_{298} (kJ/mol)
CH ₃ OH → CO + 2H ₂	+25	+91
CH ₃ OH + CO → CH ₃ COOH	-174	-97
2 CH ₃ OH → (CH ₃) ₂ O + H ₂ O	- 17	- 24
CH ₃ OH + H ₂ CO → HCOOCH ₃ + H ₂	- 30	- 71
CO + 3H ₂ → CH ₄ + H ₂ O	-143	-206
CO + H ₂ O → CO ₂ + H ₂	- 29	- 41
2CO → CO ₂ + C	- 120	- 172

Table 3-1: Thermodynamic data at 298K

A number of metals which are active for methanol decomposition have been investigated and palladium catalysts and copper based catalysts have been the most commonly reported. Less commonly studied metals are platinum [50-52], nickel [53-55], ruthenium [56], and manganese [53]. Generally speaking all of the latter metals catalyse unwanted side reactions in methanol decomposition particularly at lower temperatures compared with copper and palladium catalysts. For example on rhodium, formaldehyde formation results in selectivity loss to CO [57] whereas, as stated above, CH₄ is a commonly observed by product on nickel [48,58] and platinum catalysts [59].

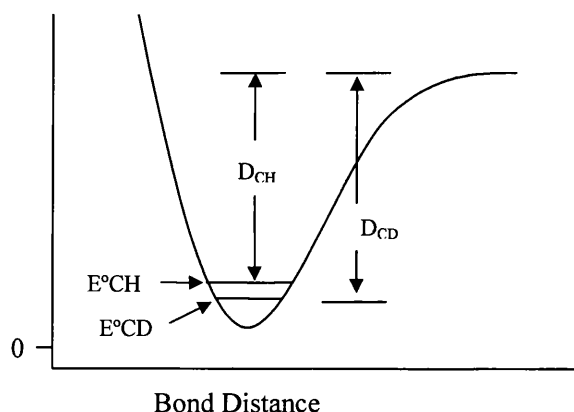
3.2.1 Mechanism of methanol decomposition

The exact mechanism of methanol decomposition and the nature of the active sites in the methanol decomposition catalysts are subject to much debate. However, it is accepted that methanol decomposition generally occurs via the following steps where (a) means that the species is adsorbed onto the surface:

- 1) $\text{CH}_3\text{OH (g)} \rightarrow \text{CH}_3\text{O (a)} + \text{H (a)}$
- 2) $\text{CH}_3\text{O (a)} + \text{H (a)} \rightarrow \text{CH}_2\text{O (a)} + \text{H}_2\text{(g)}$
- 3) $\text{CH}_2\text{O (a)} \rightarrow \text{CHO (a)} + \text{H (a)}$
- 4) $\text{CHO (a)} \rightarrow \text{CO (a)} + \text{H (a)}$
- 5) $\text{CO (a)} \rightarrow \text{CO (g)}$
- 6) $2\text{H (a)} \rightarrow \text{H}_2\text{(g)}$

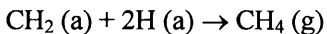
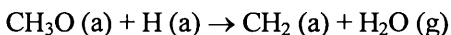
The rate determining step is believed to be the fission of the C-H bond in step 2) [60]. It is commonly accepted that this is the case in most methanol decomposition catalysts. The following description of the kinetic isotope effect is adapted from reference [146]. The primary kinetic isotope effect arises from the difference in vibrational energy levels of both hydrogen and deuterium illustrated in the following diagram.

Potential Energy

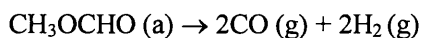


It can be observed from the potential energy diagram above copied from reference [146], that the zero-point energy of a bond to deuterium ($E^{\circ}CD$) is lower than that of hydrogen ($E^{\circ}CH$), and as a result the bond dissociation energy D_{CD} is higher. The zero-point energy is related to the vibrational frequency given by $E = 1/2h\nu$ where h is Planck's constant and ν the vibrational frequency. The vibrational frequency of a bond depends on the force constant k and the reduced mass u of the atoms involved in the bond by Hooke's Law: $\nu \propto \sqrt{k/u}$. The force constant is the same for deuterium and hydrogen but the reduced mass is larger between a carbon deuterium bond than a carbon hydrogen bond and as a result the stretching frequency is lower between carbon deuterium compared with the carbon hydrogen bond. The lower stretching frequency results in the lower zero point energy and higher bond dissociation energy between the carbon deuterium compared to the carbon hydrogen bond. It follows from an Arrhenius relationship that the relative kinetic rate of bond dissociation between carbon and deuterium is lower than carbon hydrogen. With reference to the mechanism of methanol decomposition, McKee *et al.* [60] showed that CH_3OH and CH_3OD have the same activation energies for methanol decomposition on platinum black, however activation energies for CH_3OH and CD_3OH were reported to be 14.3 and 17.5 kcal/mole respectively. The larger bond dissociation required to break the carbon deuterium bond compared with the carbon, hydrogen bond results in the higher activation energy of CD_3OH compared with CH_3OH . McKee, however reported that no similar kinetic isotope effect is observed using a ruthenium catalyst, which acts as a methanation catalyst, indicating that a different mechanism operates. It was postulated that

the following mechanism may exist for methanation:



The main methanol decomposition products over copper containing catalysts in the temperature range 150 – 250 °C are CO, CO₂, methyl formate and H₂. Lin *et al.* [61] reported on the findings of methanol decomposition over a Cu/ ZnO/ Al₂O₃ catalyst. The conclusion was that methanol decomposition to CO and H₂ occurs via the decomposition of methyl formate species on the surface of the catalyst:



Bell *et al.* [62] investigated the mechanism of methanol decomposition over Cu/SiO₂, ZrO₂/SiO₂ and Cu/ZrO₂/SiO₂ catalysts using FTIR spectroscopy, temperature programmed reaction (TPRS) and temperature programmed desorption (TPD) techniques. In that study, a Cu/SiO₂ catalyst yielded mainly CO, CO₂, H₂ and methyl formate. The formation of CO and H₂ were reported to form from the decomposition of methyl formate and the formation of CO₂ from the decomposition of adsorbed formate species via the following equation:



Adsorbed formate species were also reported to provide a route for CO formation via the following:



The FTIR spectra of the Cu/ZrO₂/SiO₂ catalyst showed that the formation of the formate intermediates occurred on the surface of ZrO₂. However, the decomposition of methanol was found to occur slowly on ZrO₂/SiO₂ and adding copper produced a catalyst with a higher activity. As a result of these findings Bell proposed that the decomposition

occurred on zirconium sites and the copper provided a route for the removal of H₂ by the reverse spillover of atomic hydrogen from zirconium species.

Much of the literature with respect to methanol decomposition has focussed on the mechanistic aspect and the identification of active sites and reaction intermediates. Although there has been a focus on improving catalyst activity and lifetime, particularly with the copper based systems, there has been no direct comparison between the activities of different types of methanol decomposition catalysts. In the present project, such data would be useful, as the CO generated by the methanol decomposition will be used in the subsequent methanol carbonylation step. In spite of the large number of studies conducted into methanol decomposition it is often difficult to compare catalyst performance on per pass yields due to the different conditions employed. The range of temperature, methanol concentration and space velocities reported are vast and somewhat arbitrary. Space time yields (STYs) represent a suitable means for comparison because they intrinsically take into account variations of conversion, space velocity and methanol concentration. The mass normalized space time yield data for recently reported literature for CO and H₂ production for various catalysts is presented in Table 3-2. Catalysts are only included if it has been possible to calculate STYs, and the names of the catalysts from the data presented are those used in the studies. The data correspond to the catalyst of highest activity within each study. Reaction temperatures and percentage methanol conversion have been included. The table also displays a ratio of STY rates for CO and H₂. This gives a crude estimation of catalyst selectivity to CO. For every 2 moles of H₂ produced there is 1 mole of CO in selective decomposition. A ratio of 7.0 therefore indicates that a CO:H₂ ratio of 2:1 occurs. An STY ratio less than 7.0 implies CO is lost to other carbon containing compounds. It should be noted that there is a limitation when applying this ratio because the methanol can be converted to by-products, which do not affect the STY CO:H₂ ratio, for example methanol dehydration to form DME.

The justification of presenting this data in STY form is the application of methanol decomposition to the current proposed application of the generation of CO feedstocks for *in situ* methanol carbonylation reactions. For the maximum efficiency, the rate of the decomposition reaction should be matched with the rate of methanol carbonylation and the catalyst must not exhibit complete methanol conversion. On inspection of Table 3-2 it is evident that most of the catalysts are based on copper and palladium. These catalysts produce synthesis gas at rates spanning a range of more than two orders of magnitude. It is

clear that catalysts which are of similar composition, can yield markedly different rates for synthesis gas production. The table provides a useful approach for making general comparisons between the different types of catalyst formulations and reaction conditions employed in methanol decomposition although the reliability of the data reported provides a specific limitation. General trends in selectivity between the different types of catalyst are also observed. For example the palladium based entries in the Table systems tend to exhibit high selectivity to CO with STY ratios of 7.0 at varying conversions and temperatures. The other catalyst groups, for example those containing copper, exhibit STY ratios below 7.0 due to the formation of by-products. There are however limitations when directly comparing the activities for various catalysts. It can be observed that many of the catalysts in the table and many of the studies reported exhibit complete methanol conversion and so are therefore reagent limited. There are also few studies which focus on more than one general type of methanol decomposition catalyst. For example, most of the studies are based on copper or palladium but no studies compare these metals directly. In the present Chapter the synthesis and testing of common types of methanol decomposition catalysts was performed under directly comparable conditions, to provide a library of catalysts and their activities. It should be noted that the temperatures and methanol concentrations employed are comparable with those for methanol carbonylation, with a temperature range of 250- 300°C and a 40% methanol concentration.

Catalyst	Reaction temperature (°C)	MeOH Conversion (%)	STY CO (g/kgcat/h)	STY H ₂ (g/kgcat/h)	STY Ratio	Ref
Ni ₃ Al	352		11625	1875	6.2	48
Cu/Cr/Mn/K	275	63.2	7142	1145	6.2	64
Cu/Cr/Mn/Na	275	62.7	6244	1068	5.9	64
Cu/Cr/Mn	275	59.8	5507	971	5.7	64
Cu/Cr/Mn/Si oxide	300	83.0	5157	768	6.7	65
PdZn/MgAl (3/1)I spc ¹	300	100	4965	712	6.9	66
Pd/MgAl (3/1) imp ²	300	99.8	4950	710	7.0	66
Pd/MgAl (3/1) spc ¹	300	100	4940	710	7.0	66
Pd/MgO imp ²	300	99.8	4930	708	7.0	66
Pd/MgAl (2/1) spc ¹	300	100	4890	703	7.0	66
Mg/Pd/Sc	300	99.0	4806	702	6.8	67
Pd/Ce _{0.8} Zr _{0.2} O ₂ cop ³	250	99.9	4943	700	7.1	68
Pd/MgCr (3/1) spc ¹	300	97.7	4831	698	6.9	66
Mg/Pd/Cr	300	97.7	4831	698	6.9	67
Pd/MgAl (3/1) spc ⁴	300	96.6	4791	687	7.0	66
Pd/CeO ₂ MS ^{5, 15}	220	80.0	4800	686	7.0	69
Pd(Mg(Al)O)/ HMS ⁶	300	96.5	4796	685	7.0	70
Mg/Pd/Al	300	95.9	4737	684	6.9	67
Pd/CeO ₂ cop ³	250	97.1	4741	674	7.0	68
Rh/CeO ₂ ¹⁶	300	100	4439	666	6.7	57
Mg/Pd/Fe spc ¹	300	97.7	4230	664	6.4	67
Pd/ZrO ₂ cop ³	250	91.4	4559	647	7.0	68
Pd(Mg(Al)O)/ HMS ⁷	250	91.7	4516	642	7.0	70
Pd/Al ₂ O ₃ imp ²	300	100	4605	636	7.2	66
Pd/(Mg(Al)O)	300	88.6	4408	629	7.0	70
Pd(Mg(Al)O) + HMS	300	87.2	4342	620	7.0	70
Rh/ZrO ₂	400	100	4177	620	6.7	57
Pd/ZrO ₂ imp ²	300	87.7	4275	619	6.9	66
Rh/CaO ¹⁶	380	100	4128	604	6.8	57
PdCu/MgAl(3/1) spc ¹	300	84.6	4217	603	7.0	66
Rh/Al ₂ O ₃ ¹⁶	400	100	3675	589	6.2	57
Pd/Ce _{0.8} Zr _{0.2} O ₂ imp ²	250	83.6	4153	585	7.1	68
Rh/MgO ¹⁶	380	100	3544	564	6.3	57
Rh/ZnO ¹⁶	380	100	2197	558	3.9	57
Mg/Pd/Ga spc ¹	300	78.1	3835	557	6.9	51
Pd/CeO ₂ ¹⁵	220	55.0	3300	471	7.0	69
Pd/La ₂ O ₃ /SiO ₂ Co- imp ^{8, 15}	227	80.5	3136	448	7.0	71
Pd/La ₂ O ₃ /SiO ₂ Cop ^{3, 15}	227	76.8	2940	420	7.0	71
Pd/La ₂ O ₃ /SiO ₂ Seq pre ^{9, 15}	227	73.1	2800	400	7.0	71

Catalyst	Reaction temperature (°C)	MeOH Conversion (%)	STY CO (g/kgcat/h)	STY H ₂ (g/kgcat/h)	STY Ratio	Ref
Pd/SiO ₂ imp ²	300	53.9	2684	382	7.0	66
Pd/CeO ₂ DP ^{10, 15}	220	43.0	2580	369	7.0	72
Pd(Mg(Al)O)	250	47.1	2336	335	7.0	70
Pd/Ce ₇₀ Zr ₃₀ USV ^{11, 15}	180	37.9	2274	324	7.0	73
Pd/HMS	300	45.4	2259	322	7.0	70
Pd/Ce ₇₀ Zr ₃₀ ¹⁵	180	36.1	2166	309	7.0	73
Pd/CeO ₂ MS-U ¹²	180	36.0	2160	309	7.0	69
Pd/CeO ₂ MS ⁵	180	33.0	1980	283	7.0	69
Pd/TiO ₂ MS ^{5, 15}	220	29.0	1740	248	7.0	74
Pd/22%CeO ₂ /10%La ₂ O ₃ /Al ₂ O ₃ ¹⁶	250	91.4	1434	205	7.0	75
Cu/ZnO/Al ₂ O ₃	260	100	1330	198	6.7	76
Pd/ZnO imp ²	300	27.9	1247	189	6.6	66
Cu/Zn/Ni	250	77.3	1277	186	6.9	77
Pd/HMS	250	25.6	1272	182	7.0	70
Pd/CeO ₂ ¹⁵	180	21.0	1260	180	7.0	69
Cu/Zn/Cr	250	72.8	1143	173	6.6	77
Pd/TiO ₂ ¹⁵	220	18.0	1080	154	7.0	74
Cu/Zn/Mg	250	67.4	939	151	6.2	77
Pd/CeO ₂ -Imp ^{2, 15}	220	15.0	900	129	7.0	72
Cu/Cr/Mn/Si ¹⁷	250	67.5	802	121	6.6	78
Cu/Zn/Fe	250	52.0	692	114	6.1	77
Cu/Zn/Al	250	49.8	680	110	6.2	77
Cu/Zn/Ga	250	48.5	606	106	5.7	77
Cu/Zn/Co	250	47.5	610	103	5.9	77
Cu/Zn/Mn	250	43.9	537	94	5.7	77
Cu/Zn/Ti	250	42.0	552	91	6.1	77
Mg/Pd/Sc spc ⁴	200	10.4	520	75	7.0	67
Mg/Pd/Cr spc ⁴	200	10.3	515	74	7.0	67
Cu/Zn	250	33.1	422	71	5.9	77
Cu/Zn/Mo	250	34.8	388	70	5.5	77
Mg/Pd/Al spc ⁴	200	8.5	425	61	7.0	67
Cu/Zn	299	89.8	397	58	6.8	14
Mg/Pd/Ga spc ⁴	200	8.4	180	50	3.6	67
Mg/Cr/Rh spc ⁴	200	6.8	334	49	6.8	67
Mg/Sc/Rh spc ⁴	200	6.6	322	47	6.9	67
Mg/Fe/Rh spc ⁴	200	6.3	301	45	6.7	67
Mg/Al/Rh spc ⁴	200	5.9	290	42	6.9	67
Mg/Pd/Fe spc ⁴	200	5.2	228	37	6.2	67
Mg/Ga/Rh spc ⁴	200	5.2	215	36	6.0	67

Catalyst	Reaction temperature (°C)	MeOH Conversion (%)	STY CO (g/kgcat/h)	STY H ₂ (g/kgcat/h)	STY Ratio	Ref
United G89 Cu/Cr/Mn	251	55.3	201	30	6.7	65
Pt/CaO (A) ^{13,16}	320	100	75	14	5.4	51
Pd/CeO ₂ (B) ^{14,16}	220	100	86	14	6.1	51
Pt/CeO ₂ (B) ^{14,16}	240	100	91	14	6.5	51
Pt/CeO ₂ (A) ^{13,16}	230	100	94	14	6.7	51
Pt/ZrO ₂ (A) ^{13,16}	260	100	90	14	6.4	51
Pt/SiO ₂ /Al ₂ O ₃ (A) ^{13,16}	320	100	88	13	6.8	51
Pt/Al ₂ O ₃ (A) ^{13,16}	290	100	88	13	6.8	51
Rh/CeO ₂ (A) ^{13,16}	230	100	64	13	4.9	51
Ru/CeO ₂ (A) ^{13,16}	270	100	41	13	3.2	51
Rh/CeO ₂ (B) ^{14,16}	270	100	68	13	5.2	51
Ru/CeO ₂ (B) ^{14,16}	280	100	74	13	5.7	51
Pd/CeO ₂ (A) ^{13,16}	280	100	68	12	5.7	51
Pt/MgO (A) ^{13,16}	280	100	70	6	11.7	51

Table 3-2: Space time yield data for methanol decomposition catalysts

Spc 2 – Catalyst precursor solution mixed for one minutes and aged for one hour at 363K¹, Imp – Catalysts prepared by impregnation², Cop – Catalysts prepared by coprecipitation³, Spc 1 – Catalyst precursor solution mixed for forty minutes and aged for one night at 363K⁴, Spc 1 – Catalyst precursor solution mixed for forty minutes and aged for one night at 363K⁵, MS – Mesoporous 6, Mass ratio Pd (Mg(Al)O) to HMS = 1/2⁶, Mass ratio Pd (Mg(Al)O) to HMS = 2/1⁷, Catalysts prepared by co-impregnation⁸, Catalysts prepared by sequential precipitation⁹, Catalysts prepared by deposition precipitation¹⁰, Catalysts prepared by ultrasonic vibration¹¹, Mesoporous cerium oxide. Prepared using ultrasonic vibration¹², Catalyst reduced with formaldehyde¹³, Catalyst reduced with hydrogen¹⁴, 100% selectivity to CO + H₂ is assumed on the basis of in the specific reference¹⁵, Space-time yields calculated with an assumed catalyst density of 2g/cm³¹⁶, 200kPa pressure¹⁷

3.3 Results and discussion: Copper methanol decomposition catalysts

3.3.1 General background

Copper based catalysts are widely studied in the decomposition of methanol since they are the basis for successful methanol synthesis and reforming catalysts in industry. Using the principle of microscopic reversibility, it has been suggested that methanol synthesis catalysts would be optimum in the decomposition reaction. However this assumption is not strictly correct since the principle of microscopic reversibility applies only to systems under equilibrium conditions and methanol synthesis is known to proceed through CO₂ hydrogenation on copper based catalysts [27]. Methanol synthesis catalysts do not always perform well in the decomposition reaction due to poor activity and stability [79]. The selectivity to CO is dependent on reaction temperature and space velocity over copper based catalysts. At low temperatures and high space velocities, methyl formate is produced, which can be decomposed further to CO and H₂ when the temperature and/or contact time is increased [46].

In the methanol synthesis reaction, the ZnO component is necessary to obtain a catalyst of high activity, selectivity and lifetime [27] but in the decomposition reaction it has been shown that ZnO is not a necessary component [65]. In a study by Cheng *et al.* [65], a series of copper based catalysts were compared for activity and stability at atmospheric pressure. CO was not selectively produced, with CO₂, CH₄, DME and methyl formate being reported by-products. It was reported that catalysts based on Cu/ZnO rapidly deactivated within the first two hours on stream, with the initial high methanol conversion of 70% falling to 20% at 250 °C. The deactivation was attributed to the dissolution of zinc into the active copper metal resulting in an increase in the lattice parameter of the copper metal and the formation of brass, observed by XRD of the spent catalyst. The most selective and stable catalysts reported by Cheng did not contain a ZnO component. A Cu/Cr/Mn/Si catalyst containing Cu metal and CuO phases exhibited a methanol conversion of 83% and CO selectivity of 92.5% at 300°C. Rapid deactivation did not occur with any catalysts not containing the ZnO component. However, lifetime studies demonstrated that after 150 hours on stream the methanol conversion continuously decreased from 73.4% to 64.3%. XRD analysis of the calcined Cu/Cr/Mn/Si catalyst showed phases corresponding to CuO and copper metal. The reported role of the silica and chromium was to increase the dispersion of the copper, improving the stability of the catalyst. It should be noted that a reduction of CO

selectivity was observed with increased chromium loadings due to DME formation. The performance of Cu/ZnO based catalysts can also be improved by the addition of nickel [77]. In a study by Lu *et al.* [77], the deactivation of Cu/ZnO catalysts was observed at 250° C. The initial methanol conversion was 33% and dropped to 19.2% after 20 hours on stream. XRD analysis of the spent catalyst illustrated that brass formation had occurred. By doping nickel, under the same reaction conditions the initial methanol conversion was 77.3% and 67.3% after 20 hours on stream. No brass formation was reported for the doped catalyst and the increased activity and stability was attributed to an increase of the copper surface area as determined by N₂O adsorption.

There are several causes for the copper catalysts to deactivate in methanol decomposition. At high temperatures, typically around 300°C, sintering of the copper metal results in larger copper particles and loss of activity [80]. Brass formation is prevalent with Cu/ZnO systems. Coke formation is also a cause of catalyst deactivation, but a cycle of oxidation and reduction has been reported to restore the catalyst activity. In a study by Cheng *et al.* [78], this approach was used with a Cu/Cr₂O₃ based catalyst. After 309 hours reaction, the methanol conversion was reduced from 67.5% to 36.9% and the CO selectivity reduced from 90.6% to 36.9%. However, the activity and selectivity was completely restored after regeneration. Cheng reported that there was little change in the BET surface area of the catalyst after reaction and that the deactivation was solely a result of carbon lay-down. The first stage of regeneration was oxidation of the catalyst under air at 300 °C for 2 hours, which removed all of the coke as carbon oxides. The next stage involved reduction under H₂/N₂ mixtures at 250°C, which resulted in formation of the active copper metal. XRD analysis of the regenerated catalyst showed that this treatment had not altered the dispersion and crystallite size of the active copper metal. It has also been shown that the addition of CO₂ into the feed can help prevent brass formation [81]. Cheng *et al.* [81] hypothesise that the oxidising atmosphere prevents carbon deposition, as well as reducing the sintering of the copper particles. Although doping increases the dispersion of the active copper catalyst as discussed, variations in preparation stages can influence the performance of the active catalyst. It has been reported that malachite or zincian malachite phases provide ideal precursors before calcination [82,83]. This results in an optimum copper dispersion in the final catalyst. Li *et al.* have also reported that neutral pH and aging is necessary to produce the desired malachite precursor phase [84]. Cheng *et al.* [82] reported that a higher dispersion of copper can be maintained in the reduced catalyst when a highly crystalline CuO phase can be avoided in the calcination step. It was reported that a

highly crystalline CuO phase can form when the calcination temperature is too high, which results in large copper particles upon reduction. The optimal calcination temperature was found to depend on the copper loading with higher copper loadings requiring lower calcination temperatures.

It is evident by inspection of Table 3-2 that a wide range of activities are exhibited by copper based methanol decomposition catalysts. Inspection of Table 3-2 shows that the most active copper methanol decomposition catalysts do not contain the ZnO component [64]. Despite these catalysts exhibiting high STYs, it is noticeable that the STY ratio is below 7.0. This is because methyl formate is formed as the main by-product. Cheng *et al.* reported that the alkali metal doping of the Cu/Cr/Mn oxide catalyst results in an increase of activity in methanol decomposition. Although the metal doping decreased the BET surface area of the catalyst, the promotional effects observed were a result of an increased dispersion of the copper, evident from increased reflection widths in the XRD patterns.

Xi *et al.* have studied various Cu/ZnO based catalysts at a temperature of 250 °C [77]. From inspection of the table, it can be seen that the un-promoted Cu/ZnO catalyst exhibits the lowest activity and selectivity. Selectivity was lost mostly to methyl formate, although DME and CO₂ by-products were also reported [77]. The addition of iron, aluminium, gallium, cobalt, manganese and titanium, all led to an increase of methanol conversion but with low selectivity. A commercial methanol synthesis catalyst can exhibit good CO selectivity without any additives. A STY CO/H₂ ratio of 6.7 is obtained for a Cu/ZnO/Al₂O₃ catalyst. The improved selectivity to CO is attributed to the addition of water into the feed preventing the formation of typical by-products such as CH₄ and methyl formate [76]. CO₂ was observed due to the water gas shift reaction. However, deactivation was also reported which is typical of methanol synthesis catalysts.

3.3.2 Catalyst characterization- Copper based catalysts

In order to probe candidates for methanol decomposition, a methanol synthesis catalyst was initially selected on the basis that these constitute a large portion of the reported studies on methanol decomposition. The methanol synthesis catalyst was based upon a commercial catalyst, the Katalco 51-8 catalyst, which has the formulation $\text{CuO}/\text{ZnO}/\text{Al}_2\text{O}_3/\text{MgO}$ (64/24/10/2wt%) [85]. In order to study the effect of Cu/Zn ratio on the activity of these catalysts, the ratio was varied and a targeted catalyst of composition $\text{CuO}/\text{ZnO}/\text{Al}_2\text{O}_3/\text{MgO}$ (44/44/10/2wt%), labelled Cu/ZnO was synthesised. Apart from Cu/Zn ratio the synthesis variables were kept constant for both catalysts.

Figure 3-2 shows the XRD patterns for the calcined Katalco catalyst and the Cu/ZnO catalyst.

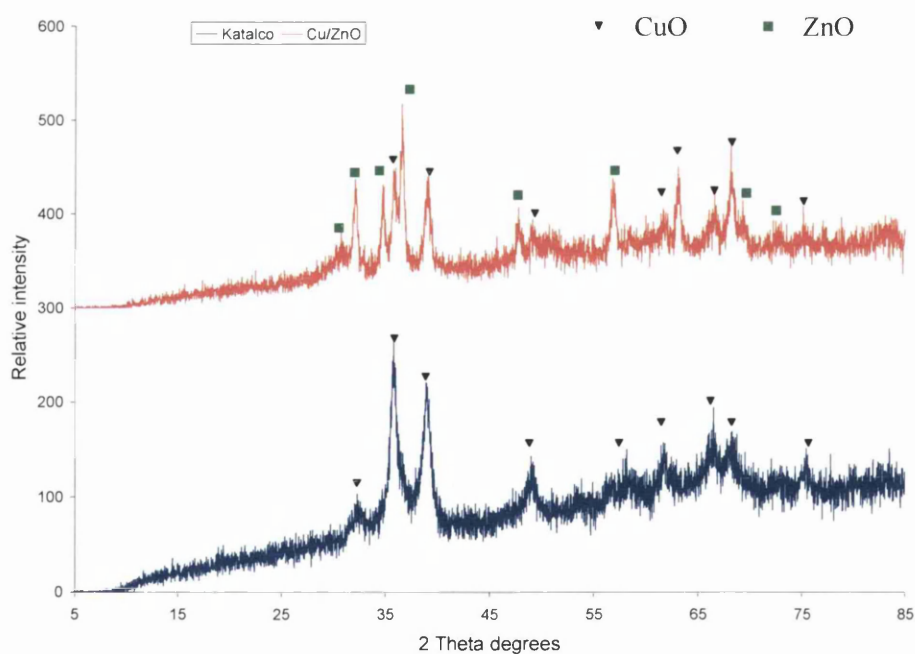


Figure 3-2: XRD pattern for calcined Katalco and Cu/ZnO catalysts

The rising backgrounds evident in these patterns are, at least partially, related to fluorescence effects with the $\text{Cu K}\alpha$ x-ray source. The calcined Katalco catalyst appears to

solely contain the CuO phase, whilst increasing the amount of zinc in the Cu/ZnO catalyst has resulted in the presence of an additional ZnO phase.

ICP analysis, is presented in Tables 3-3 and 3-4 for the calcined Katalco and Cu/ZnO catalysts respectively

Element	Calculated metal loading (wt%)	Actual metal loading from ICP analysis (wt%)
Cu	41.1	37.6
Zn	15.6	13.3
Al	3.5	5.7
Mg	0.9	0.9

Table 3-3: Elemental analysis for the Katalco catalyst

Element	Calculated metal loading (wt%)	Actual metal loading from ICP analysis (wt%)
Cu	28.3	29.5
Zn	28.7	32.0
Al	3.5	0.8
Mg	0.9	0.01

Table 3-4: Elemental analysis for the Cu/ZnO catalyst

From Table 3-3, it can be observed that there is a reasonable agreement with the calculated amounts of all the metal constituents of the catalyst. However for the Cu/ZnO catalyst, there is significantly less aluminium and magnesium than expected. The Cu/ZnO catalyst has the zinc present as ZnO, whereas the zinc present in the Katalco catalyst is amorphous.

It is evident that simply varying the Cu/Zn ratio produces two very different materials. Since the catalysts are reduced *in-situ* before catalytic testing, experiments were carried out to determine the nature of the active reduced catalyst. This was investigated by *in-situ* XRD under a H₂ atmosphere. Figures 3-3 and 3-4 are the results of these experiments for the Katalco catalyst and the Cu/ZnO catalyst respectively. It should be noted that there was an additional phase observed in Figure 3-3. This has been identified as a silicon carbide impurity from the sample holder, which has contaminated the sample for this analysis.

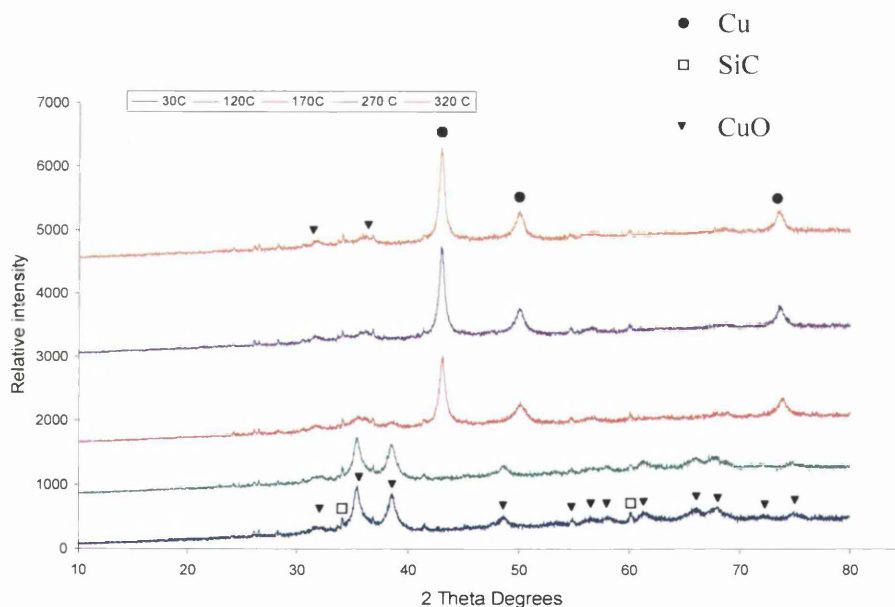


Figure 3-3: *In-situ* XRD patterns for Katalco catalyst

The reduced Katalco catalyst contains a copper metal phase which forms at 170 °C with some residual CuO remaining. This indicates that although the CuO in the calcined catalyst is reduced to the metal upon reduction, some residual CuO is evident. This is significant because the catalyst was reduced at 250°C prior to reaction, although it should be noted

that the partial pressure of hydrogen in the reactor was 20% whereas in the above *in-situ* reduction, a hydrogen partial pressure of 2% was utilised. The calcined Cu/ZnO catalyst contains CuO and ZnO and at 220 °C it is observed that the CuO is completely reduced to the metal and the ZnO phase remains.

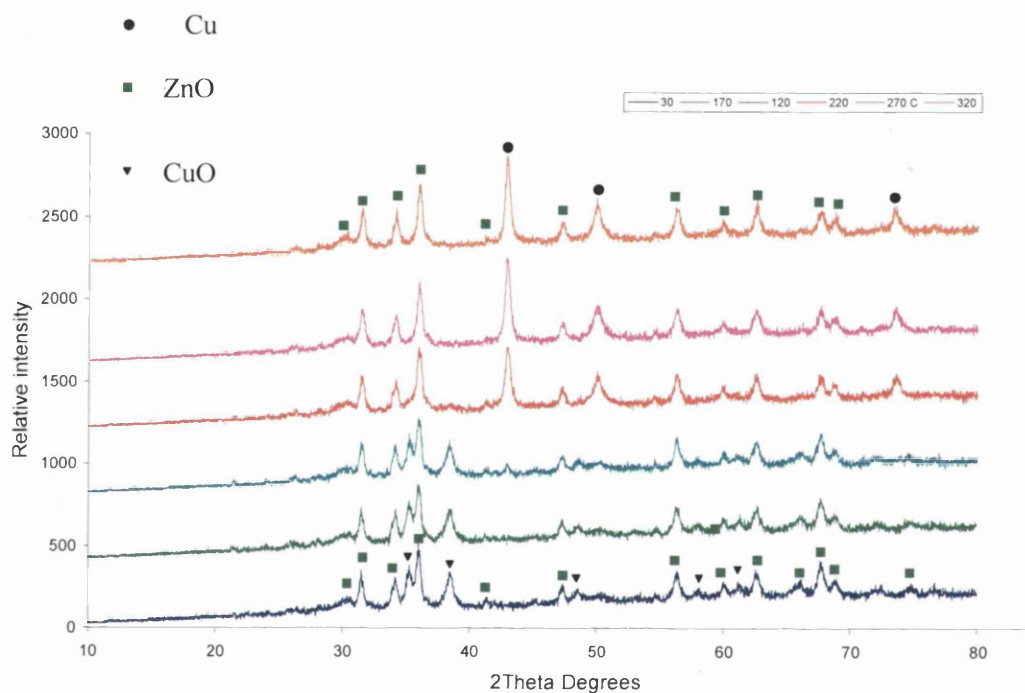


Figure 3-4: *In-situ* XRD patterns for Cu/ZnO catalyst

3.3.3 Reaction data-Copper based catalysts

Figures 3-5 and 3-6 present the data for methanol decomposition over the Katalco based catalyst at 250°C and 300°C.

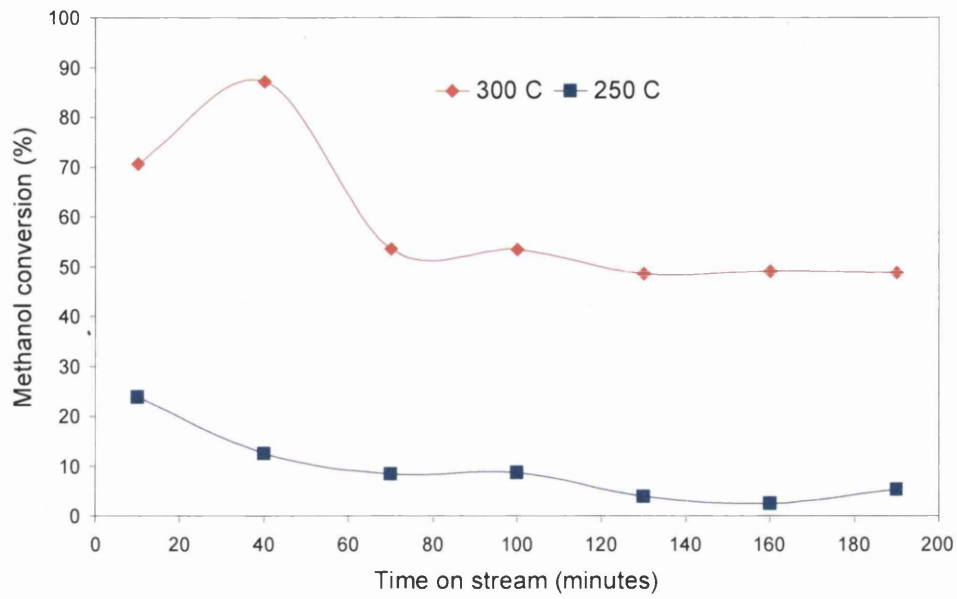


Figure 3-5: Methanol conversion, Katalco catalyst

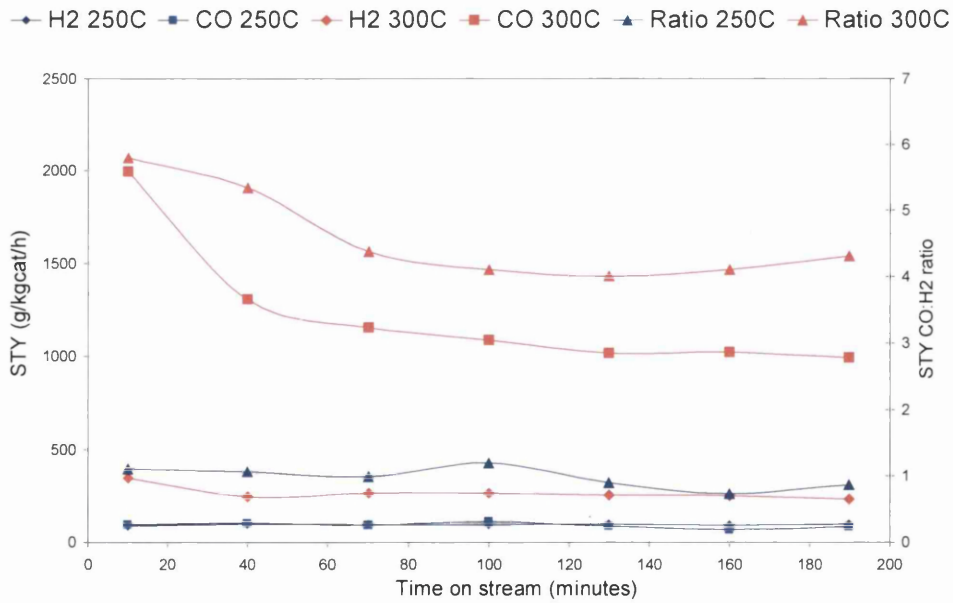


Figure 3-6: STY data Katalco catalyst

As it can be seen from Figure 3-5 increasing the temperature from 250°C to 300°C results in an increase in the methanol conversion from 5% to 50% after 190 minutes on stream. The STY for CO at 250°C is only around 95g/kg cat/h whereas at 300°C the STY is around 934g/kgcat/h after 190 minutes on stream. It is also evident that at both temperatures deactivation occurs. Figure 3-6 presents the STY production for CO and H₂ at both 250°C and 300°C. Deactivation is also evident at 300°C over the Katalco catalyst. After 10 minutes on stream, the STY value is over 1870g/kgcat/h and after 190 minutes on stream this reduces to a value approaching 935g/kgcat/h with respect to CO production. It should be noted that methyl formate was observed as the only by-product but the detection of this product was too poor to quantify with any degree of accuracy and so is omitted from these plots. As already discussed, the CO: H₂ STY ratio gives an indication of the selectivity of CO. At 250°C this ratio is low at 1.5 indicating selectivity to CO is small. However at 300°C there is an increase in the STY ratio, which is between 4 and 5. This increase is indicative of an improved selectivity to CO with the decomposition of methyl formate.

Most of the catalyst activities reported in Table 3-2 are in the temperature range 250-275°C. The activity of the Katalco catalyst at 250°C in this study is a lot lower than those reported in the table at this temperature. At 300°C STYs and conversions are obtained which are comparable to those in the table for Cu/ZnO based catalysts. For example, the Cu/Zn/Mg entry based on reference [77] which has a methanol conversion of 67.4%, an STY value of 939 g/kgcat/h for CO and an STY ratio of 6.2. The most active copper catalyst in the Table is Cu/Cr/Mn/K which has a reported CO STY value of 7142g /kgcat/h [64].

Figure 3-7 presents the conversion data for Cu/ZnO which exhibits low activity in methanol decomposition in comparison to the Katalco catalyst. This is also reflected in the lower rates of formation of CO and H₂ presented in Figure 3-8 compared with Figure 3-6 at 300°C. There is no STY data reported for CO production at 250°C for the Cu/ZnO catalyst on this plot as only a few data points were obtained and are left out of the plot for clarity. But the mean value for the CO production is presented in a summary at the end of the Chapter. The rate of product formation over the Cu/ZnO is roughly half that of the more active catalyst. After 190 minutes on stream, the Cu/ZnO catalyst has an STY value approaching 375g/kgcat/h whereas an STY value approaching 1000g/kgcat/h is observed for the Katalco catalyst at 300°C. Deactivation is evident from the Cu/ZnO catalyst as this material exhibits a substantially higher rate of formation of CO within the first 70

minutes on stream when compared to the CO formation rate approaching steady state. The low STY ratio is also consistent with CO selectivity loss to methyl formate.

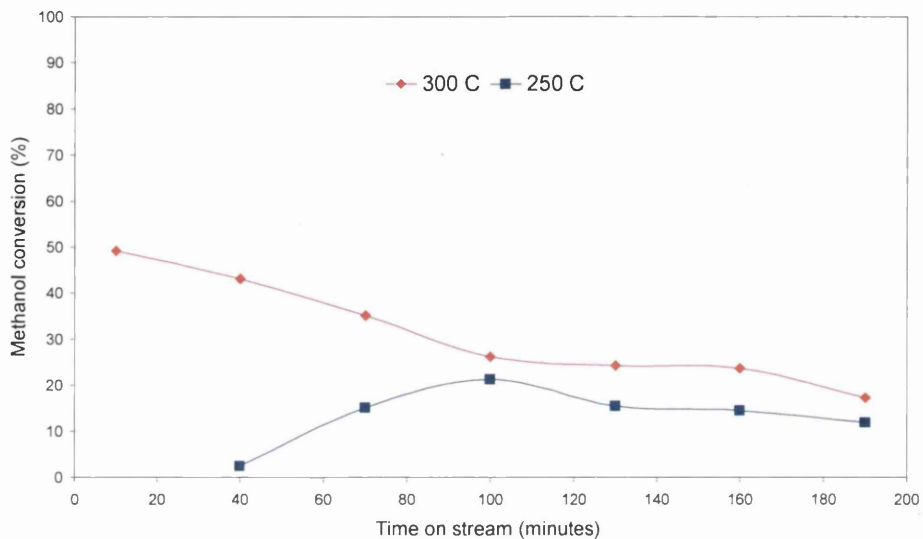


Figure 3-7: Methanol conversion, Katalco catalyst

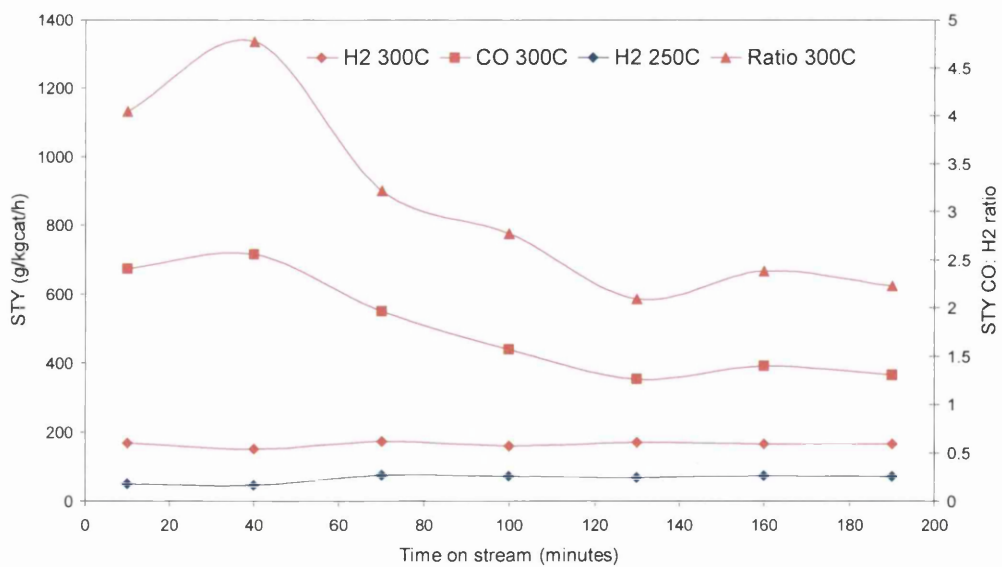
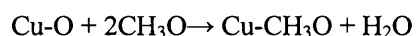


Figure 3-8: STY data Cu/ZnO catalyst

These results have demonstrated that the copper based catalysts studied exhibit very different activities in methanol decomposition. This is not surprising given the differences in their composition and structure. The main difference in the reduced active catalysts appears to be the zinc component. As described previously, zinc has a huge influence in the performance of methanol decomposition catalysts and those without this component are more active and stable. The data obtained in the present study suggest that the lower copper/zinc metal loading in the Cu/ZnO catalyst compared with the Katalco catalyst may also be responsible for its lower activity compared with the Katalco catalyst, which only exhibits the copper metal phase in the active catalyst. Figure 3-9 presents the XRD patterns for the spent Katalco and the Cu/ZnO catalyst after reaction at 300°C. Both patterns contain phases that are the same as the reduced catalysts, indicating no major phase change has occurred with both of these catalysts upon reaction. The Katalco catalyst contains copper metal reflections which are more intense compared with the Cu/ZnO catalyst. It has been suggested that metallic copper is the active phase for methanol decomposition and that the more active catalysts contain smaller copper particles in a more dispersed state [65,82]. In the present study it appears that the Cu/ZnO catalyst contains smaller copper particles due to the larger reflection widths taken from the (200) reflection in Figure 3-9. However this should be treated with caution and further studies would be required in order to obtain a measure of the copper dispersion and metal size. The copper loadings employed in the present study are also higher than those in other studies. The Cu/Zn weight ratio in the present Katalco catalyst is 2.6 and for example, the Cu/Zn weight ratio employed by Cheng *et al.* [82] ranges from 0.1 to 0.3. The higher activity of the Katalco catalyst compared to the Cu/ZnO catalyst in the present study could be due to the higher copper loading which would be consistent with copper metal being the active component. Cheng *et al.* have also studied methanol decomposition over a commercial methanol synthesis catalyst [76]. A Cu/ZnO/Al₂O₃ catalyst with a Cu/Zn weight ratio of 1.9 was studied for methanol decomposition at 290 °C. In that study it was reported that the Cu²⁺ oxidation state favours methanol decomposition by the formation of methoxy groups from adsorbed methanol as follows:



The deactivation of the Cu/ZnO/Al₂O₃ catalyst was reported to be a result of the reduction of Cu²⁺ to metallic copper during the initial stages of the reaction. This deactivation was 74

alleviated by the addition of water in the feed, which preserved the Cu^{2+} oxidation state through a redox reaction. It can be observed in Figures 3-3 and 3-4 respectively that the reduced Katalco catalyst contains CuO whereas the Cu/ZnO catalyst only contains copper metal. This may explain the higher activity of the Katalco catalyst over the Cu/ZnO catalyst. The deactivation which occurs with the Katalco catalyst may be due to the reduction of the CuO. The spent catalyst contains ZnO as observed in Figure 3-9. The absence of this phase in the *in-situ* XRD experiments could be due to the lower hydrogen partial pressure.

The deactivation of copper based catalysts is also a result of the dissolution of zinc into the copper lattice and the formation of Cu-Zn alloys [65]. Cheng *et al.* [65] compared the XRD patterns for various spent copper catalysts synthesised by co-precipitation. In that study they tested a catalyst with a Cu/Zn metal loading of 30/70 for methanol decomposition and analysed the spent catalyst in order to elucidate any phase changes and causes of catalyst deactivation. The result of this was the spent catalyst contained a copper metal phase and ZnO phase. This is consistent with the present study where these phases are also observed with the spent Cu/ZnO catalyst presented in Figure 3-9. Cheng *et al.* also observed peaks corresponding to Cu-Zn alloy formation with reflections at 42.3 and 49.3 ° 2 θ . There is no evidence of alloy formation in the present study for both the Katalco catalyst and the Cu/ZnO catalyst as there are no shifts in the positions of copper reflections or new peak reflections corresponding to alloy formation. The cubic copper phase, calculated using the (200) reflection has a lattice parameter of 0.3610 nm for both the Katalco and Cu/ZnO catalyst and this is in agreement with the lattice parameter reported for pure cubic copper metal (0.3615nm) [86].

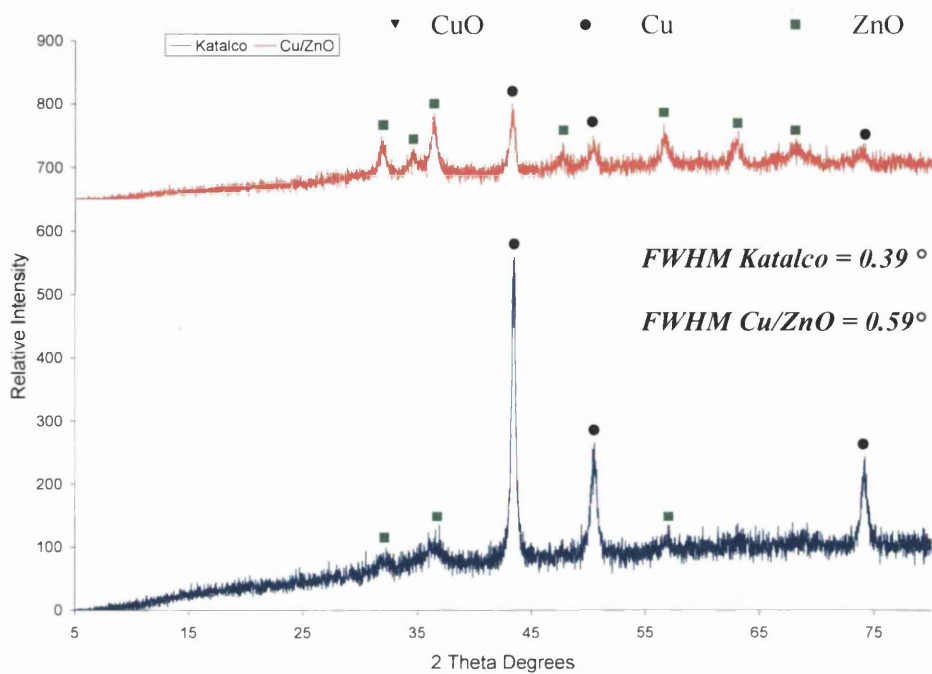


Figure 3-9: XRD patterns for spent Katalco and Cu/ZnO catalysts after 300° C reaction

The differences in activity for the catalysts could relate to differences in BET surface area. Table 3-5 displays some of the data about concerning the fresh and spent catalysts.

Catalyst	BET surface area fresh catalyst (m ² /g)	BET surface area spent catalyst (m ² /g) at 300°C	Post reaction carbon content (wt%) ¹
Katalco	51	32	0.9
Cu/ZnO	19	8	1.2

Table 3-5: Catalyst data, ¹ coke content determined by CHN elemental analysis

The Katalco catalyst has a higher surface area which may also explain its higher activity when compared to the Cu/ZnO catalyst. Both catalysts contain carbon after reaction,

which has been shown to contribute to the catalyst deactivation in methanol decomposition. In a study by Jackson *et al.* [79], the coke formed on a Cu/SiO₂ catalyst associated with the copper could not be oxidised in temperature programmed oxidation experiments. It is possible that the coke formed in these studies may also be associated with the active copper metal, thus blocking active sites and causing deactivation. Further studies would need to be carried out to determine if this is the case with these systems.

3.4 Results and discussion: Palladium methanol decomposition catalysts

3.4.1 General background

Palladium is widely studied in the decomposition of methanol because it is the most active and selective metal for the formation of CO.

The performance of palladium is dependent on many factors such as the type of support and preparation technique. Common supports employed have been ZrO₂, CeO₂, La₂O₃, Al₂O₃, TiO₂, Pr₂O₃, ZnO, Fe₃O₄ and SiO₂. In a study by Haruta *et al.* [87], TiO₂, ZnO, SiO₂ and Fe₃O₄ were shown to be less effective supports than ZrO₂, Pr₂O₃ and CeO₂. Surface analysis showed that the binding energy of the Pd 3d_{5/2} was proportional to the turnover frequency indicating that cationic palladium leads to more active catalysts.

The more active catalysts contain supports and employ preparation techniques, which encourage this strong metal support interaction. Liu *et al.* [68] demonstrated that CeO₂ doped with ZrO₂ leads to the most active catalysts in their study. A 17wt% Pd/Ce_{0.8}Zr_{0.2}O₂ catalyst prepared by the co-precipitation method exhibited the highest conversion. The co-precipitation method was reported to result in smaller palladium particles when compared to catalysts compared with impregnation, as evidenced by analysis of the XRD peak widths and higher palladium metal surface area measured by CO adsorption. The 17wt% Pd/Ce_{0.8}Zr_{0.2}O₂ catalyst prepared by the co-precipitation had a palladium metal surface area of 13.9m²/g whereas a catalyst with the same composition synthesised by impregnation yielded has a palladium surface area of 6.6m²/g. It was proposed that zirconium inclusion promoted a strong metal support interaction with the palladium and the CeO₂ support thus maintaining the palladium in a more active cationic state. It was also proposed that the co-precipitation procedure promotes smaller palladium particles which can dissolve into the CeO₂ lattice thus further enhancing this effect. A similar effect was

also obtained by doping ceria with La_2O_3 [88].

Haruta *et al.* [89] reported that palladium supported on ZrO_2 prepared by the deposition-precipitation method afforded a similar strong interaction between palladium and the support. In that study, Arrhenius plot analysis indicated that a lower activation energy is obtained with the more active catalyst. Other alternative supports include hydrotalcite and mesoporous silica [70], and synthetic anionic clays [67]. Liu *et al.* [70] reported that large surface area, palladium dispersion and a strong metal support interaction are characteristics of their active Pd/(Mg(Al)O)/HMS catalyst.

The rate-determining step in methanol decomposition is thought to be the breaking of a C-H bond of adsorbed methoxy group [60]. It is argued that this is accelerated by cationic palladium, which weakens the C-H bond. Generally the assignment of cationic Pd state has been made on the basis of XPS, although the possible influence of final state effects on the assignment of oxidation states does not seem to have been considered with highly dispersed Pd systems [68].

Palladium catalysts are the most selective in the decomposition of methanol. From inspection of Table 3-2 it is evident that most palladium catalysts exhibit a wide range of STYs. Most catalysts have an STY ratio of 7.0 which arises from 100% selectivity to CO. These systems are unlike the copper based systems where high selectivity to CO is dependent on a variety of conditions, including higher reaction temperature. Kapoor *et al.* reported that palladium supported on mesoporous CeO_2 exhibits 100% selectivity to CO at temperatures as low as 180°C [69]. There are entries in Table 3.1 where the STY ratio is less than 7.0 for palladium based catalysts which is a consequence of small amounts of by-products. CO_2 , CH_4 and methyl formate were reported by Liu *et al.* [68] over a series of palladium catalysts supported on $\text{CeO}_2/\text{ZrO}_2$. In that study, the selectivity to CO was found to decrease with increasing contact time and all catalysts deactivated due to the formation of coke although activity could be regenerated with calcination and reduction [68].

The palladium loadings vary from 3-30wt% in Table 3-1 and there is no correlation between activity and loading. Figure 3-10 is a plot of H_2 STY at 200°C as a function of loading for some of the studies represented in Table 3-1. It can be observed from this table that the high loadings employed by some studies therefore appear arbitrary and unnecessary to develop an active catalyst as there is no correlation between loading and

series of palladium supported on γ -Al₂O₃ were synthesised by impregnation and tested. These catalysts were targeted to contain palladium loadings of 1.5, 3 and 9 wt %.

Catalyst	Theoretical amount of Pd (wt%)	Actual amount of Pd from ICP analysis (wt%)	Theoretical amount of Zr (wt%)	Actual amount of Zr (wt%)
Pd/Ce _{0.8} Zr _{0.2} O ₂	17.0	8.4	9.3	8.7
Pd/CeO ₂	3.0	1.7	/	/

Table 3-6: Elemental analysis for Pd based catalysts

Table 3-6 presents the theoretical and actual loadings for the metal for each of the palladium catalysts. Whilst there is a good agreement with the amount of zirconium, the loading for palladium is consistently less than the theoretical value. One explanation for this is that during the co-precipitation, a portion of the palladium was left in solution and washed away during the subsequent washing and filtering stage of the catalyst preparation.

Figures 3-11 and 3-12 show the XRD patterns for the calcined catalysts for Pd(17wt%)/Ce_{0.8}Zr_{0.2}O₂ and Pd(3wt%)/CeO₂ respectively. Both samples show the CeO₂ support phase. There are no reflections corresponding to palladium and zirconium oxides in the present study and this is consistent with the XRD patterns from the materials produced by Liu *et al.* [68]. However Liu *et al.* reported that solid solutions are formed from the dissolution of the zirconium into the ceria lattice. They calculated the lattice constant for CeO₂ in materials containing CeO₂ and CeO₂/ZrO₂ mixed phases and found that the lattice constant was smaller with the mixed supports (0.5412nm for CeO₂ and 0.5364nm for the mixed support), indicating that the Zr⁴⁺ had dissolved into the CeO₂ lattice replacing some Ce⁴⁺. The value of the lattice constant for the cubic CeO₂ phase was calculated taking the (200) reflection in the present study. A value of 0.5403nm was obtained for the Pd(17wt%)/Ce_{0.8}Zr_{0.2}O₂ catalyst but the Pd(3wt%)/CeO₂ catalyst without any Zr⁴⁺ has an even smaller lattice parameter value of 0.5361nm indicating other factors such as lattice

defects cause a reduction in the lattice constant. It has been shown that defects can occur in ceria as a result of catalytic preparation steps [125].

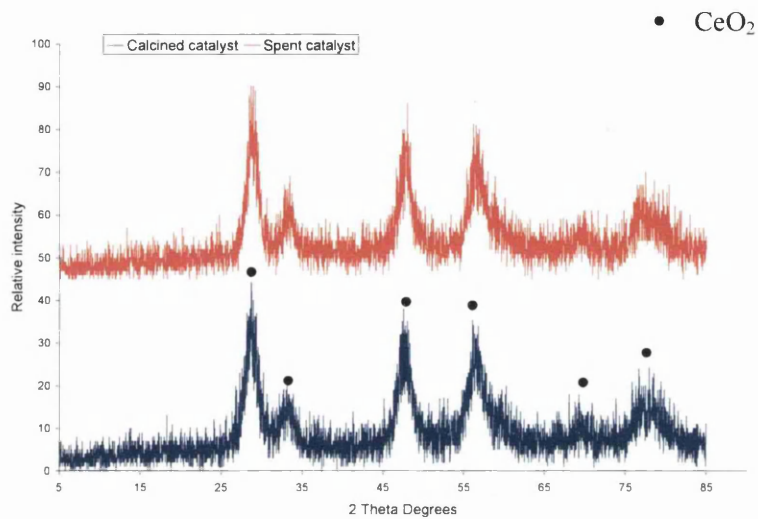


Figure 3-11: XRD pattern of calcined and spent Pd/Ce_{0.8}Zr_{0.2}O₂ catalyst at 300°C

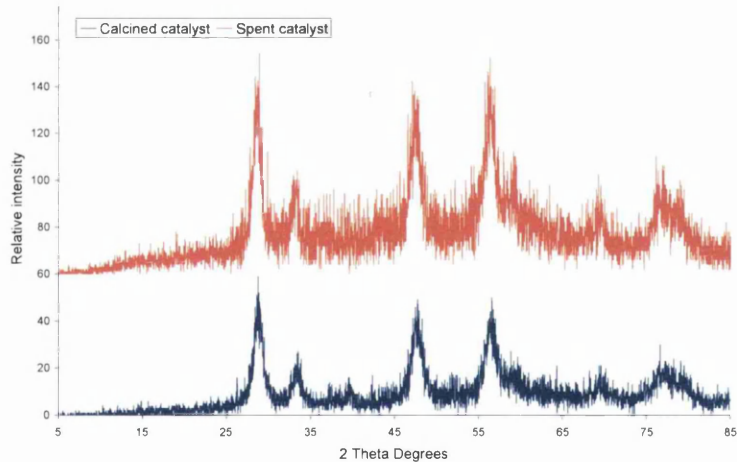


Figure 3-12: XRD pattern of calcined and spent Pd/CeO₂ catalyst at 300°C

3.4.3 Reaction data - Palladium based catalysts

Methanol decomposition experiments were carried out on both palladium based catalysts at 250°C and 300 °C. Figure 3-13 displays the methanol conversion data for Pd/ Ce_{0.8}Zr_{0.2}O₂ catalyst and Figure 3-14 the STY production for CO and H₂ at 250°C and 300°C.

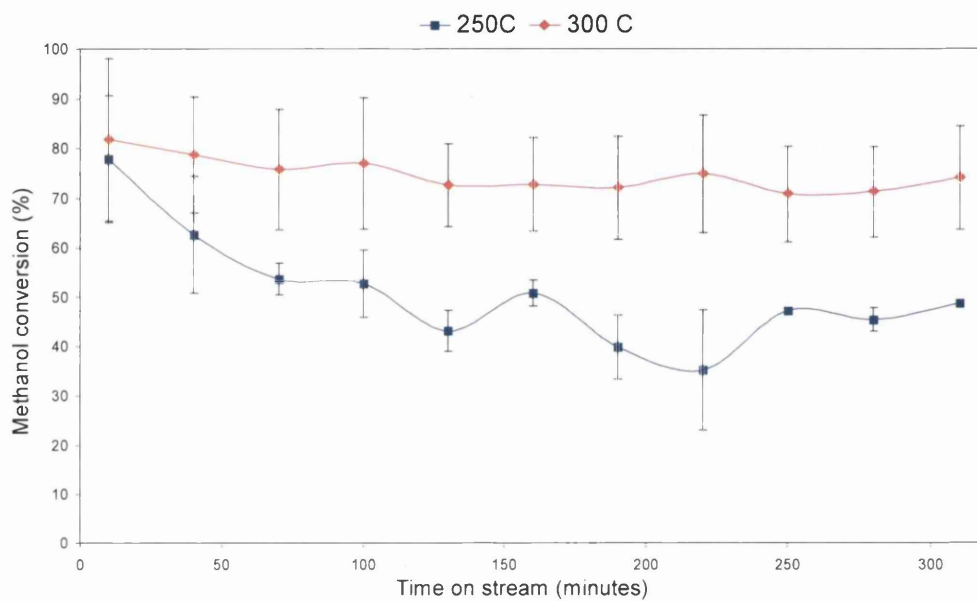


Figure 3-13: Methanol conversion, Pd/ Ce_{0.8}Zr_{0.2}O₂ catalyst

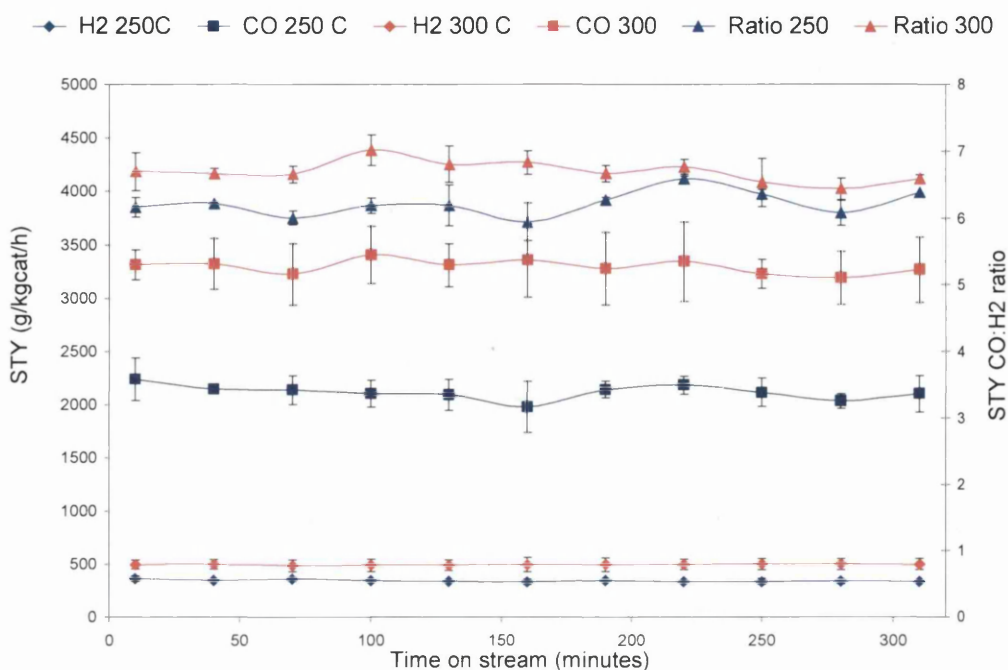


Figure 3-14: STY data Pd/ Ce_{0.8}Zr_{0.2}O₂ catalyst

The methanol conversion and activity of the catalyst increased, as expected, with increasing temperature and the STY values for CO and H₂ are larger at 300°C. The STY CO:H₂ ratio is at a value of 6.0 at the reaction temperature of 250°C however no by-products were detected. The STY CO:H₂ ratio at 300°C is closer to 7 indicating that the methanol is decomposed to CO and H₂ in approximately a 1:2 ratio. Although no by-products are detected with the present catalyst, Liu *et al.* reported that low levels of CO₂, methyl formate and CH₄ are produced over palladium based catalysts at 250°C [68] and hence the possibility of these products cannot be ruled out in the present study and may be produced in small quantities, below their detection limits. Figure 3-15 displays the methanol conversion data for the Pd/CeO₂ catalyst and Figure 3-16 the STY production for CO and H₂ at 300°C. This catalyst exhibits an activity and selectivity very similar to the Pd/Ce_{0.8}Zr_{0.2}O₂ catalyst with both catalysts having comparable methanol conversions and STY values.

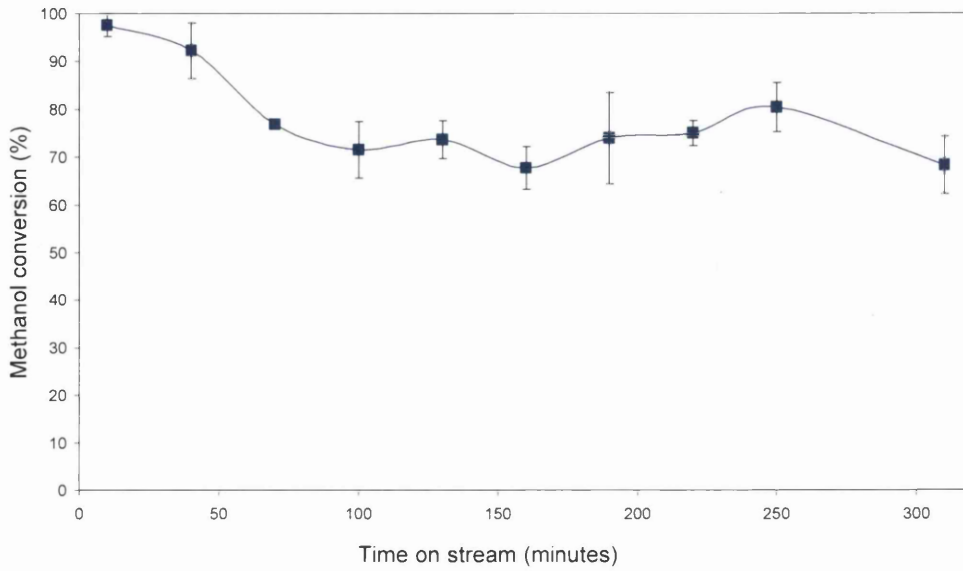


Figure 3-15: Methanol conversion, Pd/CeO₂ catalyst at 300°C

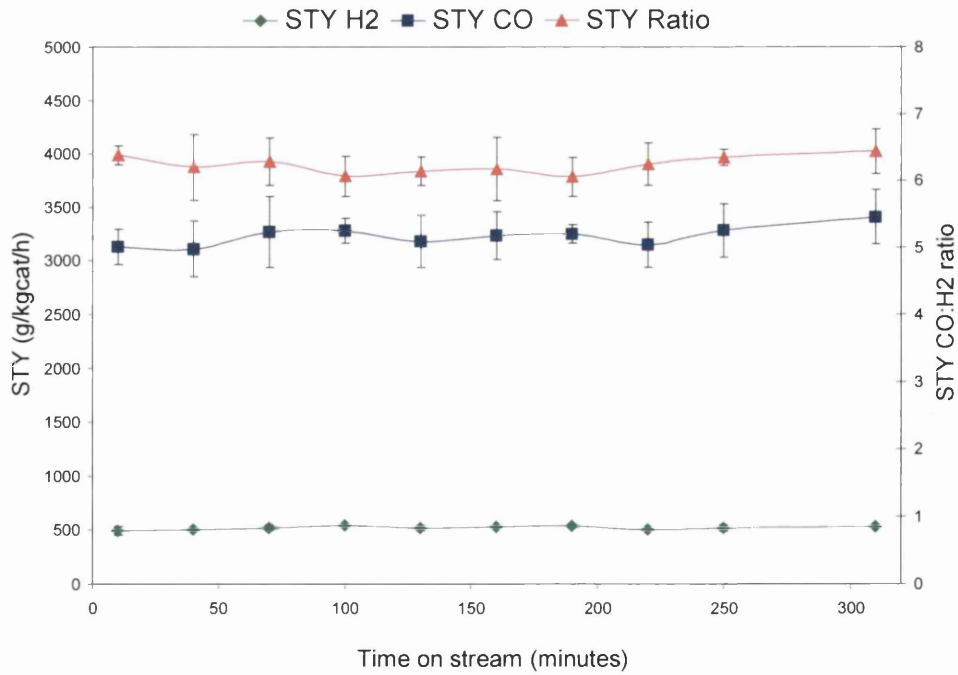


Figure 3-16: STY data Pd/CeO₂ catalyst at 300°C

In agreement with the literature regarding palladium loadings and the data displayed in Figure 3-10, there is no correlation with palladium loading and catalyst activity. It appears that such a high loading of palladium as reported in the catalyst formulation in the study by Liu *et al.* [68] is unnecessary to develop a catalyst with high activity.

Table 3-7 contains BET and CHN data for the palladium catalysts. It is apparent that the Pd/Ce_{0.8}Zr_{0.2}O₂ catalyst has the highest BET surface area of the two catalysts prior to reaction, but not afterwards. Despite having an initially larger BET surface area and a higher palladium loading, there is no marked increase in the catalyst activity as already described. However, as discussed by Liu *et al.* [68], a large palladium surface area where the palladium particles are of the magnitude 3nm are very active in methanol decomposition.

Catalyst	BET surface area of fresh catalyst (m ² /g)	BET surface area of spent catalyst (m ² /g) following reaction at 300°C for 5 hours	Post reaction carbon content (wt%) ¹
Pd/ Ce _{0.8} Zr _{0.2} O ₂	160	44	0.6
Pd/CeO ₂	85	81	0.7

Table 3-7: Catalyst data Pd/CeO₂ based catalysts, ¹ coke content determined by CHN elemental analysis

Despite the reduction of BET surface area and the accumulation of coke on both catalysts, there was little evidence of a decrease of activity with both of the studied palladium catalysts over the 5 hours of reaction in terms of CO and H₂ production. However, the methanol conversion does drop within the first 100 minutes of reaction for both palladium catalysts as observed in Figures 3-13 and 3-15. The constant production of synthesis gas and initial high methanol conversion suggests that the coke may be formed at the early stages of the reaction on both palladium catalysts in this study. However Liu and co-

workers reported that deactivation occurs over a longer time on stream. A decrease of conversion from 51% to 43% after 24 hours on stream was reported [68].

3.4.4 Palladium supported on γ -Al₂O₃

There are entries in Table 3-1 where γ -Al₂O₃ has been used in methanol decomposition to support palladium [66, 75] and rhodium [57]. High CO selectivities were achieved using γ -Al₂O₃ as a support. The Pd/Al₂O₃ entry [66] exhibits an STY ratio of 7.2. In that study DME was formed at lower temperatures, however at 300°C no DME was formed. Surface modification of the γ -Al₂O₃ can affect the performance of these catalysts. Yang *et al.* [75] has an entry in the table where the STY ratio is 7.0. The high selectivity to CO in that study was attributed to the addition of La₂O₃, which neutralized the surface acidic sites of γ -Al₂O₃ and suppressed DME formation.

Palladium supported on γ -Al₂O₃ catalysts were prepared using wet impregnation as described in the experimental section. Both cationic and anionic species may be used as precursor compounds. In order to obtain a high dispersion, the correct precursor selection depends on the pH of the impregnation solution and the point of zero charge (pzc) of the support. The pzc of a given surface is the pH at which that surface has a net neutral charge. The significance of this is that a given surface will have a net positive charge at a solution pH value less than the pzc and thus be a surface on which anions may strongly adsorb. On the other hand, the surface will have a negative charge at solution pH values greater than the pzc and thus be a surface on which cations may strongly adsorb.

For example, it has been reported that γ -Al₂O₃ has a pzc between 8 and 9 [93]. If the pH is increased above this range then the γ -Al₂O₃ surface will have a negative charge and could adsorb the cationic [Pd(NH₃)₄]²⁺ species. If the pH of impregnation is less than the pzc for γ -Al₂O₃ then the surface will have a positive charge and could adsorb the [PdCl₄]²⁻ species. SiO₂ has a pzc of 2-3 and is only suitable for cation exchange with [Pd(NH₃)₄]²⁺ [91]. Varying the impregnating pH and precursor therefore provides a synthetic tool for engineering the impregnation of metals onto supports. An example of this was demonstrated by Schwartz and co-workers who were able to deposit palladium selectively onto the SiO₂ component of Al₂O₃-SiO₂ composite oxides [91].

3.4.5 PZC of γ -Al₂O₃ support

The pzc of the γ -Al₂O₃ support was determined by potentiometric mass titration using a literature method [92]. This is carried out in two steps. Firstly a blank titration was carried out. A 75 ml solution of 0.03M KNO₃ was regulated to a high pH with NaOH(1M) and this is titrated with 0.01M HNO₃ which is progressively added and gave rise to the pH profile observed in Figure 3-17. This procedure was repeated with the solution containing a suspension of the γ -Al₂O₃ support (0.75g). This gave rise to the red profile line in Figure 3-17. The pzc is the point where the two lines cross. The reason for this is that the amount of acid necessary to achieve the given pH is the same for the blank titration and is not affected by the presence of the γ -Al₂O₃ suspension.

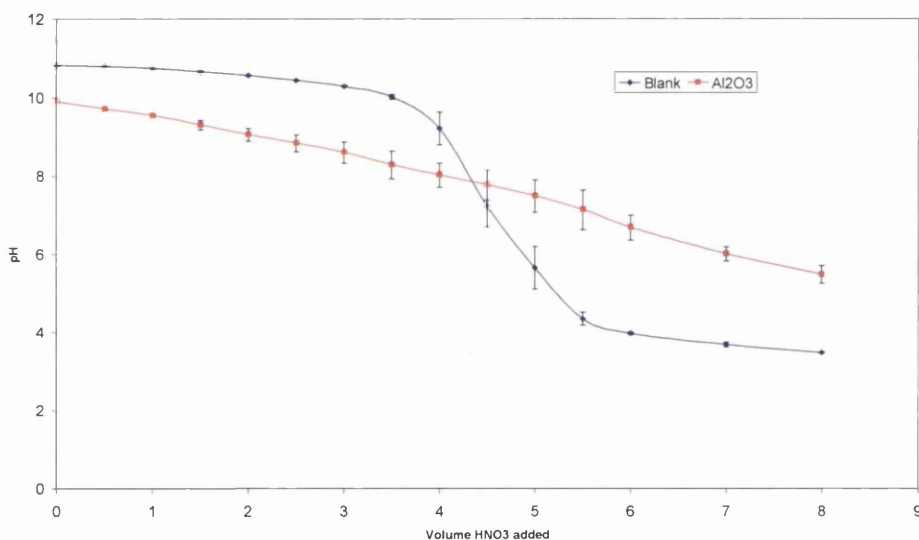


Figure 3-17: Potentiometric titration of γ -Al₂O₃

The pzc of the γ -Al₂O₃ support was determined to be 8. This value is in agreement with other studies [92, 93]. In a study by Vass and co-workers [93], the adsorption of palladium complexes was considered on γ -Al₂O₃. Figure 3-18 illustrates the effect of pH on the surface charge on γ -Al₂O₃. At pH values higher than the pzc (the pzc is represented by the dotted line) the -AlO^- species dominates and the surface of the γ -Al₂O₃ is negatively

charged. At pH values below the pzc there is an increase in the distribution of protonated AlOH_2^+ species as expected. The speciation of various palladium substrates is also illustrated in Figure 3-18. It is evident that as the pH value decreases, there is an increase in the presence of the $[\text{PdCl}_4]^{2-}$ anion in solution from a $\text{Na}_2[\text{PdCl}_4]$ precursor and a smaller distribution of the cationic palladium species. Therefore at pH 4, adsorption of $[\text{PdCl}_4]^{2-}$ will be favoured on the $\gamma\text{-Al}_2\text{O}_3$.

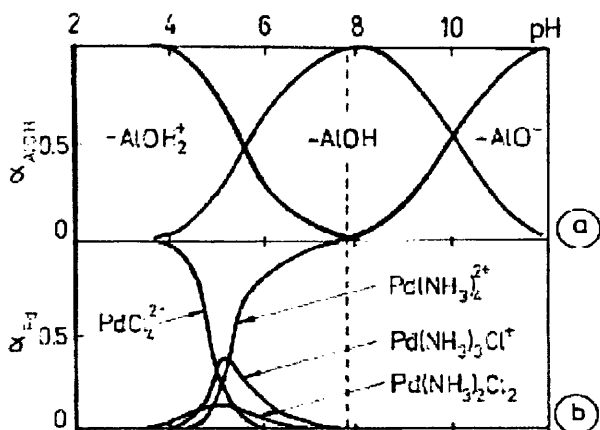


Figure 3-18: pH dependence of surface distribution of hydroxyl groups (a) and Pd species in solution (b) adapted from reference 93.

In the present study, sodium tetrachloropalladate which contains the $[\text{PdCl}_4]^{2-}$ anion was used as the palladium precursor. The pH of impregnation was 3.8. The catalysts were synthesised to contain loadings of 1.5, 3 and 9wt% palladium in order to study the effect loading will have on methanol decomposition.

3.4.6 Pd/ $\gamma\text{-Al}_2\text{O}_3$ catalyst characterisation

Figures 3-19, 3-20 and 3-21 present the XRD patterns for the 3 loadings of palladium supported on $\gamma\text{-Al}_2\text{O}_3$ applied to the present study. On each figure, are the patterns for the calcined catalyst and the spent catalyst after a methanol decomposition reaction at 300°C . It is evident that all three loadings contain the $\gamma\text{-Al}_2\text{O}_3$ phase as expected. After calcination the PdO phase is only observed with the 3 and 9wt% Pd loaded catalysts. There is no evidence of palladium metal formed after reaction with all of the spent catalysts from these

patterns.

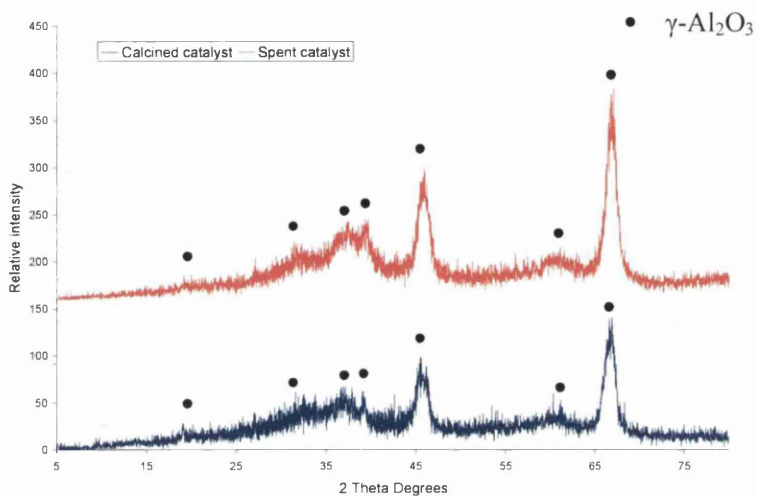


Figure 3-19: XRD pattern of calcined and spent Pd (1.5 wt%)/Al₂O₃ catalyst at 300°C

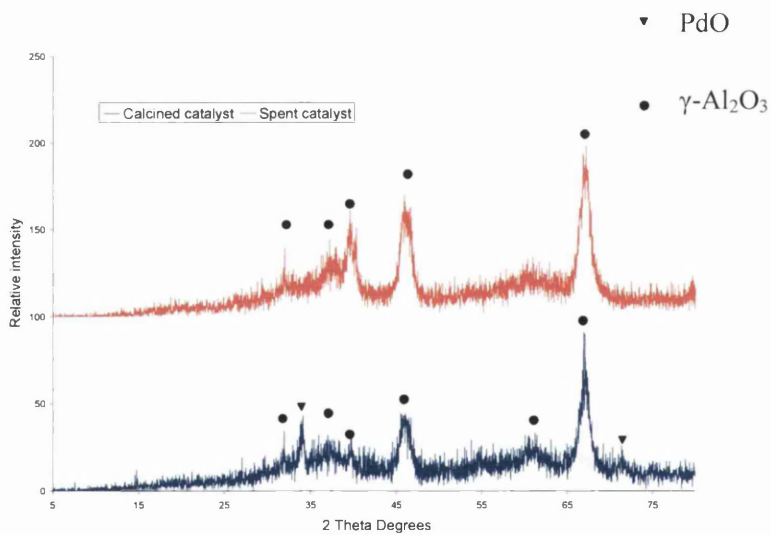


Figure 3-20: XRD pattern of calcined and spent Pd (3 wt%)/Al₂O₃ catalyst at 300°C

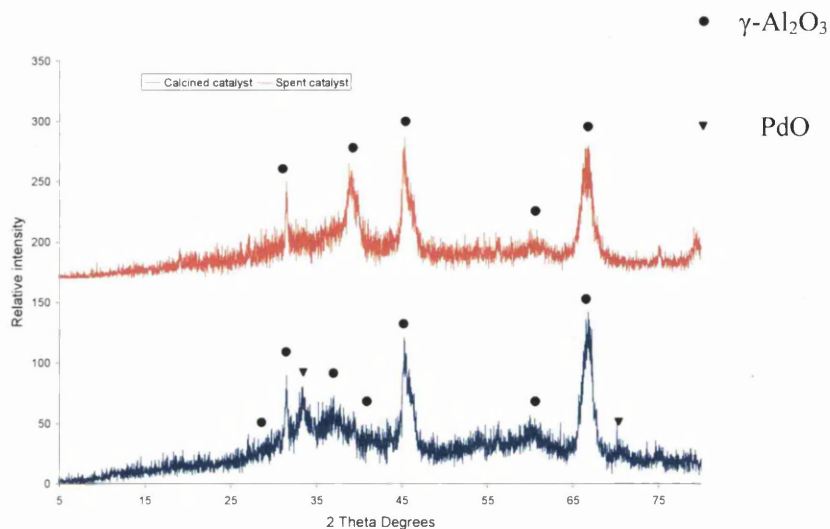


Figure 3-21: XRD pattern of calcined and spent Pd (9 wt%)/Al₂O₃ catalyst at 300°C

The absence of palladium metal reflections in the spent catalyst may possibly be attributed to the broadening and masking of adjacent $\gamma\text{-Al}_2\text{O}_3$ reflections. *In-situ* XRD and reduction experiments were carried out on both the 3wt% and 9wt% loaded catalysts in order to observe any possible evolution of a palladium metal phase upon reduction. Figures 3-22 - 3-24 display the results for the 1.5wt%, 3wt% and 9wt% respectively. It is clear that the 3 and 9wt% catalyst shows the loss of reflections corresponding to PdO which forms palladium metal upon reduction at 250 °C. For the 1.5% catalyst, the only observed phase is the $\gamma\text{-Al}_2\text{O}_3$ support. It is evident that the patterns for the *in-situ* experiments differ from those presented in Figures 3-19 to 3-21. In particular the relative intensities of the $\gamma\text{-Al}_2\text{O}_3$ reflections are different for the 9wt% sample presented in Figures 3-21 and 3-24. This may be due to the fact that the samples are loaded and contained differently for the *in-situ* analysis. If the packing of the powder in the sample holder is different then the crystallites may adopt a preferential orientation which will change the intensities of the reflections.

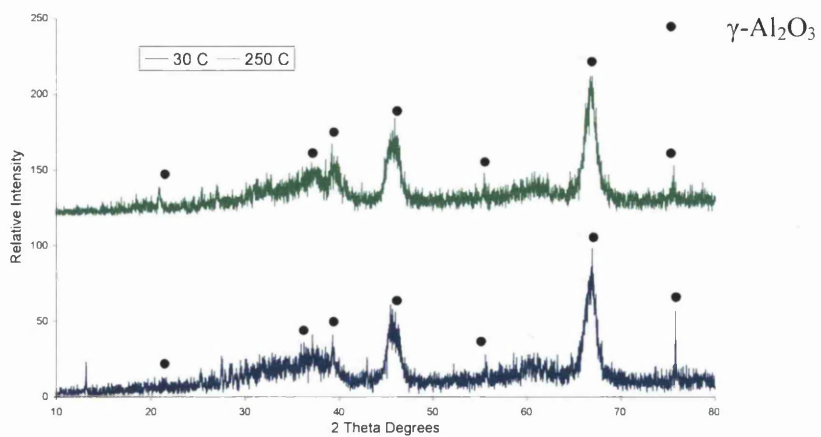


Figure 3-22: *In-situ* XRD experiment for Pd (1.5 wt%)/Al₂O₃ catalyst

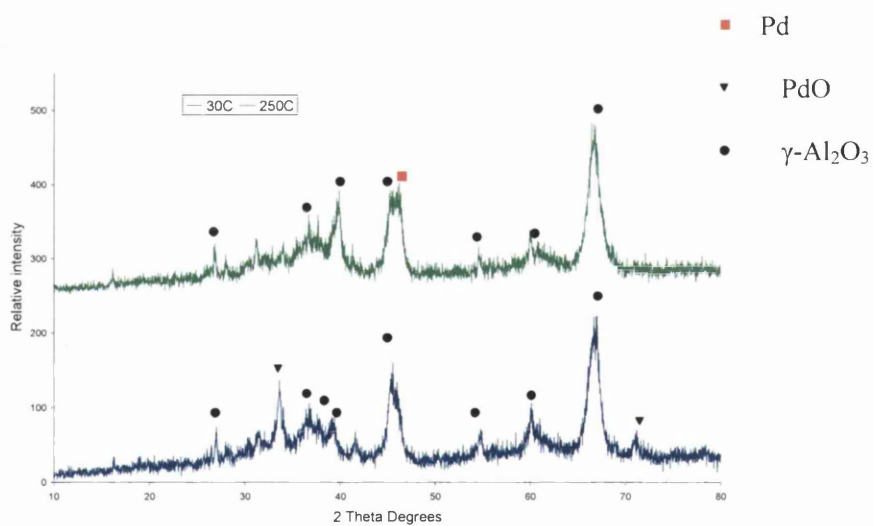


Figure 3-23: *In-situ* XRD experiment for Pd (3 wt%)/Al₂O₃ catalyst

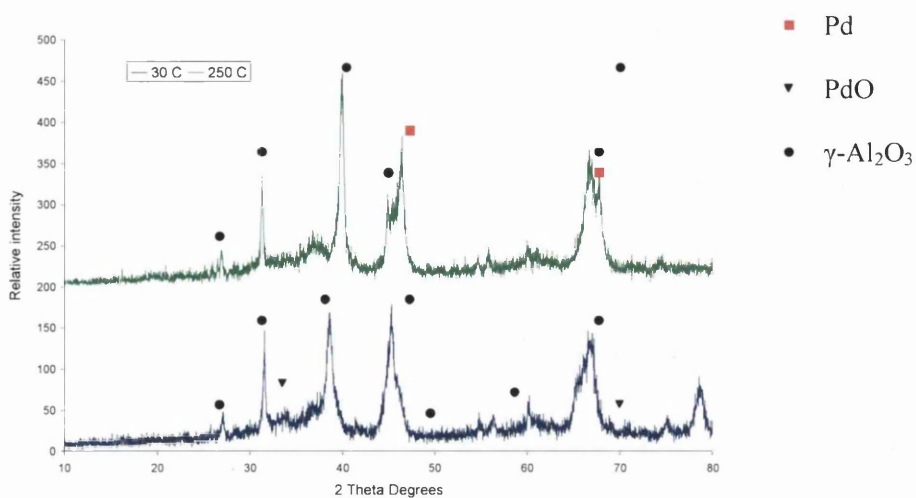


Figure 3-24: *In-situ* XRD experiment for Pd (9 wt%)/Al₂O₃ catalyst

3.4.7 Reaction data - Pd/ γ -Al₂O₃ based catalysts

Methanol decomposition experiments were carried out on the synthesised Pd/ γ -Al₂O₃ catalysts at 300 °C. The methanol conversion data is presented in Figures 3-25 – 3-27 for the 1.5, 3 and 9wt% loadings respectively.

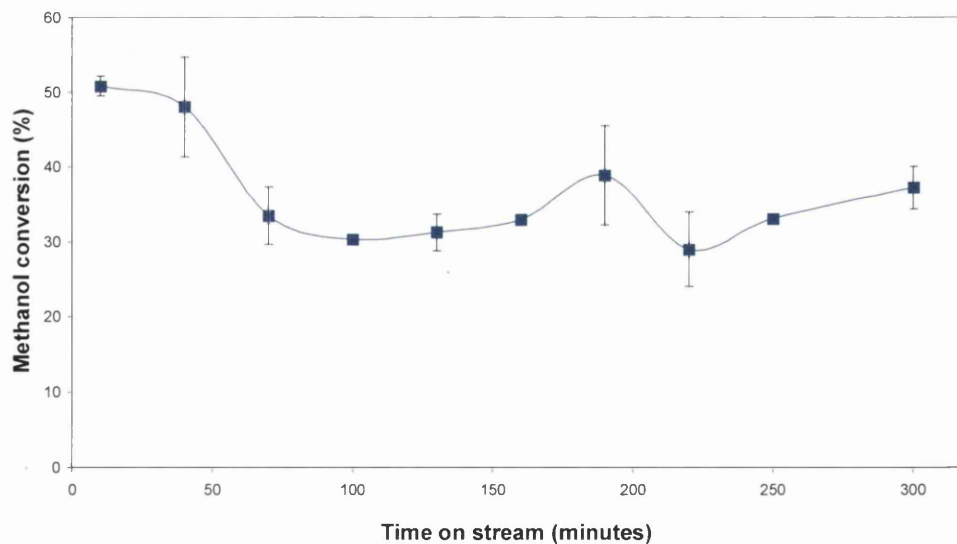


Figure 3-25: Methanol conversion for Pd (1.5wt%)/ γ -Al₂O₃ catalysts at 300°C

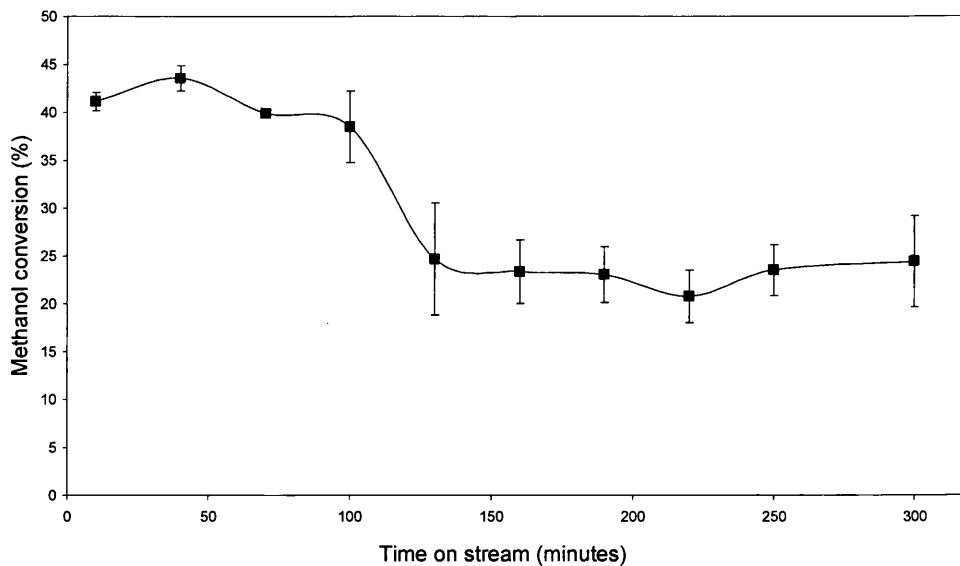


Figure 3-26: Methanol conversion for Pd (3wt%)/ γ -Al₂O₃ catalysts at 300°C

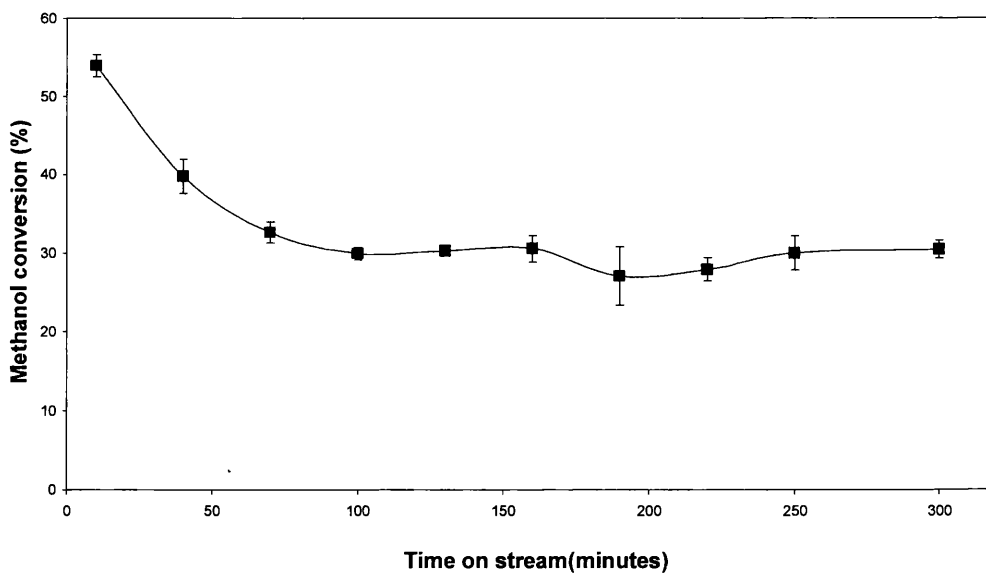


Figure 3-27: Methanol conversion for Pd (9wt%)/ γ -Al₂O₃ catalysts at 300°C

It can be observed from the methanol conversion data presented that all of the catalysts presented deactivate within the first 150 minutes on stream.

The STY data for CO and H₂ production are presented in Figures 3-28 – 3-30 and give a better indication of how these catalysts perform.

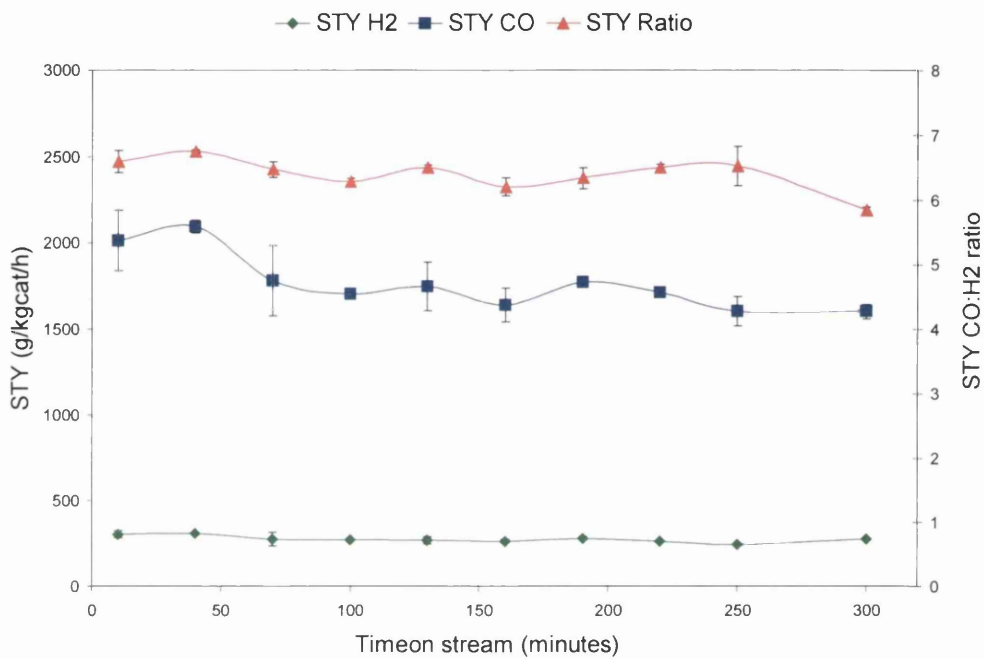


Figure 3-28: STY data at 300°C, Pd (1.5 wt%)/ γ -Al₂O₃ catalyst

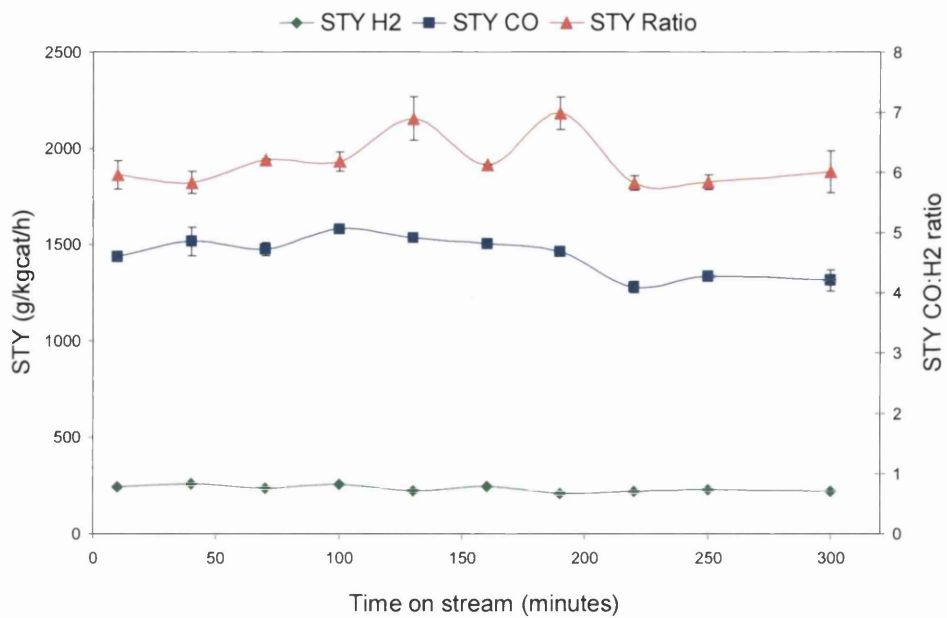


Figure 3-29: STY data at 300°C, Pd (3 wt%)/ γ -Al₂O₃ catalyst

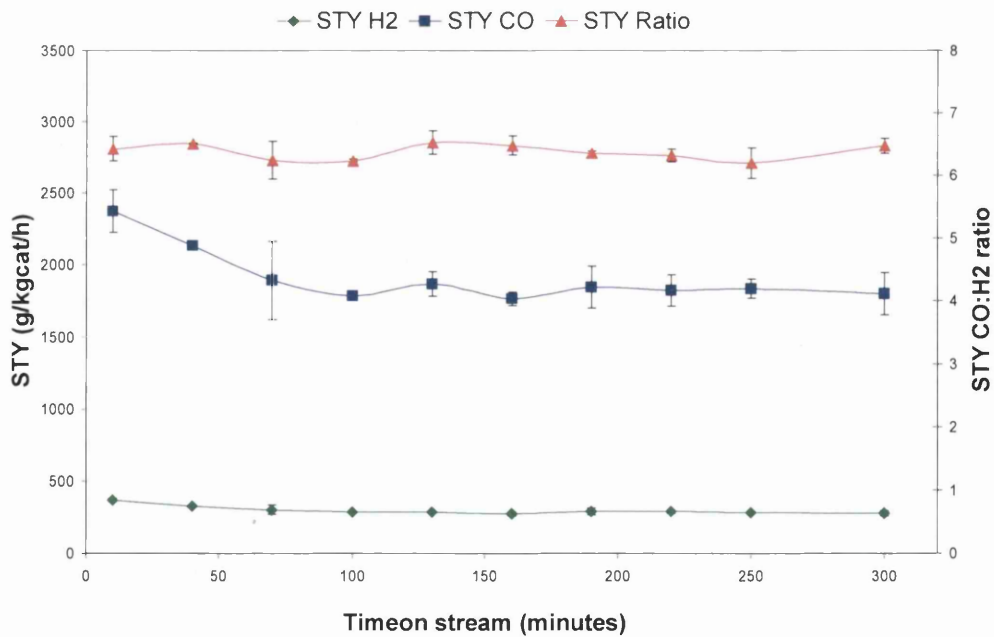


Figure 3-30 STY data at 300°C, Pd (9 wt%)/ γ -Al₂O₃ catalyst

All of the Pd/ γ -Al₂O₃ catalyst samples showed good selectivity to CO with no detected by-products and STY ratios between 6 and 7 for all the studied catalysts. The CO production for the 1.5 wt% catalyst and the 9 wt% catalyst is around 1869 g/kgcat/h. The 3wt% catalyst is less active producing around 1400g /kgcat/h for CO. There is no general trend with palladium metal loading in the present study and this is consistent with the co-precipitated palladium catalysts described previously. High loadings may however generate larger metal particles which have been shown to be less active when compared with smaller palladium metal particles which may result from lower metal loadings [68]. The fact that the 1.5wt% catalyst has similar activity to the 9wt% catalyst supports this argument, although further experiments to determine the exact particle size distribution of the palladium in each case would be required. XRD analysis shows that the reduced 9wt% contains palladium metal whereas that for the 1.5wt% catalyst only evidences the support. These palladium catalysts are active and selective in methanol decomposition, but are not as active as the Pd/Ce_{0.8}Zr_{0.2}O₂ and Pd/CeO₂ catalysts prepared by co-precipitation. This result is consistent with the literature where co-precipitation yields more active catalysts than impregnation by forming smaller palladium metal particle sizes [68]. Notably no DME was detected with these catalysts. This is consistent with other studies using γ -Al₂O₃ as a support in methanol decomposition catalysts where no DME is detected at reaction temperatures of 300°C [66]. This is surprising since methanol dehydration over γ -Al₂O₃ occurs at that temperature [45]. DME has been reported in such systems and the use of dopants has been used to suppress DME formation in other methanol decomposition studies [75]. It is possible that the role of sodium ions in the precursor material may have influence over the support properties in the present study. It has been reported that Brønsted sites are responsible for methanol dehydration to DME over γ -Al₂O₃ [94]. In a study by Sarback *et al.* [124], the effect on acidity on γ -Al₂O₃ by doping sodium ions was studied. In conclusion they reported that the sodium lowered the concentration of Lewis acid sites and reduced the strength of Brønsted sites. Table 3-8 contains data for the BET surface areas of the fresh and spent catalysts and the coke content after each reaction run. There is no significant difference between the BET surface areas between each of the loadings. The BET surface area does appear to have increased after reaction which most likely indicates the deposition of high surface area species. The interaction of N₂ with carbon is weak but generally acceptable within the limits of the BET model however further analysis of the N₂ physisorption data, and in particular, the magnitude of the C constant and shape of the isotherm would be required to establish the

validity of the BET method. All catalysts have attained coke after reaction which may explain the deactivation profiles observed for all Pd/ γ -Al₂O₃ catalysts.

Catalyst loading (wt%)	BET surface area fresh catalyst (m ² /g)	BET surface area spent catalyst (m ² /g) following a 5 hour reaction at 300°C	Post reaction carbon content (wt%) ¹
1.5	51	68	0.3
3	57	60	0.4
9	49	60	0.4

Table 3-8 Catalyst data for Pd/ γ -Al₂O₃ catalysts, ¹ coke content calculated using CHN elemental analysis

3.5 Results and discussion: Nickel methanol decomposition catalysts

3.5.1 General background

Nickel is commonly studied for methanol decomposition and it can be observed that the most active catalyst from the literature in Table 3-2 is nickel based. In a study by Matsumura *et al.* [95], the catalytic decomposition of methanol was studied at 250°C over nickel supported on SiO₂. As expected, CH₄ and H₂O were the detected by-products due to the methanation process but selectivities to CO remained above 90 % in all the reported catalysts in that study and the CH₄ selectivity was reported to increase with increasing methanol conversion. Like the palladium and copper based catalysts, nickel loading and particle size has an influence on the catalyst activity and product selectivity. Matsumura and co-workers [95] probed this relationship by comparing conventional impregnation methods with a sol-gel preparation technique. The activity of the impregnated catalysts increased with metal loadings up to 10wt%, but with the sol-gel method the activity

increased up to 40wt% nickel loadings. The NiO particles were found to sinter into larger nickel particles upon reduction on the impregnated catalysts but the nickel dispersion remained high with comparable nickel loadings using the sol-gel preparation method. The higher activity was due to the increased metal dispersion attained at high nickel loadings. In a study by the same group however, small nickel particles were reported to be a disadvantage in methanol decomposition [54]. In that study there was no direct relationship between activity and the total surface area of nickel and it was reported that the methanol conversion increased with increased concentrations of strongly adsorbed CO and H₂, and catalysts containing the smallest metal particles in the region 2-4nm were found to give the lowest methanol conversions. It was postulated that these smaller particles are of poor crystallinity and do not adsorb CO and H₂ as strongly as the larger and more crystalline nickel particles although it would be expected that strongly bound CO may decrease the rate of reaction, as reported for Pd/CeO₂ catalysts [90]. To justify their argument, Matsumura *et al.* [54] reported that the rate determining step of methanol decomposition over nickel has been postulated to be the interaction between an adsorbed surface methoxy group and adsorbed H₂, and that the larger more crystalline nickel surface would increase the number of sites supporting the methoxy intermediate. In a study by the same group [96], the exact mechanism for the gas-phase decomposition of methanol was investigated over nickel supported on SiO₂. The rate determining step was reported to be the decomposition of the methoxy group intermediate to form adsorbed CO and H₂ gas as opposed to the desorption of CO or the breaking of the carbon hydrogen bond, which has also been reported to be the rate determining step of methanol decomposition [60]. The performance of nickel can be improved by the addition of dopant metals. Haruta *et al.* [97], reported that the addition of platinum to a Ni/SiO₂ catalyst results in an increase in methanol conversion, due to the formation of Pt-Ni alloys. The most highly ranked catalyst in Table 3-2 is Ni based [48]. However this is surprising because CH₄ is often produced as a by-product. The highly active Ni₃Al catalyst was formed by leaching the aluminium with a solution of NaOH. This leaching was necessary as it was reported that unleached alloy performed poorly in methanol decomposition [48]. CH₄ and CO₂ were the detected by-products. In that study methanol decomposition was conducted in a mixed methanol and water feed however on the basis of product spectrum, methanol steam reforming was discounted as a reaction route.

In the present study, a Raney nickel catalyst was synthesised and tested for methanol decomposition to test its activity with the standard methanol catalysts described. To

complement this catalyst, a nickel-boron based catalyst was synthesised and tested for comparison. The reduction of nickel salts with sodium borohydride in an aqueous solution yields a black powder precipitate that contains both nickel and boron. Until recently this material has been thought of as an amorphous alloy on the basis of powder XRD analysis. Recently, high resolution TEM studies have shown that the particles are not amorphous but contain an ultra-fine crystalline nano structure containing nickel metal crystals (1-3nm) bound by boron containing species [98]. The interest in this material relates to the fact that it has been shown to be highly active for a wide range of hydrogenation reactions. For example, recently the NiB alloy supported on MgO, was shown to be active for the hydrogenation of sulfolene and acetophenone to sulfolane and mixtures of ethylbenzene and 1-phenylethanol respectively [99].

3.5.2 Reaction data: Ni based catalysts

Figures 3-31 to 3-34 displays the data for the NiAl catalyst runs. The methanol conversion data is presented in Figure 3-31 and the STY data for the reactions performed at 250° C and 300°C in Figures 3-32 and 3-33 respectively. The methanol conversion increases from 60% to 100% when the temperature of the reaction is increased from 250°C to 300 °C. At 300° C the catalyst conversion drops from full conversion to approximately 80%. Comparing Figure 3-14 with Figure 3-31 it is evident that the STY values for H₂ and CO on the Ni based catalyst is roughly half that of the palladium based catalysts despite the comparable methanol conversions after 100 minutes on stream. The reason for this is that in the STYs the rates are mass normalized. For all of the decomposition reactions, 0.15g catalysts were charged. In the case of NiAl catalyst, a 0.30g catalyst charge was used as 0.15g was an insufficient amount to completely cover the reactor sinter.

At 250 °C there is a constant production of CO, H₂ and CH₄. The CH₄ is produced from the methanation of CO. This is not surprising since Raney Ni has been shown to be an effective CO methanation catalyst [100]. H₂O was an observed product as a result of methanation but was not quantified. It should be noted that these catalysts still produce CO with a high selectivity and the CH₄ and CO₂ by-products are produced at much smaller STYs. The STY ratios approach 7 for both temperatures over the NiAl catalysts indicating that despite the formation of by-products, CO and H₂ are produced in a 2:1 ratio.

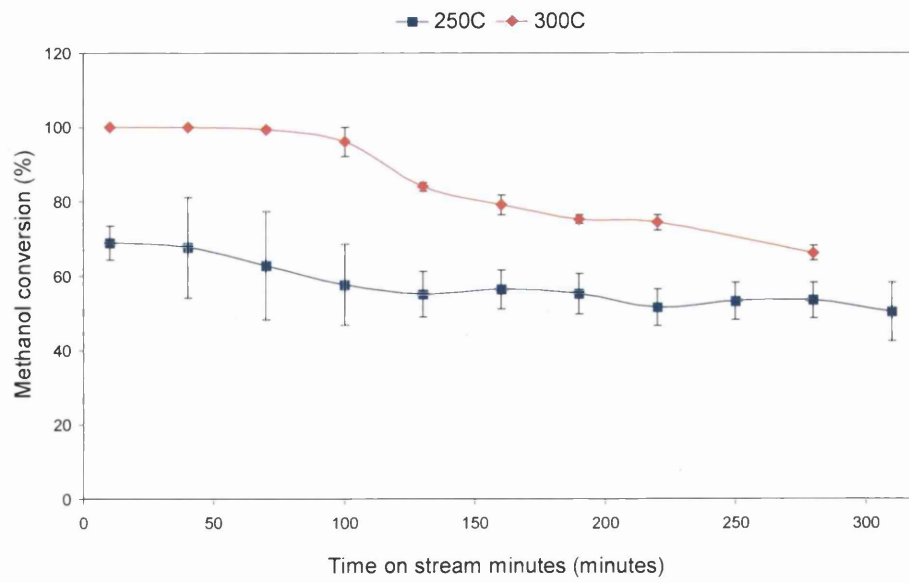


Figure 3-31: Methanol conversion for NiAl catalysts

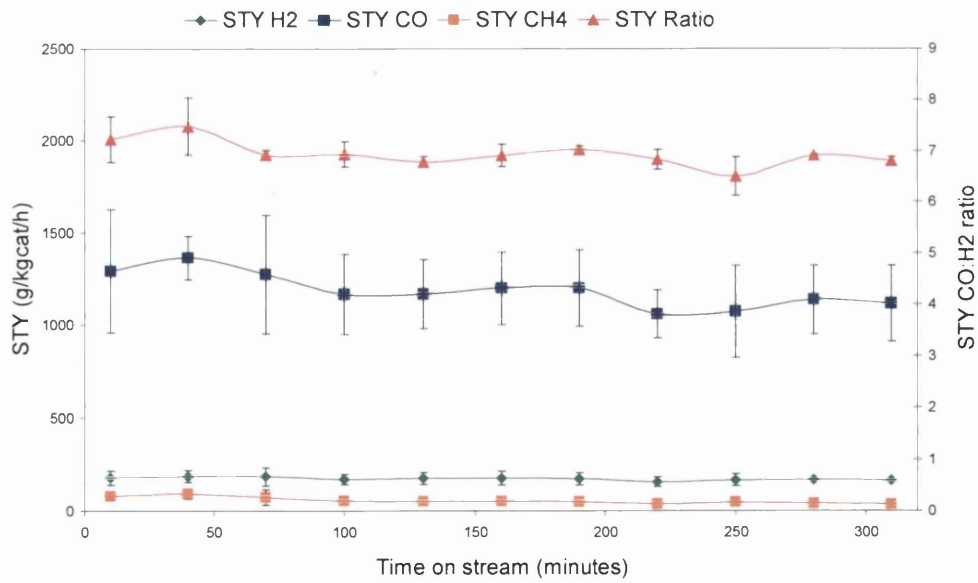


Figure 3-32: STY data NiAl catalyst at 250°C,

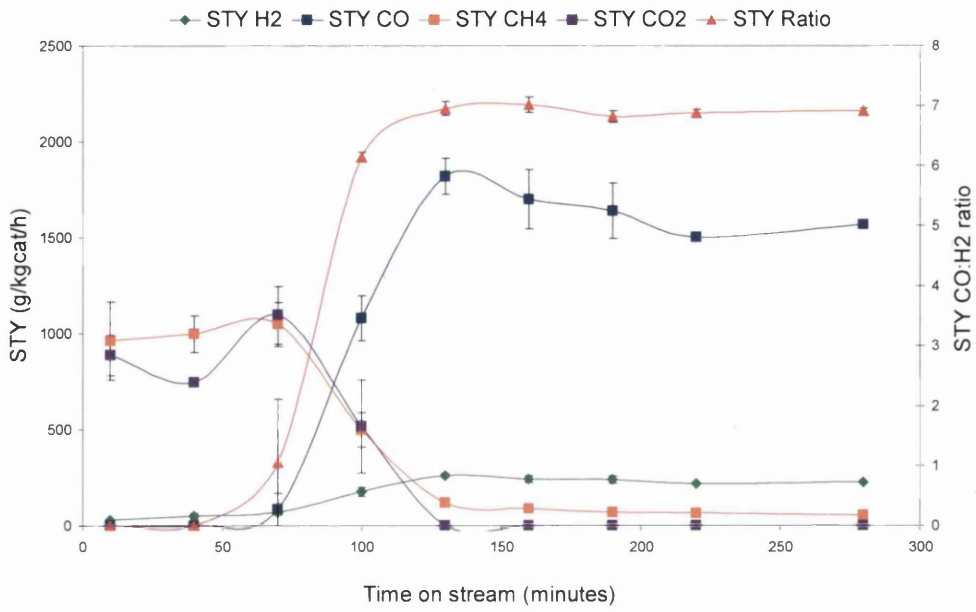


Figure 3-33: STY data, NiAl catalyst at 300°C

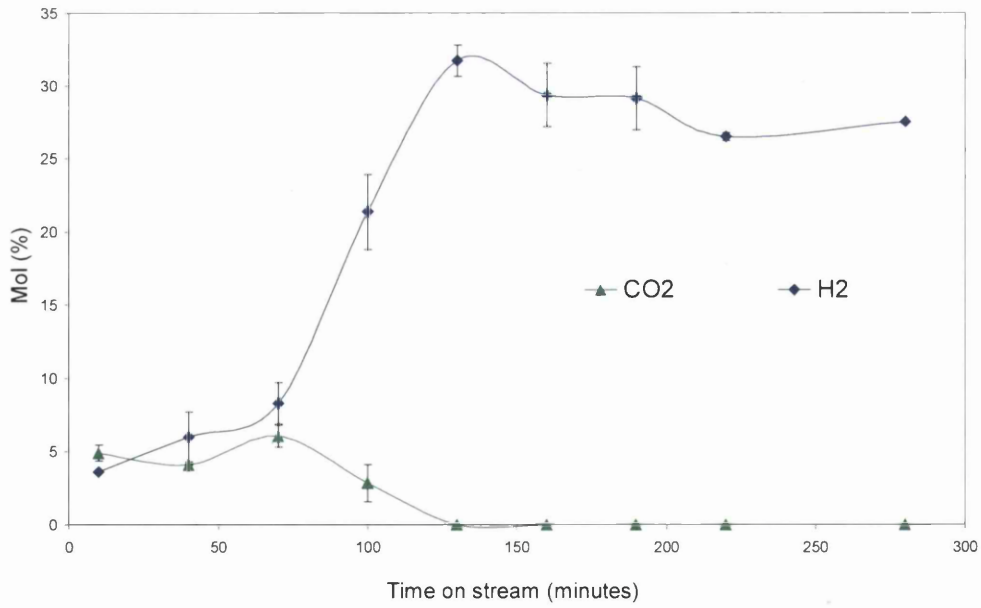
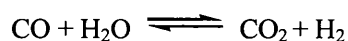


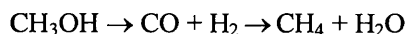
Figure 3-34: Mole percentage of CO₂ and H₂ produced at 300°C, NiAl catalyst

A different reaction profile is observed at 300 ° C compared with 250° C for methanol decomposition over the NiAl catalyst. At 300° C methanation dominates at full conversion. It is only after the conversion starts to fall that CO becomes an observed product. Once the methanol conversion starts to fall, the CH₄ production decreases and the production of CO and H₂ increases indicating that the catalyst deactivates with respect to methanation and methanol decomposition dominates after 100 minutes on stream. It can also be observed that CO₂ is produced at 300° C and follows a similar reaction profile to the CH₄ formation. It is known that the water gas shift (WGS) reaction proceeds over nickel based catalysts [101]:



The above pathway is implied from the molar ratio of CO₂ and H₂ within the first 75 minutes presented in Figure 3-34.

The observed lowering of the methanol conversion may be due to the laydown of coke on the catalyst, however no coke was observed on the spent catalyst (Table 3-9). The methanation step may occur only after the methanol has been decomposed to CO and H₂ in the following steps:



The CO and H₂ are therefore intermediates in the formation of CH₄ and are only observed once the methanation activity of the catalyst decreases. It is most likely that the cause of the observed reaction profile is simply deactivation of the catalyst with respect to methanation within the first 125 minutes on stream. Both metal sintering and coke laydown cause deactivation for nickel methanation catalysts [103]. There is a similarity between the results presented in this study and those performed by Kelley and colleagues, who performed a catalyst lifetime study on Raney nickel catalysts for methanation [100]. They reported that the catalyst deactivates after 2400 hours under standard conditions (300°C and 20 bar) and the causes of deactivation were investigated. It was found that there was an absence of any significant levels of carbon deposited on the deactivated catalyst after 2400 hours on stream. This is consistent with the findings presented in Table 3-8 where no coke was observed in analysis of the spent catalyst in the present study over a 5 hour reaction run. The primary cause of deactivation reported by Kelley was the sintering of nickel crystallites and the subsequent decrease in catalyst surface area. It is possible that in the

present study, this may be the cause of deactivation although this should be treated with caution as in the present study, direct methanation is not being performed and it occurred only as a secondary reaction after methanol decomposition.

Figure 3-35 is the XRD pattern for the NiB catalyst, exhibiting an amorphous pattern as expected. Figures 3-36- 3-38 illustrate the data for methanol decomposition over NiB. This catalyst is as active as the most active palladium based catalyst in the present study. The STYs exhibited are comparable to the most active Pd/Ce_{0.8}Zr_{0.2}O₂ catalyst at 300°C.

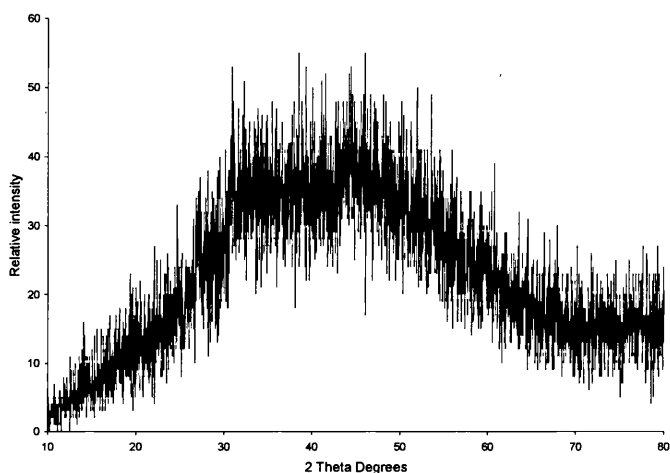


Figure 3-35: XRD pattern of NiB material

CH₄ is produced only at 300 °C over the NiB catalyst but the STY ratio indicates CO selectivity is high and CO and H₂ are produced in a 1:2 ratio. An activation profile for CO and H₂ is observed in Figure 3-40, although the NiB catalyst did not produce as much CH₄ as the NiAl catalyst within the first 100 minutes of reaction.

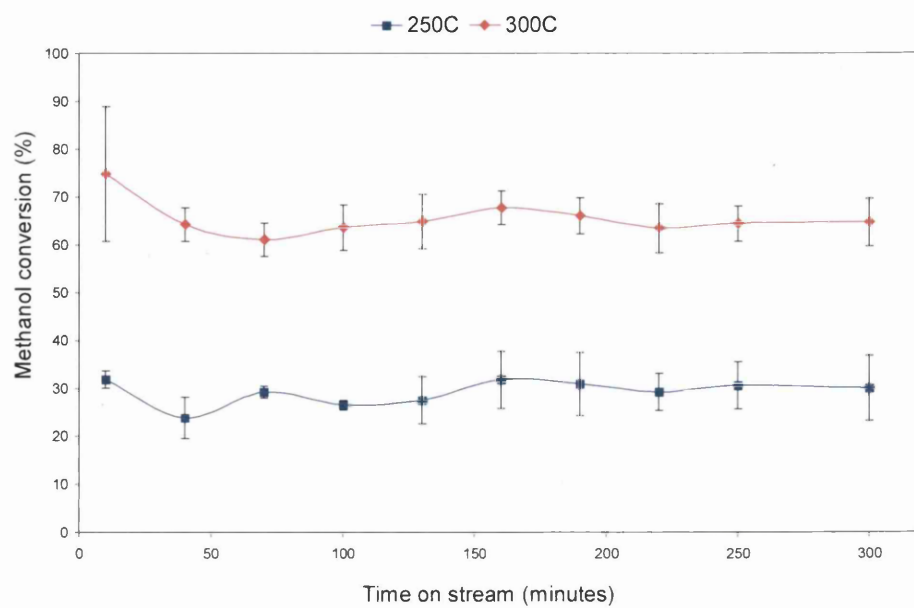


Figure 3-36: Methanol conversion for NiB catalyst

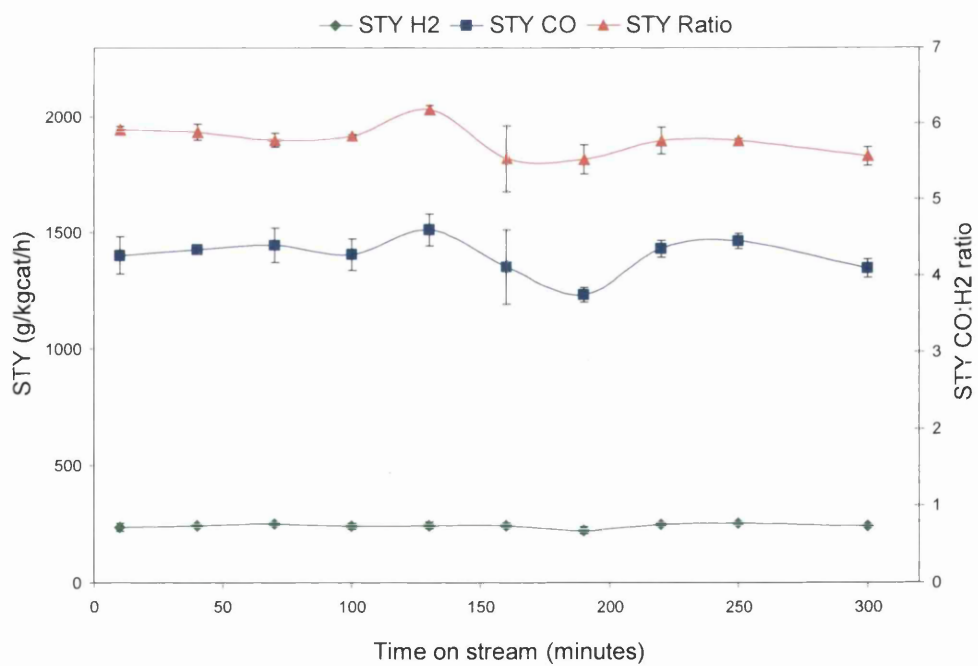


Figure 3-37: STY data at 250°C, NiB catalyst

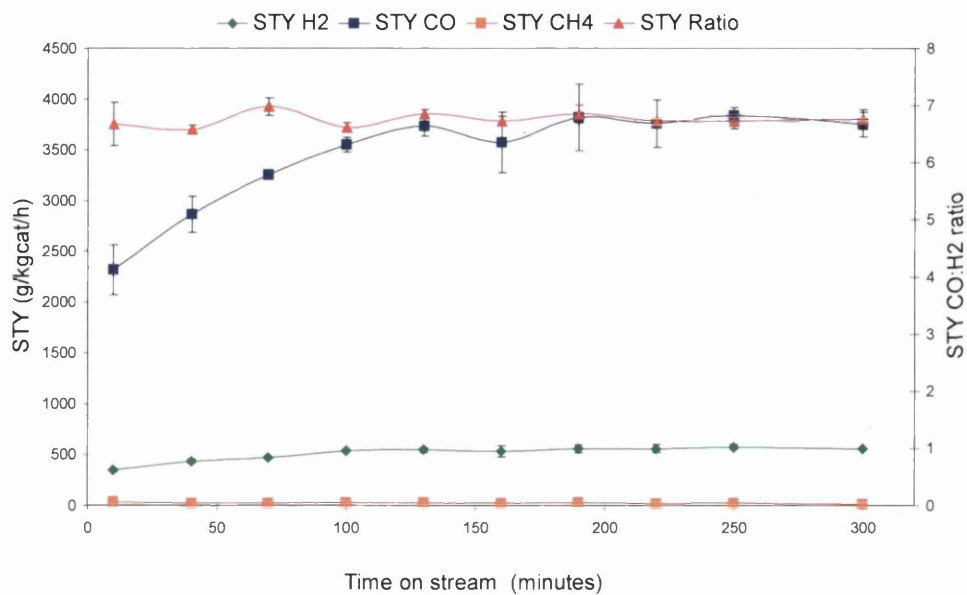


Figure 3-38: STY data at 300°C, NiB catalyst

Catalyst	BET surface area fresh catalyst (m ² /g)	BET surface area spent catalyst (m ² /g) at 300°C	Post reaction carbon content (wt%) ¹
NiAl	/	/	0
NiB	6	18	2.7

Table 3-9 Catalyst data for Ni catalysts, ¹ coke content calculated using CHN elemental analysis

It has been demonstrated that Raney nickel is active in methanol decomposition. Whilst CO is the major carbon containing product over this catalyst, an interesting reaction profile is observed with respect to by-product formation. CO is however produced at a higher rate by the novel application of a nickel boron catalyst.

3.6 Conclusions

Table 3-10 displays the summary for the activities of all the reported methanol decomposition catalysts in this Chapter. In conclusion, various methanol decomposition catalysts based on literature have been tested under directly comparable conditions and CO is produced at varying rates and selectivities. It can be observed from Table 3-10 that the catalysts prepared from palladium are more active than those based on copper and this agrees with the literature where copper based catalysts are perform poorly in the decomposition of methanol. It can also be observed that there is no relationship between palladium loading and catalyst activity in the present study and this is in agreement with the literature. The novel application of an amorphous nickel-boron alloy in methanol decomposition has however yielded the most active catalyst and exhibited STY production rates for CO and H₂ at rates similar to the most active palladium based catalysts. This suggests that active methanol decomposition catalysts may spread to a wider range of materials other than those commonly reported in the literature.

Catalyst	Reaction Temperature (°C)	Methanol conversion (%)	STY CO (g/kgcat/h)
NiB	300	66 ± 5	3445 ± 168
Pd(17wt%)/CeO ₂ ZrO ₂	300	74 ± 11	3291 ± 262
Pd (3wt%)/CeO ₂	300	78 ± 3	3228 ± 181
Pd(17wt%)/CeO ₂ ZrO ₂	250	51 ± 2	2116 ± 129
Pd(9wt%)/Al ₂ O ₃	300	33 ± 2	1911 ± 99
Pd(1.5wt%)/Al ₂ O ₃	300	36 ± 2	1767 ± 53
Pd(3wt%)/Al ₂ O ₃	300	30 ± 2	1443 ± 8
NiB	250	29 ± 3	1400 ± 36
NiAl ¹	300	86 ± 1	1340 ± 37
NiAl ¹	250	57 ± 8	1184 ± 213
Katalco	300	55	1173
Cu/ZnO	300	31	495
Katalco	250	16	106
Cu/ZnO	250	7	84

Table 3-10: Methanol conversion and CO STY formation rate for all studied methanol decomposition catalysts. 0.15 g catalyst loaded. Methanol concentration = 40mol % in Ar, Total flow = 40ml/min. 0.3 g catalyst loaded¹

4 Methanol decomposition over transition metal carbide and nitride materials

4.1 General introduction

In the previous chapter, common types of transition metal based methanol decomposition catalysts were synthesised and tested in order to make comparisons under comparable reaction conditions. Transition metal nitrides and carbides are of interest for the methanol decomposition reaction, due to the reputed ability of these materials to exhibit catalytic properties similar to platinum group metals. These materials present good alternatives due their lower cost and higher stability. There have been numerous examples in the literature where some metal carbide materials exhibit behaviour similar to that of the noble metals. For example it has been shown that molybdenum and tungsten carbides exhibit activity in CO hydrogenation [104]. In a study by Davis *et al.* [104], the face centred cubic (fcc) carbide phases of both tungsten and molybdenum catalyzed the formation of CH₄ and CO₂ via methanation and water-gas shift (WGS) reactions respectively. In a high pressure study using potassium doped β -Mo₂C carbides, Sun *et al.* [105] demonstrated that this material is active in the hydrogenation of CO to C₁-C₄ alcohols and C₁-C₄ hydrocarbons with the product distribution dependent on the level of potassium doping. Increasing the potassium doping was found to drastically increase the selectivity to alcohol formation. The gas phase hydrodechlorination (HDC) of mono- and di-chlorobenzenes has been shown to occur over α -Mo₂C/SiO₂ catalysts [106]. In that study the supported carbide catalyst was found to be more stable than a Ni/SiO₂ catalyst an established HDC catalyst. The catalytic behaviour of metal nitrides has mainly focused on γ -Mo₂N. For example it has been shown to be active in NO decomposition [107] and NH₃ synthesis [108]. Metal nitride catalysts have also been investigated for hydrogenation reactions including those for aromatics [109] and alkenes [110] which are reactions normally catalysed by platinum group catalysts. In light of these findings it is perhaps surprising that there has been little work exploring these carbide and nitride catalysts for methanol decomposition.

Metal carbides have however been shown to catalyse the dehydrogenation of methanol to methyl formate [111]. WC exhibited 81% selectivity to methyl formate whilst Mo₂C was found to selectively decompose methanol to CO with 100% selectivity at 20% conversion. Very recently Solymosi and co-workers have demonstrated that Mo₂C formed on

activated carbon and carbon nanotubes proved to be an effective catalyst for the decomposition of methanol to yield CO and H₂ [112]. The complete conversion of methanol was obtained at 350 °C and the CO selectivity was 67%. Formaldehyde, CH₄, C₂H₆ and CO₂ were observed as by-products and the production of formaldehyde was reported to increase with increasing Mo₂C loadings and temperature. The optimal catalyst loading was 5 wt% and activated carbon was found to be the superior support. The product spectra were the same for both supports although the carbon nanotube catalysts were less stable and rapid deactivation occurred within the first 100 minutes on stream. After 400 minute reaction runs these materials never reached steady state.

Molybdenum carbide and nitrides of interest are interstitial. They exist as close packed metal structures of molybdenum with the nitrogen and carbon atoms occupying interstitial sites within the lattice. Figures 4-1 and 4-2 are representations of the β -Mo₂C and γ -Mo₂N structures respectively. Figures 4-1 and 4-2 are adapted from reference [113] where the large spheres represent molybdenum atoms and the small spheres, carbon and nitrogen atoms. The structure of the β -Mo₂C polymorph is a hexagonal close packed arrangement of molybdenum atoms with half of the octahedral holes occupied by carbon atoms. The structure of the γ -Mo₂N polymorph can be described as a face centred cubic array of molybdenum atoms with the nitrogen atoms occupying one half of the octahedral sites. The δ -MoN structure can be described as a hexagonally close packed arrangement of molybdenum atoms with the nitrogen atoms occupying all of the octahedral interstitial sites and is analogous to NiAs.

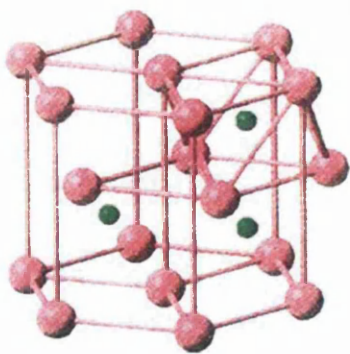


Figure 4-1: Hexagonal close packed β - Mo₂C

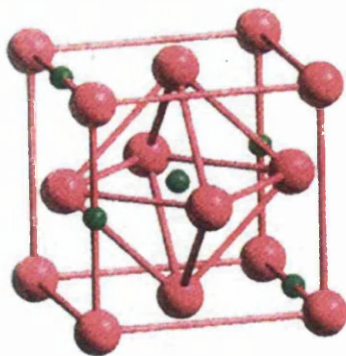


Figure 4-2: Face centred cubic γ -Mo₂N

It is the interaction between the molybdenum and these interstitial carbon atoms and nitrogen atoms which are thought to result in the catalytic behaviour of these materials. The origins of the behaviour of carbides, akin to the platinum group metals is discussed by Eberhart *et al.* [114] who conducted electronic structure calculations on WC. In that study the carbon p orbitals were found to hybridise strongly with the metal d orbitals, and the carbon s orbitals were found to hybridise with the metal s orbitals to form π and σ bonds respectively. The donation of electrons from the carbon atoms to the metal was argued to result in an increased concentration of pd electrons to the metal.

4.1.1 Synthesis of transition metal carbides and nitrides

Nitrides and carbides are classified as binary, ternary and quaternary, ie containing one, two and three metals respectively. There are many phases of nitrides and carbides, which have been synthesised and characterized with many new synthetic procedures resulting in the formation of new novel phases. In the present study of methanol decomposition have focussed on γ -Mo₂N, β -Mo₂N_{0.78} and β -Mo₂C phases as these have been studied the most widely in catalysis and could be synthesised by the most easily accessible methods. These materials are synthesised from the temperature-programmed reactions of molybdenum oxide and sulfide precursors, as described in detail in the experimental section.

The synthesis of β - Mo₂C is based on the temperature programmed reaction of MoO₃ with CH₄. The choice of carburization agent can affect the structure of the carbide. In a study by Xiao *et al.* [115], molybdenum carbides were prepared using CH₄/H₂, C₂H₆/H₂ and C₄H₁₀/H₂ mixtures. The resulting materials were characterized and the transformation pathways are summarised in Figure 4-3. Using CH₄ resulted in the hexagonal close packed (hcp) β -Mo₂C phase, whilst the cubic closed packed (ccp) alpha phase carbide (α - MoC_{1-x}) was formed using C₄H₁₀/ H₂ as the carburization agent. Using a C₂H₆/H₂ mixture resulted in a mixed phase carbide with the hexagonal phase predominant. The presence of H₂ in the feed mixtures was reported to reduce the amount of amorphous carbon deposited on the carbide material and the surface area of β -Mo₂C was larger when using C₂H₆ compared with CH₄. It was also reported that higher surface area carbides were an advantage as they were more active for the hydrodenitrogenation of pyridine [115].

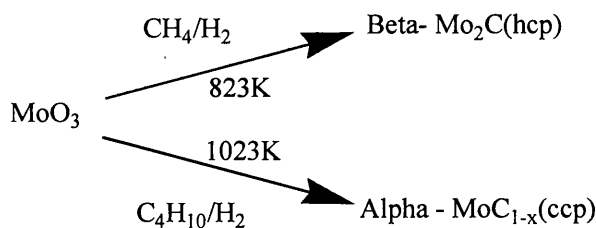


Figure 4-3: Effect of carburisation agent on the structure of Mo carbides

In a study by Hanif *et al.* [116], the optimal surface area using CH_4 was $70\text{m}^2/\text{g}$ and a surface area of $110\text{m}^2/\text{g}$ was formed using C_2H_6 at the optimum carburization temperature of 1073K . XRD studies illustrated that the reduction of the MoO_3 to the carbide occurred at lower temperatures resulting in smaller particles being formed and hence a larger surface area. Excessive temperatures above the optimum value resulted in sintering and a loss of surface area. In the present study, we were restricted to CH_4 as a carburization agent, however the synthesis were performed in mixtures of CH_4 and H_2 with low temperature ramping rates in order to give maximum surface areas.

The preparation of the nitride materials used in the present study are explained in detail in the experimental section. The synthesis of $\gamma\text{-Mo}_2\text{N}$ is normally performed by the temperature ammonolysis method, applied in the present study. Using different carburization agents can enhance the surface area of metal carbide based materials. The surface area of metal nitrides are a function of the synthesis variables applied during the temperature programmed reaction synthesis procedure. In particular high surface area $\gamma\text{-Mo}_2\text{N}$ materials are obtained by having high space velocities of NH_3 and controlled temperature ramping rates [117].

4.2 Results – Catalyst characterization

MoS_2 was the precursor material used in the synthesis of the $\delta\text{-MoN}$ and MoO_3 was the precursor material for the synthesis of all the other carbide and nitride materials. The XRD patterns of these precursors are displayed in Figure 4-4. Both materials are highly crystalline and are of low surface area. The surface area of MoO_3 is $4\text{m}^2/\text{g}$ and that for MoS_2 is $3\text{m}^2/\text{g}$. It can be observed that upon the formation of nitride and carbide materials, the reflections for the nitride and carbide phases become broad and less intense. This is due to the formation of smaller particles and an increase in disorder which occurs during

the temperature programmed reactions resulting in increased surface areas as observed in other studies [116].

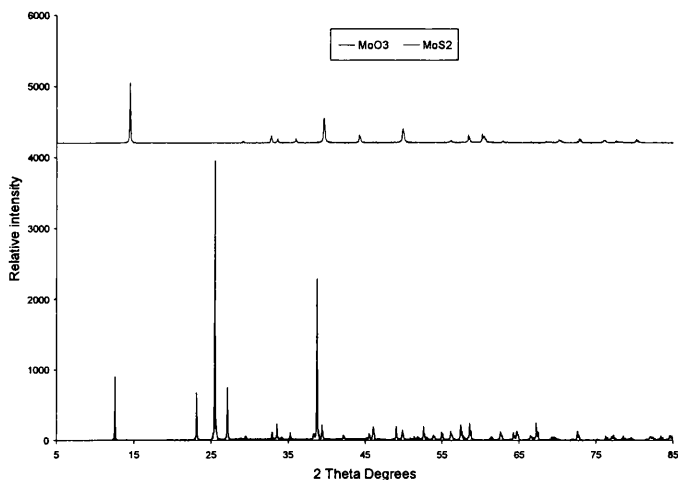


Figure 4-4: XRD pattern of MoS₂ and MoO₃ precursor materials

Figure 4-5 displays the XRD patterns for the spent β -Mo₂C catalysts after methanol decomposition. It should be noted that this material was synthesised on the methanol decomposition reactor and was not removed prior to reaction to prevent re-oxidation. As a result there are no patterns for the fresh catalysts. It can be observed that the two XRD patterns presented in Figure 4-4 are different. Pattern (a) is a pure phase β -Mo₂C material whereas pattern (b) containing an additional MoO₂ phase. These materials were synthesised under identical reaction conditions outlined in the experimental section. This was the temperature-programmed reaction of the MoO₃ precursor under CH₄/H₂ mixtures. The only difference between the preparation was the dwell time. The reaction was dwelled for 1 hour to synthesise the mixed phase carbide and it took a dwell time of 4 hours to completely convert all of the oxide into the pure phase carbide. Hanif and co-workers studied the phase evolution of the formation of β -Mo₂C [116]. In that study a number of techniques were used to elucidate the steps involved in the carburization of MoO₃ in mixtures of CH₄ and H₂. In particular the evolution of individual phases were observed during *in situ* XRD and carburisation experiments in mixtures of CH₄ and H₂. At

400 °C, H₂ reduced the MoO₃ to MoO₂ with the release of H₂O. The first carburisation of MoO₂ occurred at 550°C with the formation of an oxycarbide species (MoO_xC_y). The second carburization step occurred between 600 and 700 °C with some of the oxycarbide being reduced into the β-Mo₂C phase. Above 700° C all traces of the oxide disappeared with the formation of the pure phase β-Mo₂C. The carburization temperature employed in the present study was 650°C, which was sufficiently high to yield a pure phase carbide in the present study. There was no formation of an oxycarbide species in the XRD pattern of the spent catalyst as illustrated in Figure 4-5. It appears that the formation of the carbide occurs via the direct carburization of the MoO₂ species and the 4 hour dwell time is required for the complete conversion to the MoO₂ to the pure phase β-Mo₂C.

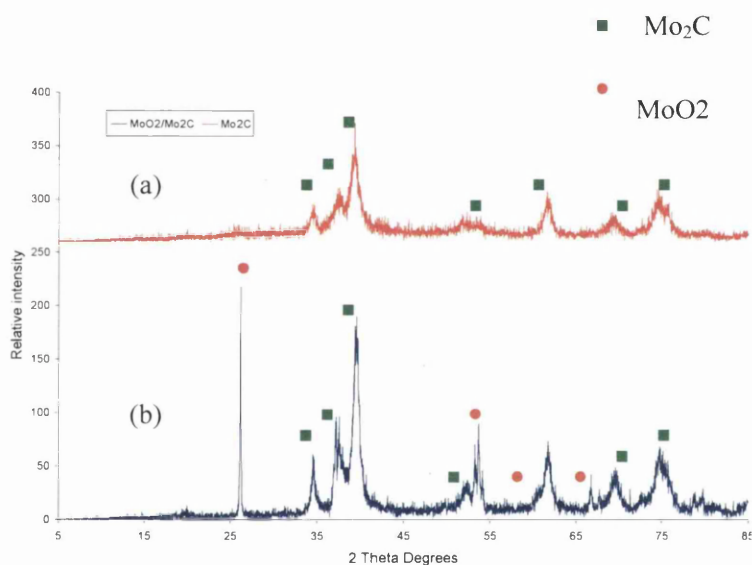


Figure 4-5: XRD of pure phase β-Mo₂C and mixed phase carbide. (a) 4 hour dwell time and (b) 1 hour dwell time

Figures 4-6 – 4-8 are the XRD patterns for the synthesised nitride materials. Figure 4-6 is the pattern for the β-Mo₂N_{0.78} phase, Figure 4-7 the γ-Mo₂N phase and Figure 4-8 the δ-MoN phase. Included in the Figures are the patterns for both the fresh catalysts and spent catalysts after a methanol decomposition reaction. It can be observed that the nitride

materials were all pure phases and no change of the bulk structures occurs after the methanol decomposition reactions.

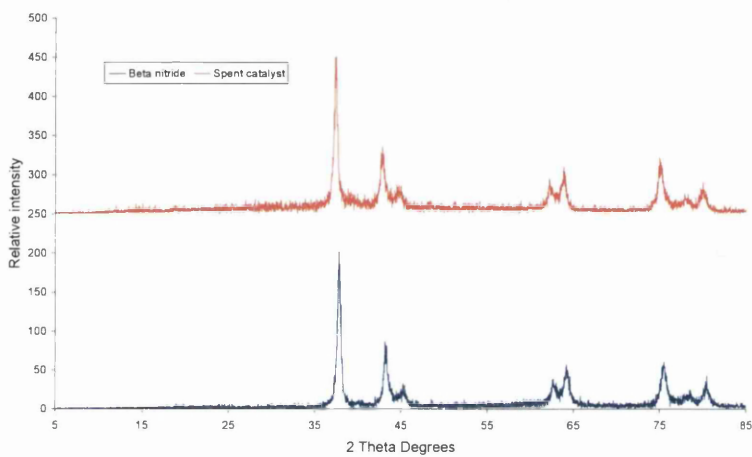


Figure 4-6: XRD of pure phase β -Mo₂N_{0.78}

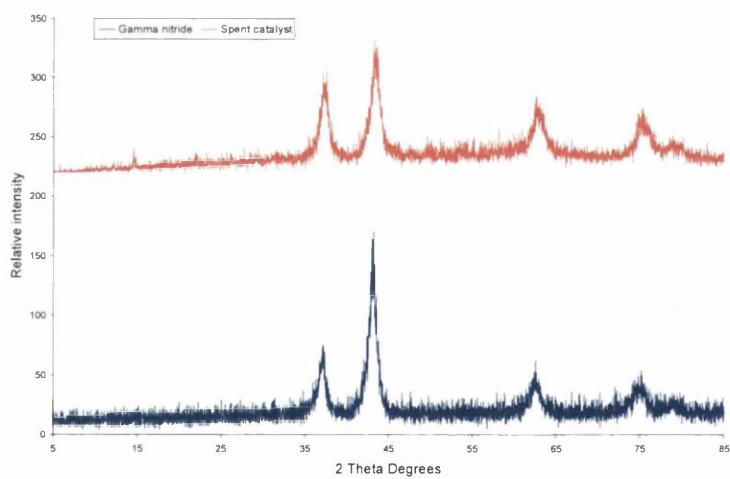


Figure 4-7: XRD of pure phase γ -Mo₂N

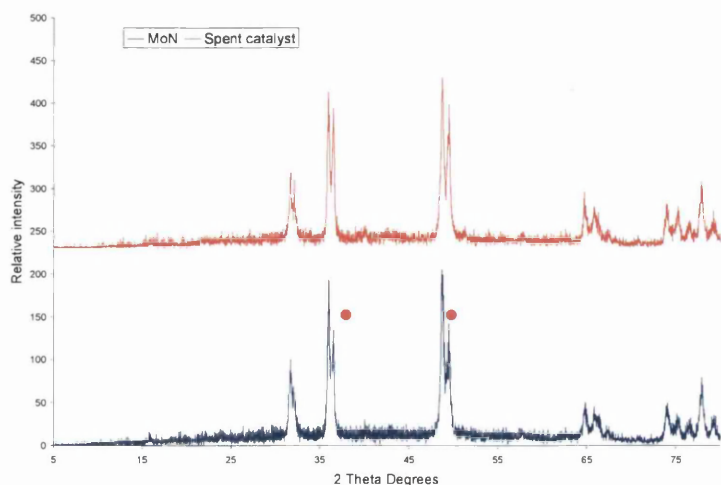


Figure 4-8: XRD of pure phase δ - MoN

It can be observed from Figure 4-8 that some of the peaks appear as doublets. The synthesis route to δ - MoN employed in the present study was the ammonolysis of low surface area MoS₂ as described in the experimental section. As noted by Marchand *et al.* [118], the temperature and final dwell time influences the surface area of the resulting nitride. In that study, a low surface area nitride (5m²/g) was synthesised at 785°C and a dwell time of 60 hours whilst at a temperature of 850° C and dwell time of 24 hours a high surface area (15m²/g) δ -MoN was synthesised. Marchand explains however, that a mixture of both high and low surface area δ - MoN can occur at both conditions, and other synthesis conditions such as space velocity need to be controlled in order to obtain either phase. In the present study a temperature of 785°C and dwell time of 60 hours were employed. The XRD pattern illustrates that there are additional shoulder peaks represented by red dots in Figure 4-8. It has been shown that it is possible to obtain 3 different forms of hexagonal, stoichiometric δ - MoN, by varying the preparation technique. In a study by Ganin et al [147], 2 different forms of δ - MoN were synthesised by the reaction of MoCl₅ or MoS₂ with ammonia by varying the synthesis method. In addition a third form could be synthesised by the reaction of Mo metal with ammonia. Crystal structure refinements from powder XRD indicated that all 3 phases contained different crystal structures. In the present study, the shoulder peaks present were rationalised by Marchand as a result of low and high surface area phases. However it is unlikely that this would result in shifts in XRD reflections. Based on the study of Ganin, it is more plausible that in the present study

there is the existence of 2 phases of δ - MoN, although further investigation would be required to confirm this hypothesis.

Catalyst	BET surface area of fresh catalyst (m ² /g)	BET surface area of spent catalyst (m ² /g)
β -Mo ₂ C	/	13
β -Mo ₂ C/MoO ₂	/	10
β -Mo ₂ N _{0.78}	9	4
γ -Mo ₂ N	85	28
δ - MoN	16	13

Table 4-1: BET surface areas of nitride and carbide catalysts,

Table 4-1 presents the surface area measurements for the synthesised catalysts. It can be observed that the nitride phases exhibit a wide range of surface areas with γ -Mo₂N having the highest surface area consistent with other studies [116].

4.3 Methanol decomposition

In the methanol decomposition studies, the reaction profiles show all of the observed products with the exception of CO₂. This is because there were issues with its detection as it was a low level product and it has been omitted from the plots for clarity. However, the mean value for its production, calculated from the sample readings when CO₂ was detected, has been presented on each of the plots. A standard error is also presented - calculated on the basis of the standard deviation of all of the CO₂ readings as described in Appendix 1.1.4

4.3.1 Precursor materials

The MoO₃ precursor materials were tested for the decomposition of methanol. The catalyst was inactive at the standard reaction conditions of 300 °C and methanol was only

converted at 400 °C. The conversion data is presented in Figure 4-9. Figure 4-10 presents the reaction profile. The STY ratio is below 7, indicating preferential selectivity loss to carbon containing products. CH₄ and CO₂ were the only observed by-products. With reference to Figure 4-11, it is evident that this material deactivates rapidly in the first 150 minutes on stream. The STY values are however very low and the molybdenum trioxide precursor material is not very active for the decomposition of methanol.

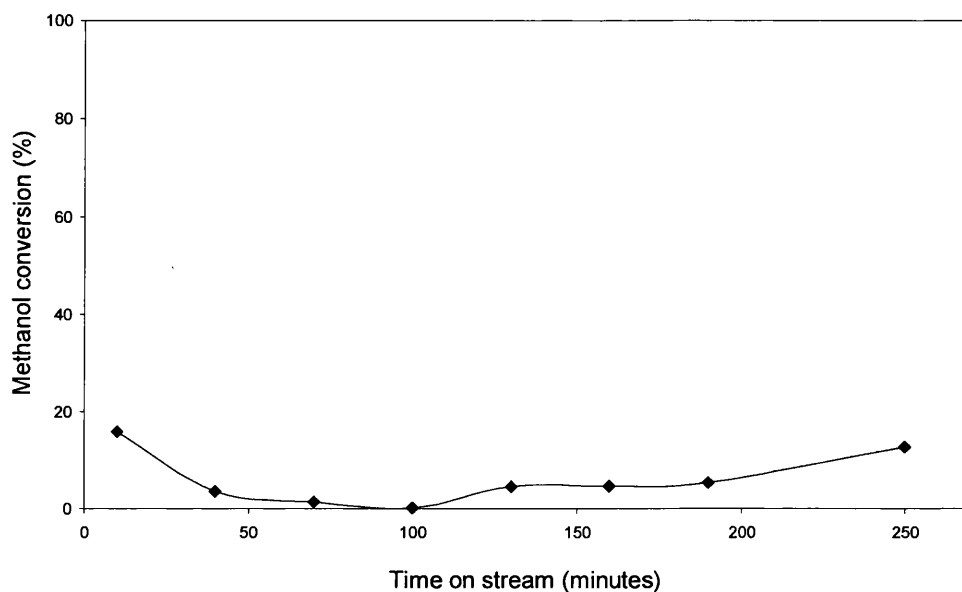


Figure 4-9: Methanol conversion for MoO₃ at 400°C

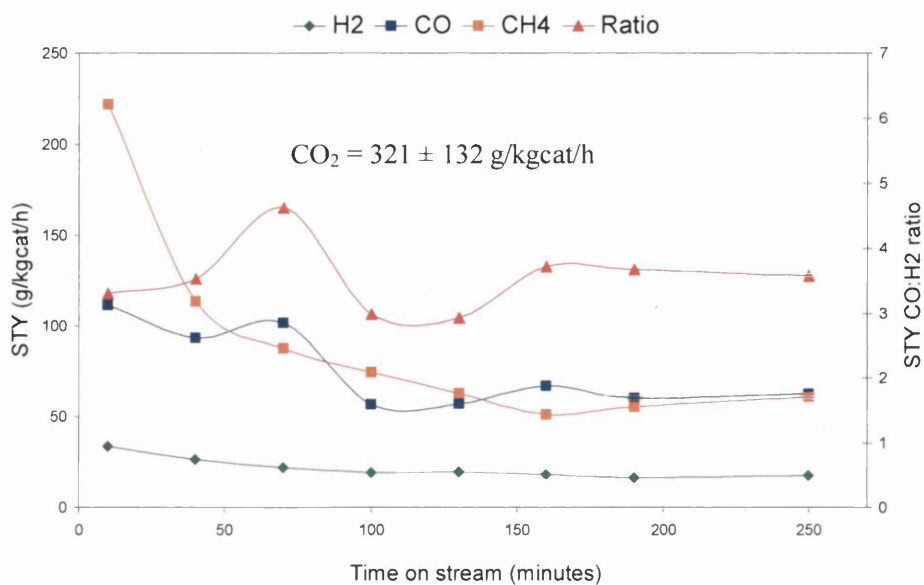


Figure 4-10: Methanol decomposition for MoO₃ at 400°C

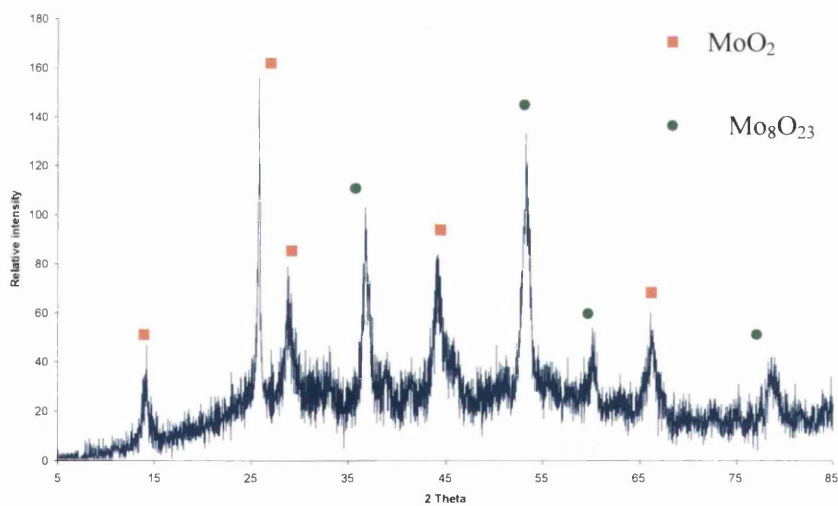
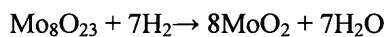
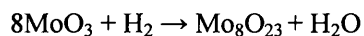


Figure 4-11: XRD pattern of spent MoO₃ catalyst

Figure 4-11 is the XRD pattern for the spent MoO₃ catalyst. It can be observed that there are no longer any reflections corresponding to MoO₃ indicating that during methanol decomposition, the MoO₃ has been reduced to MoO₂ and Mo₈O₂₃. This is not

surprising since it has been demonstrated that MoO₃ can be directly reduced under H₂ at 550 °C to MoO₂ [119]. In the present study the reaction temperature was 400 °C but it has been shown that the reduction of MoO₃ occurs slowly at this temperature under hydrogen via a Mo₄O₁₁ intermediate product [122]. Mo₈O₂₃ is observed in Figure 4-11 and it is possible that this is an intermediate reduction product and MoO₂ is produced from the following set of sequential reductions.



It is unknown whether the CO or the hydrogen produced from the decomposition are the reducing agents, although the low CO:H₂ STY ratio suggests CO may be the reducing agent.

4.3.2 Methanol decomposition – Carbides

The reaction data for the catalytic run of the mixed phase β-Mo₂C/MoO₂ catalyst is presented in Figures 4-12 and 4-13. The reaction was performed at 300 °C. CO, H₂ and CH₄ were the only observed products. It can be observed that the mixed phase catalyst deactivates rapidly within the first 50 minutes on stream and approached steady state at around a 25 % methanol conversion. Figure 4-13 illustrates that CO and H₂ decomposition products are produced and CH₄. No CO₂ was observed with the mixed phase carbide material.

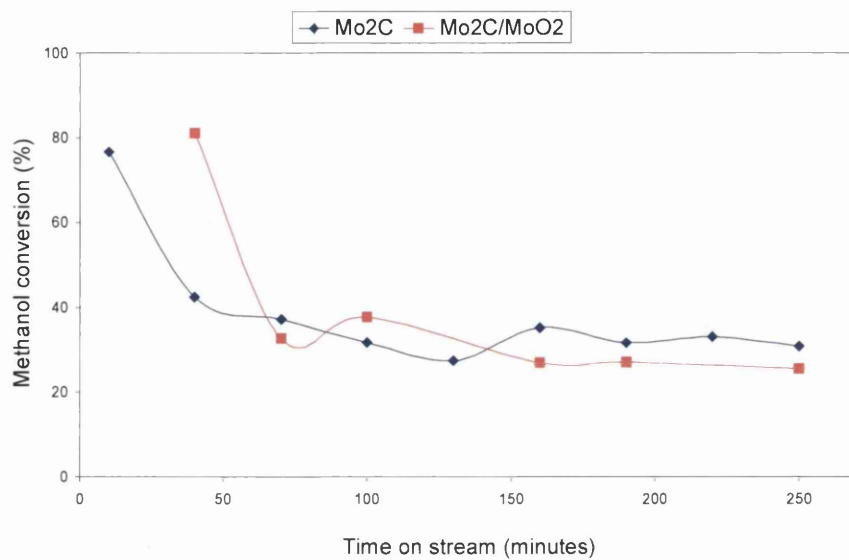


Figure 4-12: Methanol conversion for β -Mo₂C/MoO₂ and β -Mo₂C at 300 °C

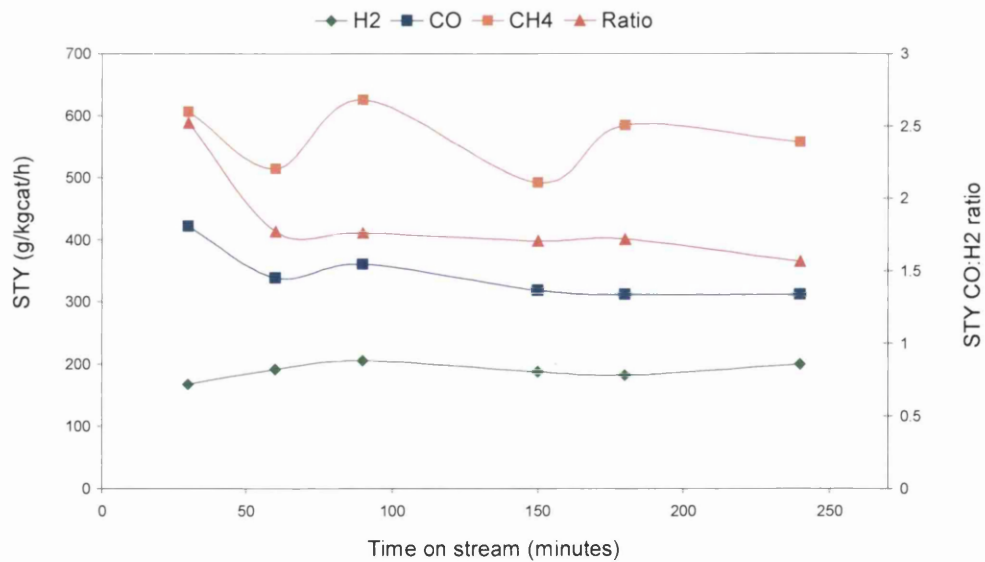


Figure 4-13: Methanol decomposition β -Mo₂C/MoO₂ at 300 °C

Figures 4-12 and 4-14 are the data for the pure phase β -Mo₂C. In addition to CO, H₂ and CH₄ products, observed with the previous mixed phase catalyst, CO₂ is also produced 120

with a mean value of 1176 g/kgcat/h. The pure phase β -Mo₂C deactivates within the first 100 minutes with the methanol conversion dropping and this is also evident when looking at the formation of the products in Figure 4-14 where the formation rate of CH₄ and CO decreases within this time.

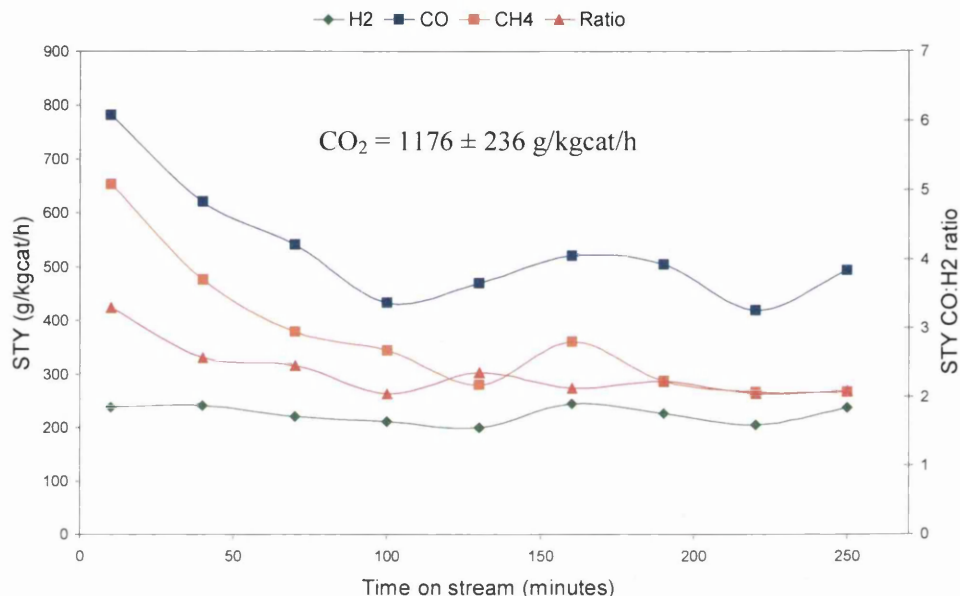


Figure 4-14: Methanol decomposition β -Mo₂C at 300°C

With reference to Figure 4-12 there is a comparable methanol conversion with the pure and mixed phase carbides. After 200 minutes on stream the mixed phase catalyst has a CO STY of 327 g/kgcat/h whereas the pure phase carbide produces CO at 421 g/kgcat/h. The most striking difference between the 2 materials is the production of CO₂ which is not detected over the mixed phase catalyst. The product spectrum with the pure phase catalyst is analogous to that in the study by Solymosi and co-workers described in the introduction section [120]. In that study, there was no selectivity data reported over the pure phase catalysts. However in agreement with the present study, H₂, CO, CH₄ and CO₂ were the main products. The low STY CO:H₂ ratios present over both carbide catalysts suggest that CO selectivity is lost, possibly to a product which is not detected. It has been shown that Mo₂C supported on carbon produces formaldehyde as the major carbon containing product in the temperature range 250-300° C [112]. It is possible that in the present study that this

product is formed but not detected, since it may be below the detection limits of the system.

4.3.3 Methanol decomposition – Nitrides

Figure 4-15 is the methanol conversion data for the $\beta\text{-Mo}_2\text{N}_{0.78}$ catalyst and the reaction was carried out in a temperature programmed regime due to the rapid deactivation profile observed. It is evident that the $\beta\text{-Mo}_2\text{N}_{0.78}$ catalyst is less active than both of the mixed phase and pure phase carbide catalysts which achieve comparable conversion at a lower temperature of 300 °C to that observed at 400 °C. CO, H₂ and CH₄ were the observed products over $\beta\text{-Mo}_2\text{N}_{0.78}$ and the STY data is presented in Figure 4-16. The production of both CO and H₂ increases with increasing temperature but the CH₄ production increases from 300-350°C and decreases when the temperature is increased to 400°C indicating that the selectivity to CH₄ is reduced. The STY ratio is between 6 and 7 at all temperatures and indicates that CO and H₂ are produced in a ratio around 2:1.

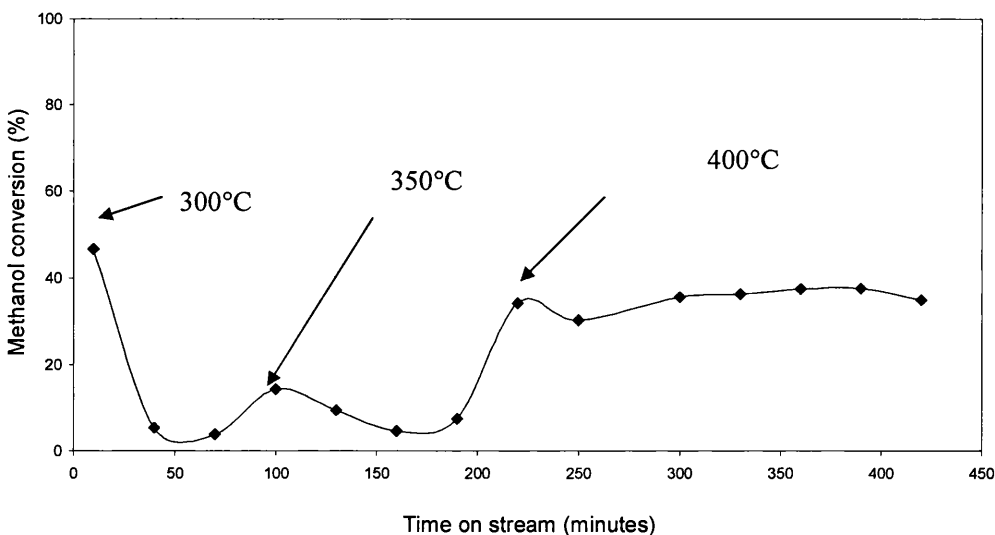


Figure 4-15: Methanol conversion for $\beta\text{-Mo}_2\text{N}_{0.78}$ at 300°C/350°C and 400°C

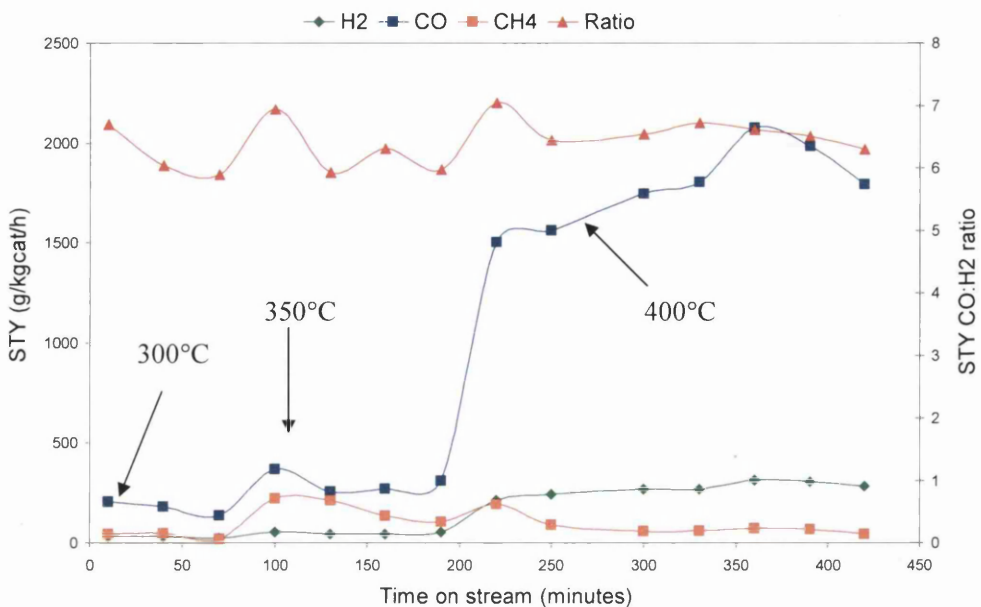


Figure 4-16: Methanol decomposition for $\beta\text{-Mo}_2\text{N}_{0.78}$ at 300°C/350°C and 400°C

Figures 4-17 and 4-18 illustrate the reaction data for methanol decomposition over $\gamma\text{-Mo}_2\text{N}$ at 250°C and 300°C. At both temperatures, this catalyst has a high initial activity but the catalyst rapidly deactivates as the methanol conversion falls, and the production of CO, H₂ and CH₄ decreases. It can be observed in Figure 4-18 that the CO:H₂ STY ratio increases when the temperature is increased from 250 °C to 300°C, but the ratio is between 4 and 5 at 300 °C indicating preferential CO selectivity loss. CO₂ was not an observed product at 250°C but was produced at 300°C with a mean STY value of 508 g/kgcat/h.

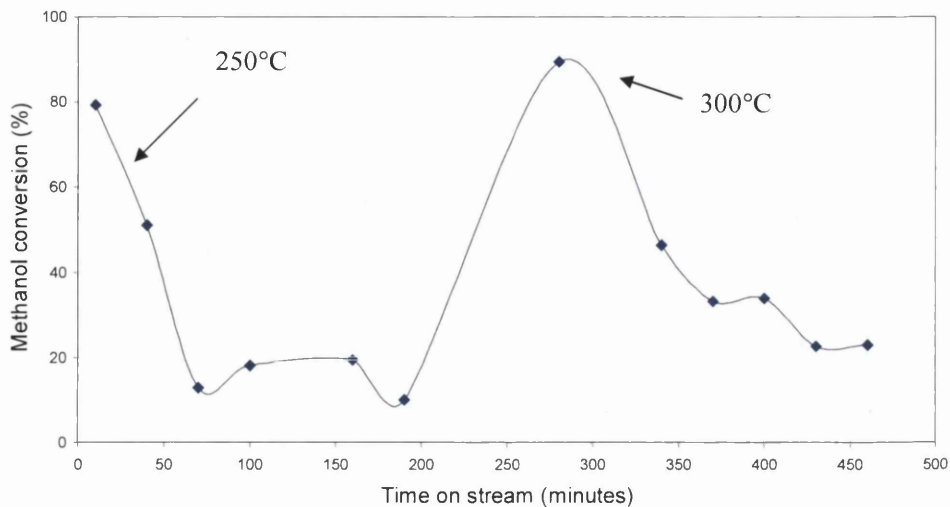


Figure 4-17: Methanol conversion for $\gamma\text{-Mo}_2\text{N}$ at 250°C and 300°C

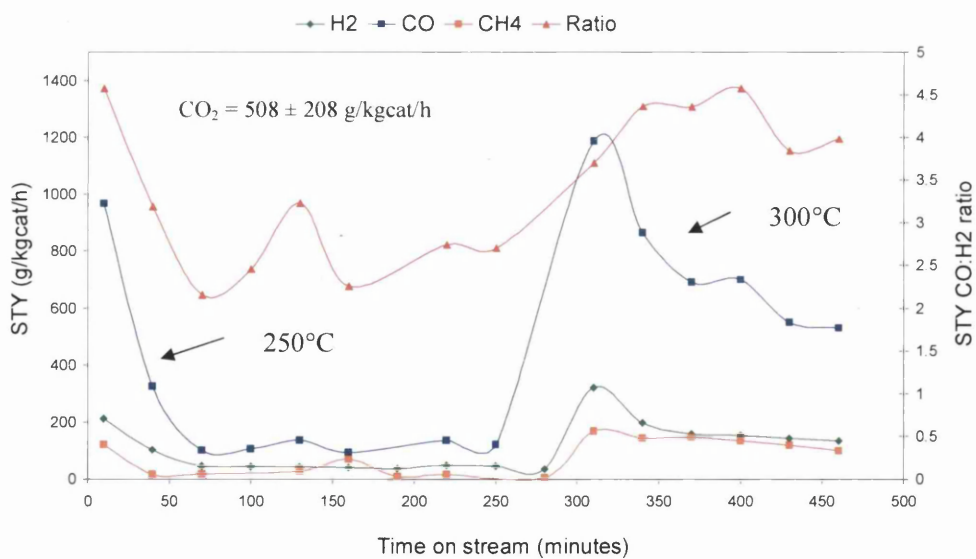


Figure 4-18: Methanol decomposition for $\gamma\text{-Mo}_2\text{N}$ at 250°C and 300°C

Figures 4-19 and 4-20 illustrate the reaction data for $\delta\text{-MoN}$ at 250°C and 300°C. It can be observed that the activity of this catalyst is low at these temperatures as the methanol

conversion is less than 10%. Trace amounts of CO, H₂, and CH₄ are observed products at 250 °C. When the temperature is increased to 300 °C, CO₂ becomes the major product. It can be observed that the STY CO:H₂ ratio is very low below 2 indicating CO preferential selectivity loss. Based on the high CO₂ production rate is most probable that the CO is being converted to CO₂ via the water-gas shift reaction or the Boudouard reaction.

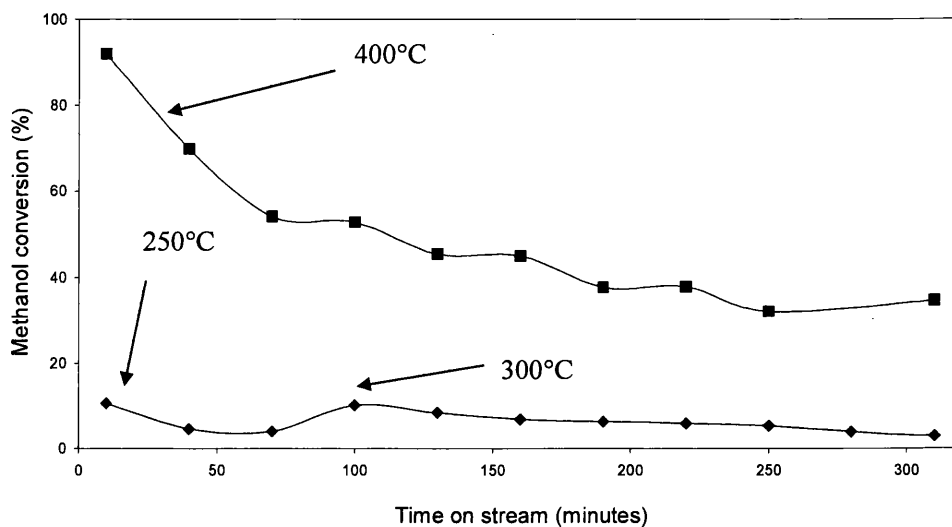


Figure 4-19: Methanol conversion for δ - MoN at 250°C, 300°C and 400°C

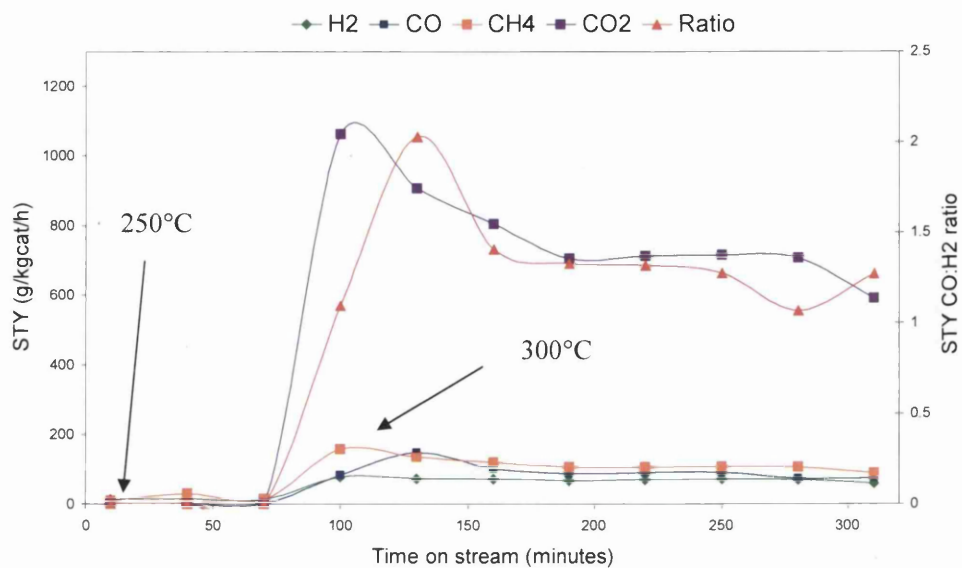


Figure 4-20: Methanol decomposition for δ -MoN at 250°C and 300°C

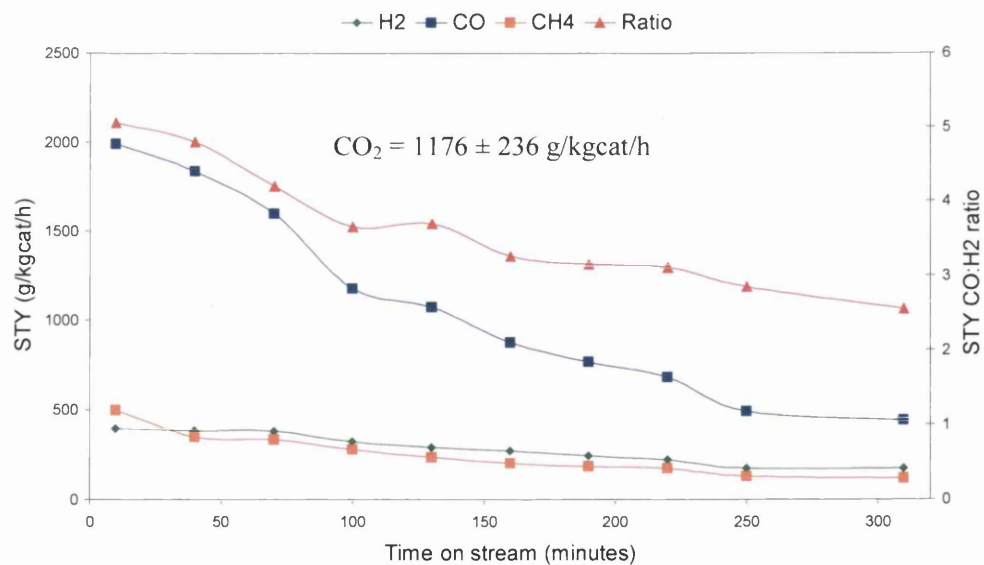


Figure 4-21: Methanol decomposition for δ -MoN 400°C

Figures 4-19 and 4-21 show the methanol conversion and product production activity for δ -MoN at 400°C. This catalyst has a high initial methanol conversion which decreases

with time on stream. CO, H₂, and CH₄ are produced at this temperature. CO₂ was produced also and the mean rate of production is 1176 g/kgcat/h.

It is evident from inspection of the previous Figures that all of the carbide and nitride catalysts exhibit different activities in methanol decomposition. CO and H₂ are observed products indicating that these catalysts are active for the decomposition of methanol. However all of the nitrides and carbides tested in the present study are not very selective in the formation of CO, with a notable exception being β -Mo₂N_{0.78} which is the most active for CO formation at 400 °C with only a low formation rates for CH₄ observed. The high selectivity to CO is also reflected in the high CO: H₂ STY ratio observed in Figure 4-16 and the largest STY value for CO over this series of catalysts.

CH₄ is a commonly observed by-product produced with all of the reported materials. This is not surprising since it has been shown that CO hydrogenation occurs over both γ -Mo₂N and β -Mo₂C at 300°C [121]. In that study, Reimer and co-workers reported that CH₄ was the main product with C₂H₄ and C₂H₆ by-products produced. γ -Mo₂N and α -Mo₂C were reported to be twice as active when compared with β -Mo₂C. The difference in activity was attributed to differences in the structure of the principle planes exposed by each face.

In the present study CO₂ is observed over γ -Mo₂N, β -Mo₂C, and δ -MoN which exhibits the highest formation rate for CO₂ at 400° C. Notably CO₂ is not produced over Mo₂C/MoO₂ and β -Mo₂N_{0.78} materials. There is certainly an issue with CO₂ detection as there was a large degree of oscillation and this is reflected with the high errors reported for the mean STYs. The production of CO₂ has been postulated to occur via the WGS reaction in the present study. In order for the WGS reaction to occur, a source of water is required. Methanation produces water which is observed in the product spectrum for all of the reported nitrides and carbides. It follows that CO₂ is produced by the sequential reactions of methanation followed by WGS. In a study by Davis *et al.* [104], CO hydrogenation was studied over the fcc polymorph of molybdenum and tungsten carbides. In that study, CH₄ and CO₂ were reported as the major carbon containing products at 270°C over a α -Mo₂C catalyst. At that temperature the selectivity of CO₂ was reported to be 55% and the selectivity of CH₄ 40%. In a CO hydrogenation study over α - and β - Mo₂C by Reimer *et al.* [121], CH₄ is always observed although no CO₂ was observed. In the present study further studies would need to be performed to gain a further understanding as to the nature of these materials with respect to CO₂ production.

Figure 4-25 displays the mean methanol conversion at 300°C as a function of BET surface area for all of the studied nitride catalysts. There is a relationship observed whereby the larger surface area materials exhibit the greatest activity with respect to the nitride catalysts. The carbide catalysts exhibit a methanol conversion similar to that of $\gamma\text{-Mo}_2\text{N}$ although it should be noted that the BET surface areas in the plot are of the spent catalysts. The surface area may not simply explain the high activity of the carbide catalysts. In a study by Aika *et al.* [108], a series of nitride and carbide catalysts were studied for ammonia synthesis. In that study a $\beta\text{-Mo}_2\text{C}$ material was more active than a $\gamma\text{-Mo}_2\text{N}$ despite having a smaller BET surface area ($32\text{m}^2/\text{g}$) compared with $140\text{m}^2/\text{g}$ for the nitride. It should also be noted that a high methanol conversion does not necessarily mean that the catalyst is more active in the formation of CO due to the formation of by-products. For example the most active nitride material is $\gamma\text{-Mo}_2\text{N}$ but this also exhibits a high selectivity to CO_2 and CH_4 .

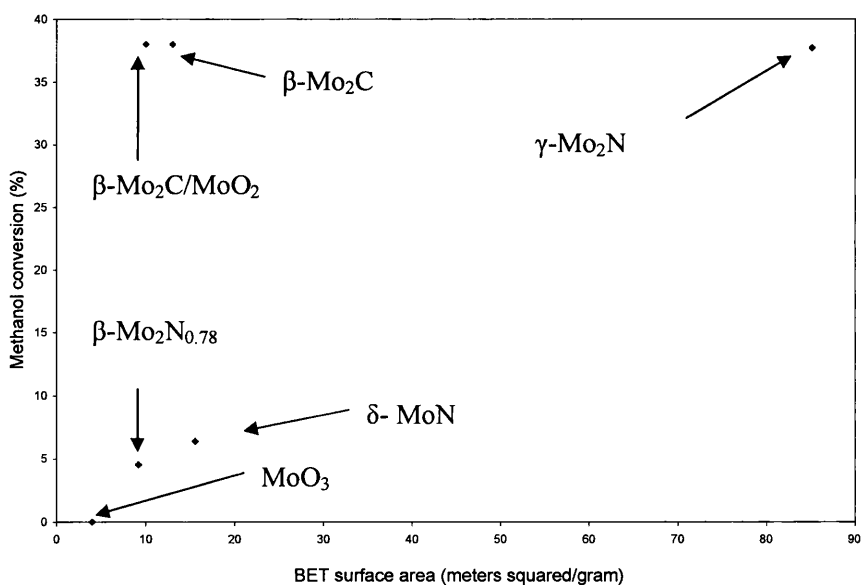


Figure 4-22: Methanol conversion at 300°C for molybdenum nitride and carbide catalysts as a function of BET surface area

4.3.4 Carbon and nitrogen analysis of nitride and carbide catalysts

A common trend is that all of the catalysts deactivate with time on stream. It can be observed from Table 4-1 that the spent catalysts have a lower surface area. The XRD patterns for all of the spent catalysts indicate that the bulk structure of the carbide and nitride materials remains unaffected after the reaction. Table 4-2 displays the CHN data for the fresh and spent samples. This has been used to calculate the amount of coke on the catalysts after reaction. It can be observed that carbon has accumulated on all of the spent catalysts. It is also evident that the nitride catalysts have lost nitrogen when comparing the pre- and post-reaction elemental analysis. In ammonia synthesis it has been shown the catalyst stability is reduced by the exchange loss of carbon and an increased amount of nitrogen over carbide catalysts [108].

Catalyst	Carbon content (wt%)	Amount of N in fresh catalyst (wt%)	Amount of N in spent catalyst (wt%)	Theoretical amount of N (wt%)
β -Mo ₂ C	0.8 ¹	/	/	/
β -Mo ₂ N _{0.78}	3.6	5.5	5.4	5.4
γ -Mo ₂ N	0.9	9.6	7.3	6.8
δ - MoN	1.9	12.7	12.3	12.7

Table 4-2: CHN data for nitrogen content and coke content on spent catalysts. It was assumed that the fresh catalyst contains 5.9wt% carbon¹

4.3.5 Conclusions

Molybdenum carbides and nitrides are active for the decomposition of methanol and behave similarly to the transition metals reported in the previous chapter. Table 4-3 displays the STY value for the highest rate of CO formation for the nitride and carbide materials. Common to all of the nitride and carbides is the production of CH₄. This behaviour is often exhibited by nickel-based catalysts as observed in the previous chapter. Although nitride and carbide catalysts act like nickel based materials in the present study with respect to CH₄ production it should be noted that the nitrides and carbides are active at higher temperatures compared with the nickel based catalysts. The carbide and nitride materials are also less selective to CO formation with the notable exception of β -Mo₂N_{0.78} which exhibits the largest STY formation rate for CO amongst the set of molybdenum nitride and carbide catalysts.

Catalyst	Reaction Temperature (°C)	STY CO (g/kgcat/h)
NiB	300	3820
β -Mo ₂ N _{0.78}	400	2081
NiAl	300	1817
δ -MoN	400	1989
γ -Mo ₂ N	300	1189
β -Mo ₂ C	300	784
β -Mo ₂ C/MoO ₂	300	422
MoO ₃	400	112

Table 4-3: STY data for CO production over molybdenum carbide and nitride catalysts

5 Methanol carbonylation

The project discussed in this thesis is concerned with the halide free heterogeneous catalytic production of acetic acid via a route involving only methanol as a feedstock. As discussed, the proposed route involves the incomplete decomposition of a methanol feedstream followed by a methanol carbonylation step. In such a system, the decomposition catalyst must not be too active in the given temperature range in which the carbonylation occurs in as this would deplete reactant methanol. A high selectivity to CO is also desirable. In the present study methanol decomposition catalysts were tested in the range 250 – 400 °C and the activities were summarised at the end of the previous results Chapters. Hydrogen was the major by-product of the methanol decomposition and the results presented illustrate that CO and H₂ were produced with varying ratios. It was demonstrated that at a temperature of 300°C, palladium and nickel based methanol decomposition catalysts produced CO at the highest rates and selectivity.

Several catalysts are active for the halide free, carbonylation of methanol as discussed in Chapter 1. In the present study, a copper mordenite catalyst was selected for the atmospheric carbonylation of methanol because it has been shown that this material is active for carbonylation in the temperature range at which CO production occurs over the methanol decomposition systems to be run in parallel [19].

5.1 Methanol Carbonylation

The methanol carbonylation experiments were carried out at atmospheric pressure and conditions which are similar to those required by a methanol decomposition catalyst in a coupled system. As discussed in Chapter 1, the copper mordenite catalyst behaves in a characteristic manner with respect to carbonylation. Initially hydrocarbons are the main products formed via methanol to gasoline (MTG) chemistry. Some of the hydrocarbons produced in this phase are polymethylbenzenes which are retained within the pores of the mordenite and were not quantified in the current study. As noted by Smith and co-workers [19], such products accounted for less than 15% of the methanol converted, even in the initial stages of the reaction where MTG is at a maximum. The second phase of the reaction was reported to be an increase in acetyls formation [19] and acetic acid and methyl acetate became the major products. In the final phase of the reaction, the selectivity

to acetyls started to reduce after 10 hours on stream and was replaced by the formation of DME, which became the major product.

Figure 5-1 contains the STY data for methanol carbonylation at 300 °C. As part of the current study, three separate reactions were run and the reaction was stopped after 180, 330 and 600 minutes on stream. STY data was calculated for each given product. It should be noted the 600 minute run was a continuation of the 330 minute experiment using the same catalyst re-started the next day and hence the plot is not representative of a continuous reaction. It does however present the activities for the main products as a function of the time that the copper mordenite is exposed to the reactant mixture. In addition to the main products reported, trace amounts of hydrocarbons and oxygenates, including C₄–C₅ hydrocarbons, ethanol, acetaldehyde, acetone, propionic acid, ethyl acetate and methyl formate were detected. It is evident from Figure 5-1 that methanol carbonylation at atmospheric pressure follows a similar trend as to that 10 bar. The production of methane, ethylene and propylene indicative of MTG and methanol to olefin (MTO) chemistry decreases after 600 minutes on stream, whilst the production of DME increases. There is also evidence of deactivation with respect to the production of acetyls because acetic acid and methyl acetate have the lowest STY values after 600 minutes on stream. However Smith and co-workers observed deactivation with respect to acetyls only after 15 hours on stream [19].

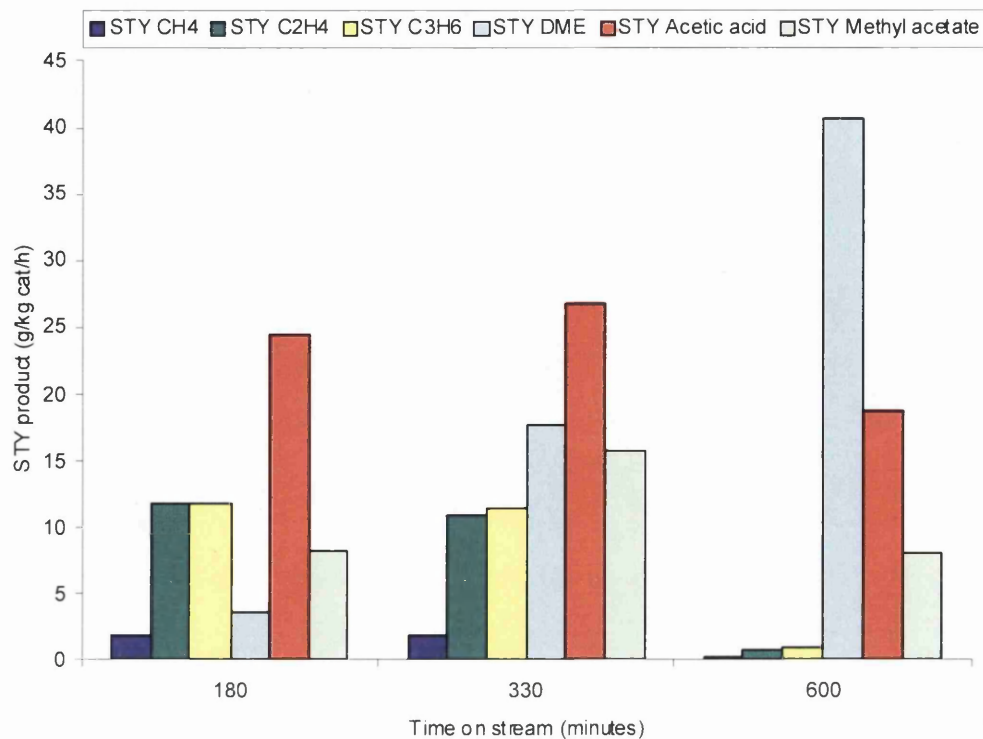


Figure 5-1: Methanol carbonylation over copper mordenite. Reaction temperature = 300 °C, GHSV = 2421 h⁻¹, volume of catalyst = 5 ml, CO/methanol molar ratio = 12

The production of polymethylbenzenes was not directly quantified but elemental analysis was carried out on the samples to determine the amount of carbon accumulated on the mordenite during the separate stages of reaction. The results are presented in Table 5-1. In addition, an experiment was carried out whereby the mordenite was taken off stream after 60 minutes and analysed for carbon content. No STY data is presented in Figure 5-1 for this because there was an insufficient volume of liquid collected in the knock-out pot to quantify the products.

Time on stream (minutes)	0	60	180	330	600
Carbon content (wt %)	0	4.2	8.1	9.2	9.9

Table 5-1: Carbon content on spent copper mordenite catalysts after various times on stream

It is evident that most of the carbon is laid down on the mordenite within the first 180 minutes on stream. This is consistent with MTG chemistry being at a peak within the initial stages of the reaction [19]. Figure 5-2 is the N₂ physisorption isotherm for the fresh copper mordenite catalyst. It can be observed that the isotherm is a composite Type I and Type IV isotherm (BDDT classification [129]), which indicates that the copper mordenite structure contains both micropores and mesopores. The total pore volume of the fresh copper mordenite was calculated to be 0.21ml/g.

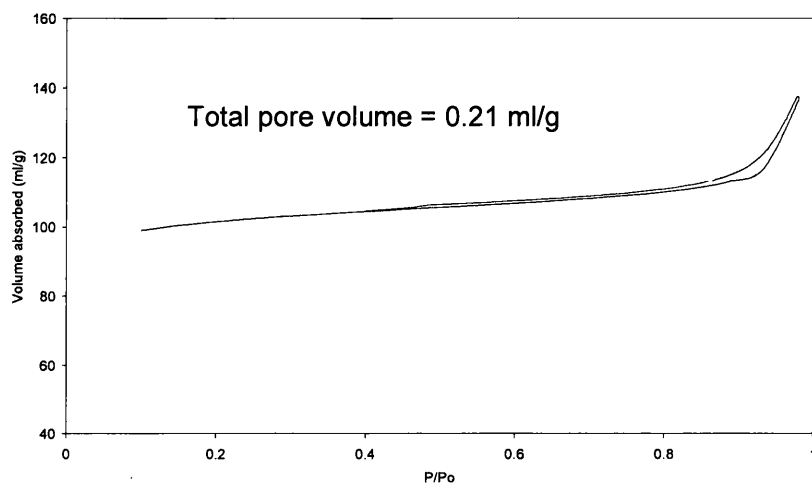


Figure 5-2: N₂ isotherm for fresh copper mordenite containing type H3 hysteresis

Figure 5-3 and 5-4 present the BET physisorption isotherms for spent copper mordenite samples after 60 minutes and 330 minutes on stream respectively. Both isotherms are type IV which indicates that the sample has lost its microporosity. The total pore volume is also greatly reduced, even after 60 minutes where the total pore volume is 0.05ml/g. This is consistent with the production of polyaromatic species in the initial MTG phase of the reaction, which block the micropores of the catalyst [19].

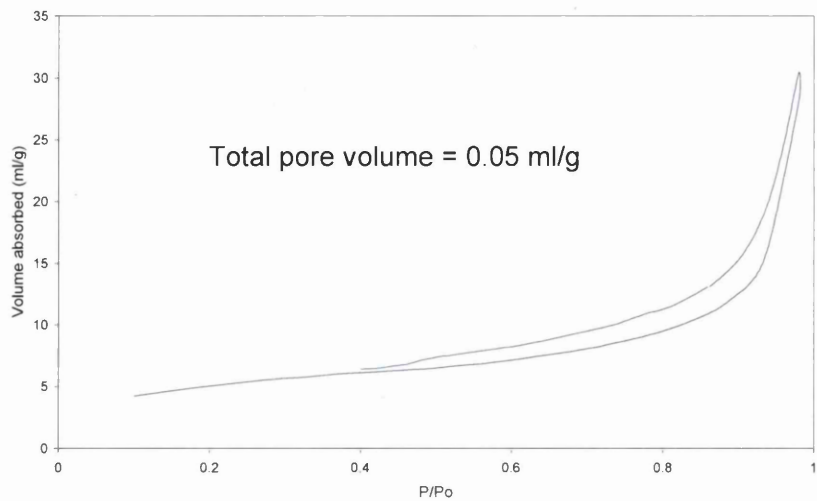


Figure 5-3: N₂ physisorption pattern of Spent copper mordenite after 60 minutes on stream containing type H3 hysteresis

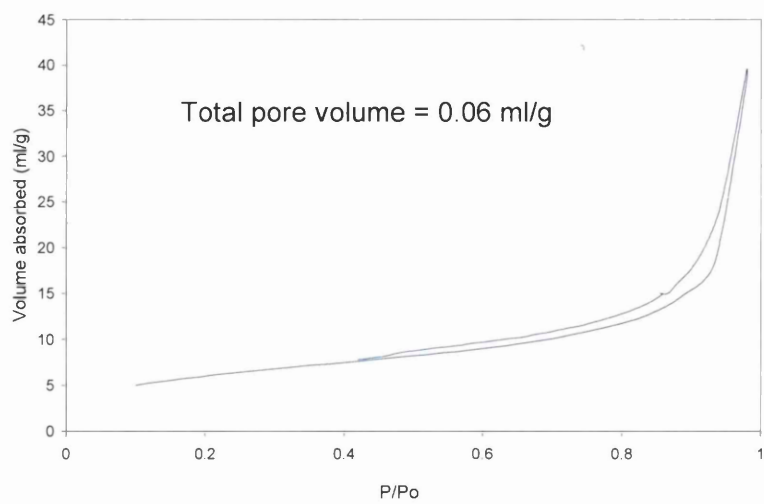


Figure 5-4: N₂ physisorption pattern of Spent copper mordenite after 330 minutes on stream containing type H3 hysteresis

Despite the pores being blocked within the first 60 minutes on stream, it is evident from Figure 5-1 that acetyl formation is not reduced as a result of carbon laydown and the blocking of the pores. This is in agreement with the study by Smith and co-workers, who reported that acetyl synthesis only becomes significant once the pore system became blocked in the initial MTG phase of the reaction [19]. It is also evident from these isotherms of the copper mordenite that a hysteresis loop occurs with IUPAC type H3. This indicates that the mordenite may have slit like pores or particles with a plate like morphology [148].

5.1.1 TGA analysis of spent copper mordenite

In order to analyze the carbon which was deposited on the copper mordenite, thermal gravimetric analysis (TGA) was carried out. The aim of this analysis was to investigate the possible types of carbon which may be deposited on the mordenite at various times on stream under reaction conditions and determine the coking profile. Figure 5-5 presents the results of a TGA experiment where weight losses are represented by peaks in the derivative plots. Experiments were carried out under both air and argon for fresh copper mordenite sample and various spent samples. It can be observed that the fresh catalyst loses weight within the first 200 °C. This weight loss can be attributed to the loss of moisture retained within the pore structure of the mordenite. On Figure 5-5, the plots labelled (b), (c) and (d) are the TGA experiments for the spent catalyst after 60, 180 and 330 minutes on stream respectively under air. It is evident from plot (b) that after only 60 minutes on stream, a form of carbon is deposited on the catalyst which is observed by a weight loss in the temperature range 700-1000° C. The TGA plots for (c) and (d) show an additional weight loss around 400° C, which is absent after 60 minutes on stream. This illustrates that after 60 minutes on stream, the copper mordenite catalyst has retained a secondary species which is lost at a lower temperature. The result for the TGA experiment carried out under argon on the spent copper mordenite catalyst after 330 minutes on stream is displayed as plot (e) in Figure 5-5. It is evident from this that the weight loss is a result of a desorption or decomposition of retained species and not the direct oxidation of carbon by a gas-phase oxidant.

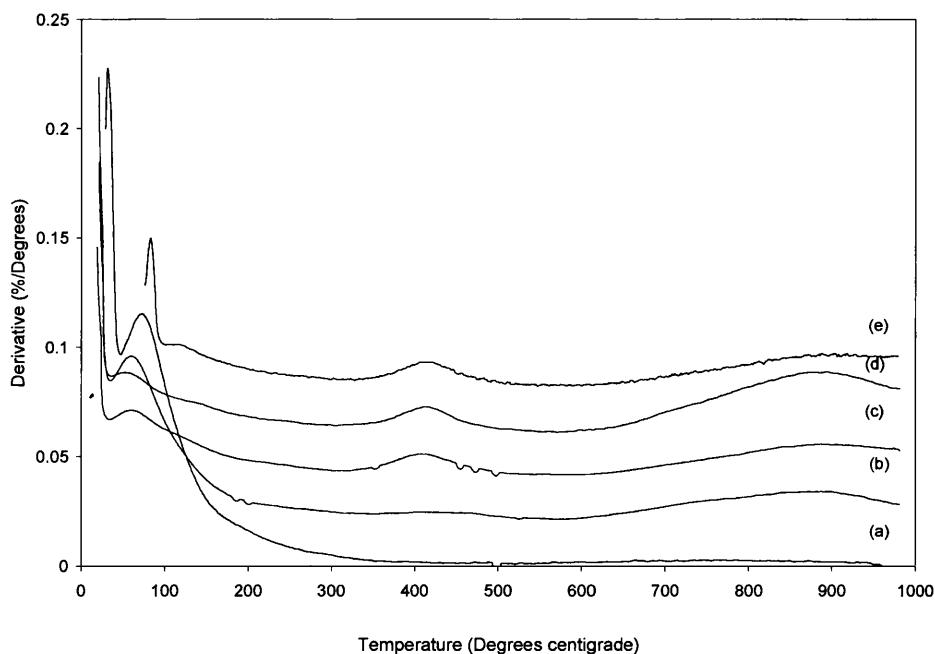


Figure 5-5: TGA derivatives of copper mordenite performed under air. (a) fresh copper mordenite (b) Spent mordenite 60 minutes on stream (c) Spent mordenite 180 minutes on stream (d) Spent mordenite 330 minutes on stream (e) Spent mordenite 330 minutes on stream under argon

It is possible that during the carbonylation reaction, the copper mordenite retains two different types of carbonaceous deposit. In conjunction with the N_2 physisorption data analysis and CHN analysis it appears that the high temperature weight loss which occurs with spent mordenites taken off stream after 60 minutes is the species which blocks the pores within the earlier stages of the reaction. After 180 minutes the emergence of the secondary species, which desorbs at a lower temperature is evident. It is possible that this species is not associated with the pores and is on the surface of the mordenite. In a study by Henriques and co-workers, the nature of the coke formed from ortho-xylene isomerization was investigated over H-mordenite in a 2.6% O_2 in He atmosphere and $7^\circ C/min$ ramp rate [125]. The content of this coke was mostly polyaromatic which is consistent with the type of coke formed during methanol carbonylation in the initial methanol to gasoline stage of the reaction. It was reported that the coke was oxidised in the $800-1000^\circ C$ temperature range. This is in agreement with our study. In a study by Gabelica *et al.* [126], the formation of coke was studied for the methanol to gasoline reaction at $370^\circ C$. Several zeolites were investigated including H-mordenite. It was discovered

that deactivation occurred due to coking which is consistent with the methanol carbonylation profile whereby methanol to gasoline activity drops within the first stage of the reaction. The saturation of coke occurred at 8.7wt% after 100 minutes on stream. This is in close agreement with the amount of coke formed in the present study presented in Table 5-1. Gabelica suggested that coke formed on ZSM-5 is restricted to the outer surfaces as opposed to the larger internal pores of mordenite which can accommodate larger carbonaceous species [126]. With respect to the present study, coke formed on the external surface of mordenite may only occur after the pores become blocked. However, the presence of weight loss features under an inert atmosphere suggest that desorption or decomposition of carbonaceous species is more probable as opposed to the oxidation of carbonaceous species. The lower temperature desorption feature in the present study could however be attributed to the decomposition of acetate species which may have adsorbed onto the surface of the mordenite during methanol carbonylation. In support of this, the presence of the low temperature TGA feature does not occur during the initial MTG stage of the reaction and the emergence of the desorption feature around 400°C occurs when acetic acid and methyl acetate formation becomes an emerging reaction pathway. In addition, TPD studies of adsorbed acetic acid over a range of materials have shown that surface acetate species, formed on HZSM-5 decomposes in the range 405-585 °C [136]. Such acetyl groups have been clearly observed as surface intermediates via FTIR spectroscopy during DME carbonylation over H-mordenite [21].

5.1.2 XRD analysis of copper mordenite

Figure 5-6 contains the XRD patterns for the fresh and spent copper mordenite catalysts after 330 minutes on stream. Figure 5-7 is the simulated powder pattern for mordenite adapted from reference [124] Cu K α radiation. It is evident that no significant structural change occurs after reaction and this is in agreement with the other methanol carbonylation study [19].

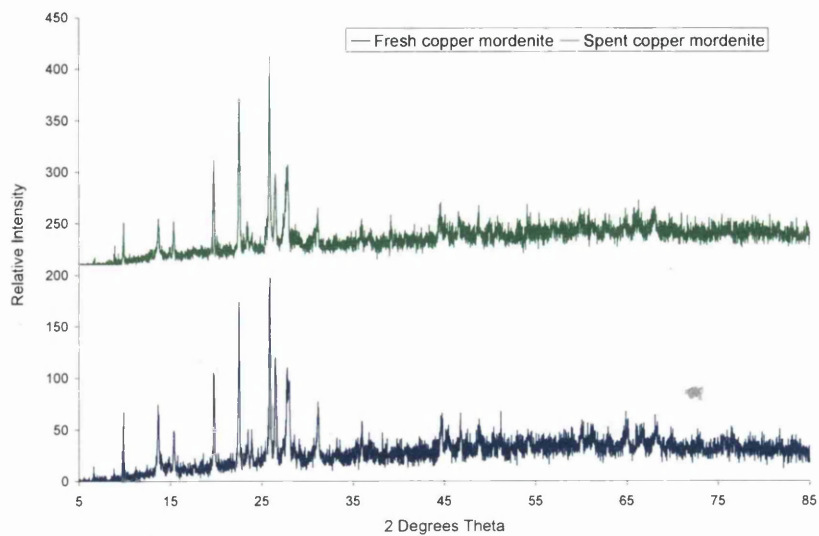


Figure 5-6: XRD pattern of fresh and spent copper mordenite catalyst

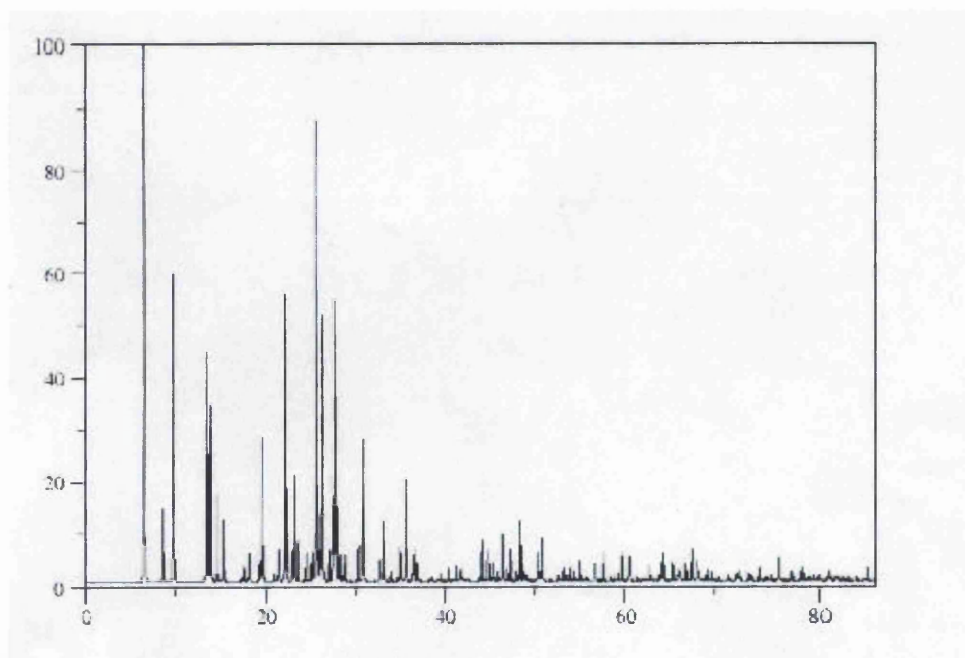
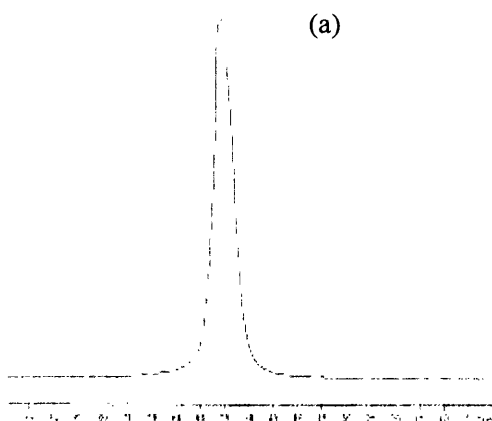


Figure 5-7: Simulated XRD pattern for mordenite adapted from reference [124]

Interestingly there was no copper oxide or copper metal observed with the fresh and spent copper mordenite catalysts respectively. This is surprising since copper oxide is observed in the XRD patterns of impregnated copper mordenite samples in the loading range of 3-10wt% copper [128], which is within the loading range employed in the present study. In addition the analysis of the spent copper mordenite catalyst yielded large copper metal particles easily detectable by XRD analysis [19].

5.1.3 ^{27}Al and ^{29}Si NMR study of mordenite samples

In conjunction with the XRD patterns, the ^{27}Al and ^{29}Si MAS NMR spectra provide a further insight into the structural nature of the mordenite as they are useful techniques, which give information about the structure of the aluminium and silicon containing species in zeolites. In the present study this is of interest because changes in the nature of the aluminium structure, eg dealumination of the framework may coincide with changes in the acidic nature of the material and in turn the catalytic behaviour. Figure 5-8 presents the ^{27}Al spectra of the parent H-mordenite samples. The fresh and spent copper mordenite samples and an NH_4 -mordenite sample for comparison. It should be noted that the samples were left in an open atmosphere for several months prior to the analysis. This prevents dehydration and quadrupolar line broadening.



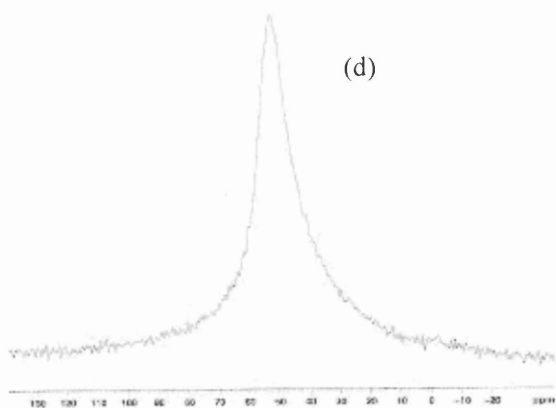
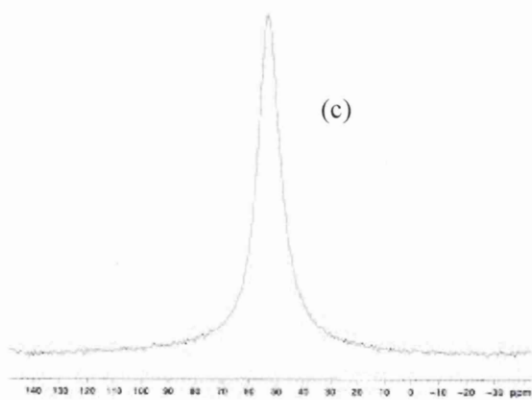
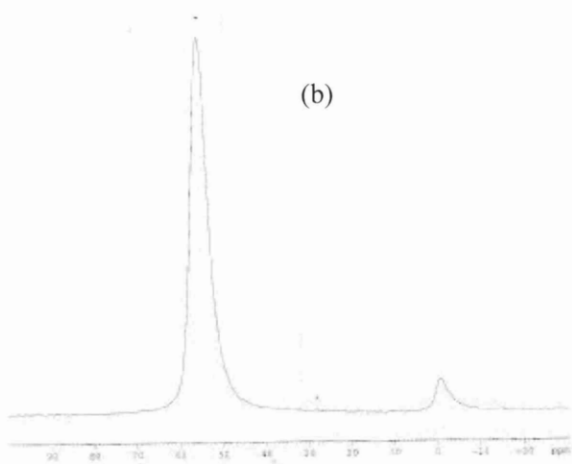


Figure 5-8: ^{27}Al MAS NMR spectra for (a) $\text{NH}_4\text{-Mor}$ (b) H-Mor (c) Cu-Mor (d) Spent Cu-Mor

All samples contain a peak at 53ppm, which is the tetrahedrally coordinated framework aluminium and in addition the H-mordenite sample contains a peak at 0 ppm, which is typical of octahedral non-framework aluminium [131,132]. As discussed by Chen *et al.* [131], the tetrahedrally coordinated aluminium is associated with Brønsted acidity whilst the generation of extra-framework aluminium may be associated with an increase in the number of Lewis acid sites. The dealumination of mordenite can result in a decrease in the number of strong Brønsted acid sites and an increase in Lewis acid sites [134]. In addition, the relative strengths of these sites can also depend on the distribution of the framework aluminium ions [134]. In terms of the behaviour of the copper mordenite with respect to methanol carbonylation, this is significant because many of the reaction pathways observed are dependent on the acid function of the mordenite catalyst. For example the formation of acetic acid is postulated to occur at Brønsted sites [19]. In addition a kinetic study of methanol dehydration to form DME suggested that adjacent Brønsted sites and basic sites are active over dealuminated mordenites [133] and the coking and aging of mordenite has also been shown to depend on the access and availability of strong Brønsted acid sites [126]. In the present study, the only peak corresponding to extra- framework aluminium is in the parent H-mordenite present in Figure 5-8(b), although there is also the possibility of this feature present in the spent copper mordenite sample in Figure 5-8(d). In addition, the broadening of the tetrahedral peaks is evident for the copper mordenite samples and may mask the presence of a resonance corresponding to extra-framework aluminium at 0ppm. Although there is no direct evidence of extra framework aluminium with the copper mordenite samples, it has been reported that this broadening of the tetrahedral resonance is due to the presence of non framework tetrahedral aluminium [19, 135], and this can also be caused by the presence of paramagnetic copper in these samples. However, it is evident that the spent copper mordenite catalyst in Figure 5-9 contains a broader resonance at 53ppm when compared with the fresh copper mordenite catalyst and possibly a greater degree of disorder of the tetrahedral aluminium.

The framework Si/Al ratio can be determined from the ^{29}Si MAS NMR spectra using the following equation as reported by Liu *et al.* [130]:

$$Si/Al = \frac{\left[\sum_{N=0}^4 I_{Si}(nAl) \right]}{\left[\sum_{N=0}^4 1/4nI_{Si}(nAl) \right]}$$

Figure 5-9 contains the ^{29}Si MAS NMR spectra for the mordenite samples.

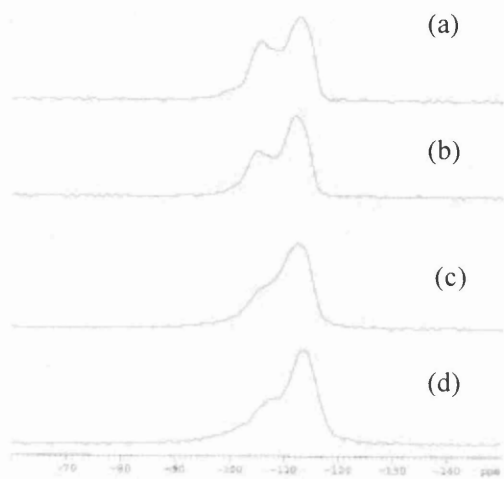


Figure 5-9: ^{29}Si MAS NMR spectra for (a) $\text{NH}_4\text{-Mor}$ (b) H-Mor (c) Cu-Mor (d) Spent Cu-Mor

All samples contain resonances with chemical shifts of -117ppm and -108ppm . These correspond to $\text{Si}(0\text{Al})$ and $\text{Si}(1\text{Al})$ respectively [137]. Si/Al ratios were calculated from the intensities of these peaks using a Gaussian peak fitting function and are displayed in Table 5-2.

Sample	Si/Al ratio
(a) $\text{NH}_4\text{-Mor}$	9
(b) H-Mor	9
(c) Fresh Cu-Mor	6
(d) Spent Cu-Mor	8

Table 5-2: Si/Al ratios for mordenite samples

The Si/Al ratio is expected to be 10 for the mordenite. The NMR indicates that the ratios for NH₄-mordenite and H-mordenite samples are 9. It seems that loading copper onto the mordenite reduces this ratio but there is an inherently large error applying peak integration to the two peaks which are difficult to deconvolute, and hence caution should be exhibited when performing comparisons. In addition, it has been reported that this ratio can be smaller than the one given by the lattice composition, due to a discrepancy resulting from silanol groups contributing to the -108ppm line [151]. Although there is the possibility of a degree of disordering of the framework aluminium in the ²⁷Al spectra and the presence of extra-framework octahedral aluminium, there appears to be no dealumination of any of the samples. This would lead to an increase in the Si/Al ratio which is not observed with any of the mordenite samples presented in Table 5-2. Although dealumination occurs in the presence of acid or water, it should be noted that the conditions of dealumination are more severe compared to that of the methanol carbonylation in the present study. For example, dealumination has been achieved using concentrated 6 M HCl or steam treatment at 600°C [137]. The impregnation of metal ions from an acidic solution is known to cause dealumination [143].

5.1.4 Methanol carbonylation summary

Under standard conditions it is clear that there are a lot of similarities with the present methanol carbonylation study and that previously carried out at higher pressure [19]. Both studies have concluded that most of the coke is formed in the initial phase of the reaction and the micropores of the mordenite become blocked as a result. The formation of acetyls and DME was shown to occur as major pathways once the initial methanol to gasoline and methanol to hydrocarbon processes cease and the mordenite micropores become blocked. This suggests that different sites exist at which these reactions occur, as it is known that the MTG and MTO processes occur on strong Brønsted acid sites [126] and acetyl formation occurs exclusively with zeolites containing eight membered channels [22]. In addition, the possibility of coking profiles has been discussed and the possibility of dealumination during methanol carbonylation investigated.

5.2 Methanol carbonylation studies under different feed conditions

Methanol carbonylation was carried out with differing feed compositions. The importance of this is that hydrogen is the major co-product of methanol decomposition and the partial

pressures of CO, H₂ and methanol required for the methanol carbonylation step will be dictated by the performance of the methanol decomposition catalyst. In this section, the influence of hydrogen partial pressure on carbonylation efficiency is probed. Table 5-3 displays the STY data for the main products for methanol carbonylation under varying conditions over a 300 minute reaction run. Various CO/H₂ partial pressures, reaction temperatures and methanol partial pressures are reported. The errors are presented for those reactions which were repeated. The first observation is that there is a high degree of error with the analysis and in particular, the analysis of acetic acid, methyl acetate and DME. As a result a degree of caution should be exerted with the interpretation of the figures. Despite this, several trends are observed. Under all conditions it is evident that the methanol conversion is greater than 93%. Limitations of the analytical procedure prevented the detection and CO and CO₂.

Product	300 °C	350 °C	300 °C	300 °C	300 °C	300 °C
	CO	CO	CO/H ₂ = 4	CO/H ₂ = 2	CO/H ₂ = 0.5	CO ¹
Acetic acid	24 ± 5	36 ± 5	45 ± 5	19	8	31
Methyl acetate	10 ± 1	5 ± 1	9 ± 1	5	3	12
DME	19 ± 5	27 ± 5	19 ± 2	13	12	41
CH ₄	1 ± 0.1	3 ± 2	1 ± 0.1	1	2	1
C ₂ H ₄	2 ± 0.4	5 ± 2	3 ± 0.1	3	7	4
C ₃ H ₆	3 ± 0.4	6 ± 0.4	4 ± 0.1	4	9	5
Methanol conversion (%)	96 ± 0.2	97 ± 1	93 ± 0.6	96	96	94

Carbon deposition(wt %)	9 ± 0.1	12	9	9	6	4 ± 0.1
-------------------------	---------	----	---	---	---	---------

Table 5-3: STY values for methanol carbonylation(g/kgcat/h). GHSV = 2400 h⁻¹, volume of catalyst = 5 ml, CO/methanol molar ratio = 10. ¹ CO/methanol molar ratio = 4

Inspection of Table 5-3 shows that increasing the temperature from 300 °C to 350°C does not result in an increase in the acetyls formation rate whilst the maximum formation rate occurs at a CO/H₂ ratio of 4. It is notable that, contrary to the case of larger partial pressures, activity is enhanced by low partial pressures of hydrogen. Since the catalysts have been reduced with hydrogen at 300°C prior to reaction, it seems unlikely that this is due to reduction of copper ions. One possibility is that the nature of the carbon deposited, either in terms of its quantity or its functionality, is influenced by this procedure. Further studies would be required to prove this. At higher hydrogen partial pressures the reduced rate of acetyls production may be explained by the corresponding decrease in CO partial pressure as it has been demonstrated that in DME carbonylation over a mordenite catalyst, the carbonylation rate increased linearly with CO partial pressure [21]. A decrease in this ratio results in a lowering of acetyl production. The lowest production rate occurs when the CO/H₂ ratio is 0.5, the ratio corresponding to selective methanol decomposition. The formation of DME decreases with lower CO/H₂ ratios and a maximum value of 41g/kgcat/h is observed when the methanol partial pressure is increased. This is consistent with a study where the dehydration of methanol to DME was studied over mordenite in the temperature range of 200-300°C [133]. In that study it was reported that increased methanol partial pressures yielded higher formation rates of DME and the kinetic order with respect to methanol was between 0.5 and 1. The production of methane, ethene and propene does not follow any particular trend with varying conditions. However, the formation of these products occurs via many possible routes. In a study by Guisnet *et al.* [138], the mechanism of methane, propene and ethene from DME and methanol was investigated over mordenite at 530°C. Whilst C₃-C₇ hydrocarbons were reported as primary products, ethene and methane were reported to occur from the cracking of higher alkanes and demethylation of polymethylbenzenes respectively. The amount of carbon deposited on the copper mordenite is generally high and this is not surprising considering its acidic nature. The highest amount of carbon results from methanol carbonylation at the increased temperature of 350°C with a value of 12 wt% whilst increasing the hydrogen partial

pressure reduces the amount of coke observed on the spent catalyst, possibly due to the hydrogenation of surface carbonaceous species. The inhibiting effect of H₂ on coke formation has also been reported for ortho-xylene isomerization over mordenites [127]. However in the present study, there is no evidence that coke formation causes deactivation with respect to acetyl production as most of the carbon is deposited in the initial stages of the reaction before carbonylation activity dominates. It has been reported that deactivation occurs with water formation, competing for CO binding sites inhibiting carbonylation rates [21]. In the present study, methanol dehydration to DME and hydrocarbon formation provide a source of water.

5.3 Coupled methanol decomposition and carbonylation experiments

The idea of mixing two separate heterogeneous catalysts together is not a new one. In a study by Ramos *et al.* [140], the direct synthesis of DME from synthesis gas was achieved in one reactor by combining a commercial methanol synthesis catalyst with a series of methanol dehydration solid acid catalysts. In that study, physical mixtures of the catalysts yielded a maximum DME selectivity of 60% and CO conversion of 30%. It was concluded that the overall rate of DME formation was influenced by the nature of the acid catalyst. DME formation increased with the more acidic acid catalysts and this resulted in an increase in the overall CO conversion due to an equilibrium shift in the methanol synthesis reaction. In another study, the direct steam reforming of DME to produce H₂ occurred by combining a H-mordenite DME catalyst with a CuO/CeO₂ steam reforming catalyst [141]. In that study, the deactivation of the overall system was attributed to the coking of the steam reforming catalyst and not the H-mordenite catalyst. It is clear that there are many considerations when combining two catalysts into one system.

In the present study, methanol decomposition reactions were carried out using palladium and copper catalysts and were coupled with copper mordenite carbonylation catalyst in both mixed bed and stacked bed configurations. In the stacked bed configuration, the methanol decomposition catalyst was placed above the copper mordenite catalyst in the downflow reactor. The CO and H₂ STY values are normalised with respect to the mass of the methanol decomposition catalyst. DME, CO₂, CH₄, methyl acetate and acetic acid STY values are normalised with respect to the mass of the copper mordenite. The most important difference between the current analysis and the analysis in the previous section is that CO₂ and CO are quantified. The detection of CO₂ is of importance in the present

study because it is a major product arising from the water gas shift reaction in the homogeneous carbonylation of methanol in the Cativa and Monsanto processes currently used industrially for the production of acetic acid [4]. However, limitations in the analysis of the mixed catalyst system set-up meant that many of the products observed in the direct methanol carbonylation are not observed or quantified, eg ethane and propene formation indicative of MTO chemistry.

Both a palladium and a copper catalyst based on a Katalco methanol synthesis catalyst were selected due to the fact that they represent the most commonly studied catalysts in the literature. The activities of the catalysts are summarised in Table 5-4. It can be seen that the palladium catalyst is significantly more active in the production of CO. The low STY CO/H₂ ratio for the Katalco catalysts is due to the fact that this catalyst is less selective to CO formation.

Catalyst	Temperature (°C)	STY CO (g/kgcat./h)	CO/H ₂ STY ratio
Pd (3wt%)/CeO ₂	300	3228 ± 181	6.5
Katalco	300	1174	4.2

Table 5-4: Summary of selected methanol decomposition catalysts at 300°C.

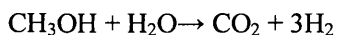
5.3.1 Coupled methanol decomposition and carbonylation experiments:

Experimental results

The analysis of acetic acid and methyl acetate was performed off-line after the reaction was completed and the results are displayed in Table 5-5. In addition, the mean CO₂ production rate is presented for each experiment.

It can be observed in Table 5-5 that CO₂ is produced for all catalyst conditions and bed configurations. A probable route for CO₂ production is the water- gas shift reaction, which is a source of selectivity loss in the homogeneous methanol carbonylation route. Water-

gas shift activity has been reported to occur over copper containing solid acid catalysts. In a study by Andrade and co-workers, a Cu- ZSM-5 catalyst showed good water gas shift activity in the temperature range of 300-400°C [139], the temperature range in which methanol carbonylation is currently conducted. However, the water gas shift reaction is moderately exothermic ($\Delta H = -41.1 \text{ kJmol}^{-1}$) [149] and the equilibrium constant decreases with temperature. At 300 °C, the equilibrium constant is 38.8 [149], so more thermodynamically favourable routes to CO₂ production have to be considered in the present study. Another possibility is the steam reforming of methanol via the following equation:



This reaction occurs over copper based catalysts and in addition the pathway is thermodynamically favoured at elevated temperatures. At the carbonylation temperature of 300 °C employed in the present study, in the methanol steam reforming reaction pathway it has been shown that a methanol conversion of greater than 95% is achieved with CO₂ and H₂ the only reported products [150]. This is a probable route to CO₂ production observed in the present study. Another possible route is the reduction of oxidic fractions from the surface of the mordenite by methanol, H₂ or CO. The discussion is primarily academic as further investigation would be required to confirm this hypothesis.

It was reported that the active catalyst contained copper metal ions and copper oxide clusters [139]. In the present study, although no copper was evidenced by XRD analysts but the presence of copper metal and copper oxides have been observed in the analogous copper mordenite catalyst used in methanol carbonylation [19].

Methanol Decomposition Catalyst	Bed Configuration	STY Acetic Acid (g/kgcat/h)	STY Methyl acetate (g/kgcat/h)	STY CO ₂ (g/kgcat/h)
Pd/CeO ₂	Stacked	9.85 ± 0.5	0.75 ± 0.35	133 ± 29

Pd/CeO ₂	Mixed	1.45 ± 0.1	0.3	93 ± 17
Katalco	Stacked	6.5 ± 0.6	0.4	236 ± 46
Katalco	Mixed	0.3 ± 0.1	0.07	152 ± 26

Table 5-5: STY values for acetyl formation at 300°C. GHSV = 2625 h⁻¹ (calculated with respect to the Cu-MOR catalyst), methanol (39mol%) feed in argon 0.15g Cu-Mordenite catalyst. 0.15g decomposition catalyst

It can be observed in Table 5-5 that both acetic acid and methyl acetate are produced for both copper and palladium catalysts in both bed configurations with methyl acetate being a minor product. It is notable that the palladium methanol decomposition catalyst and a stacked bed configuration yields higher acetyl formation rates.

The results for the Katalco catalyst are displayed in Figures 5-10 - 5-12. On inspection of Figure 5-10, it can be seen that the methanol conversion is around 90 % for both stacked and mixed bed configurations. DME is also observed as a result of methanol dehydration over the copper mordenite. For both the mixed and stacked bed configurations, it can be observed that the DME follows an activation profile. This is consistent with the trend observed in direct methanol carbonylation whereby DME formation increases with time on stream. However the mixed bed configuration yields more DME produced at a rate of around 841g/kgcat/h compared with the stacked bed which has a peak formation rate of 374g/kgcat/h.

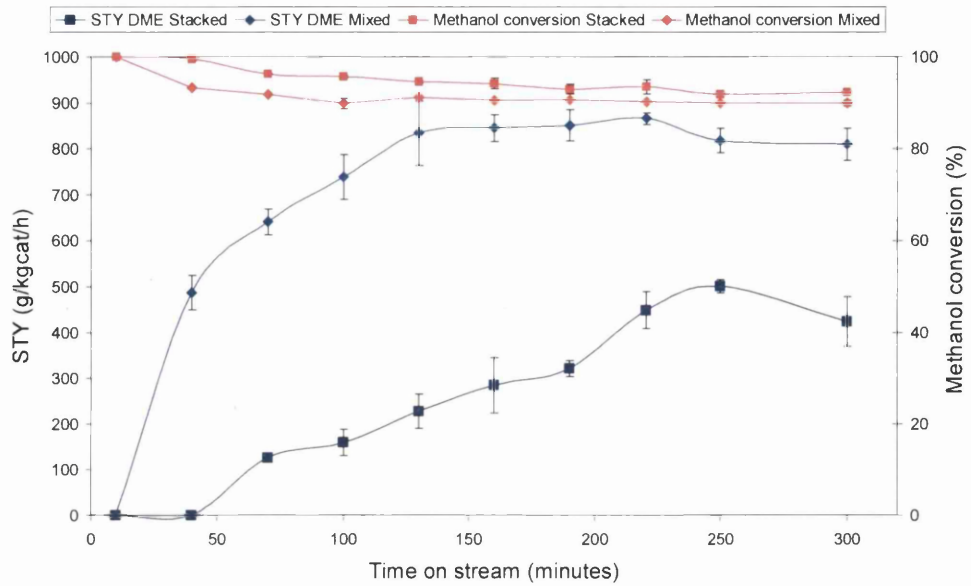


Figure 5-10: STY DME and methanol conversion for the Katalco catalyst

Figures 5-11 and 5-12 present the data for CO, H₂ and CH₄ production over mixed and stacked beds respectively for the Katalco catalyst.

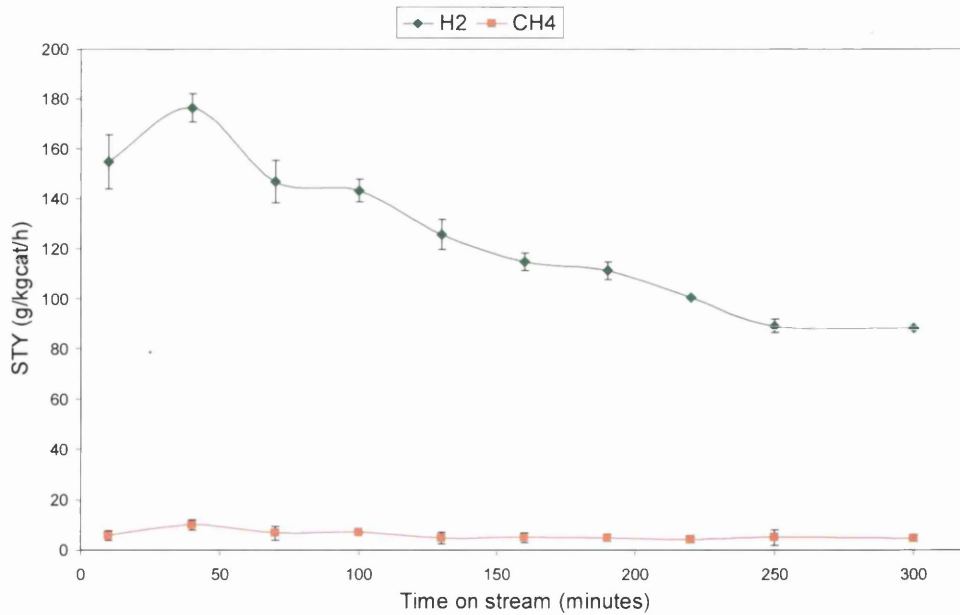


Figure 5-11: H₂ and CH₄ STY data for the Katalco catalyst (mixed bed configuration)

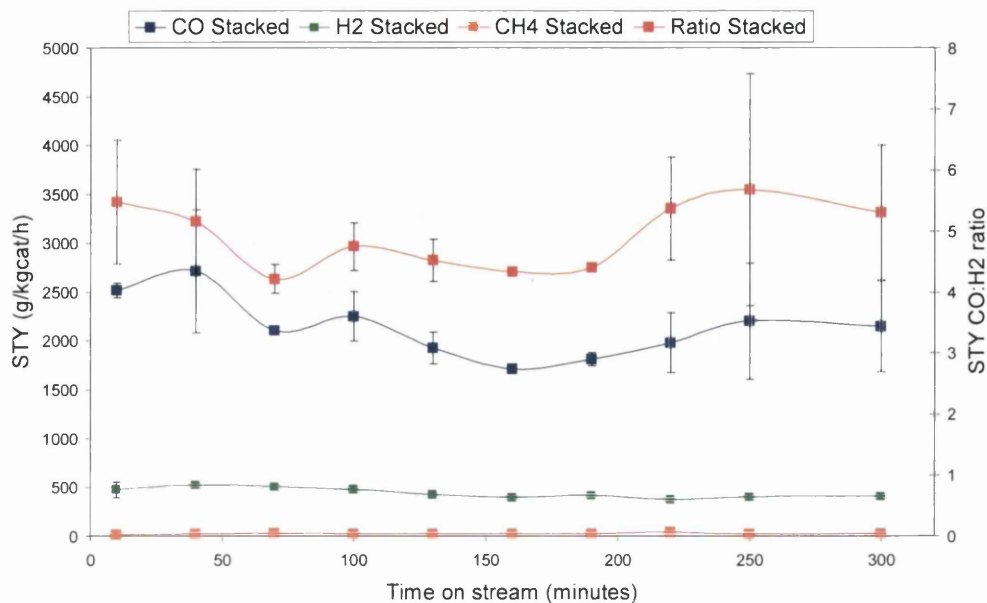


Figure 5-12: CO, H₂ and CH₄ STY data for the Katalco catalyst (stacked bed configuration)

It is noticeable that there is no CO produced in the mixed bed configuration presented in Figure 5-11. However H₂ is observed indicating that the decomposition of methanol occurs and the CO produced is below the detection limit. It can also be observed that CH₄ is produced, which is a by-product of the interaction of methanol and the copper mordenite catalyst, since this product is not observed with methanol decomposition over both the palladium and Katalco catalysts. The stacked bed configuration however yields a different product spectrum to that of the mixed bed configuration. CH₄ is also observed with the stacked bed configuration but the main difference concerns the behaviour of the methanol decomposition. CO and H₂ are now observed products from the methanol decomposition and their rate of formation is higher compared with the mixed bed. When comparing the STY values for the direct methanol decomposition in Table 5-4 with that of Figure 5-12 it is evident that there is more CO produced when the Katalco catalyst is coupled with the copper mordenite carbonylation catalyst compared with direct methanol decomposition. Comparing Figure 5-12 with Table 5-4 indicates that the STY CO/H₂ ratio remains unaffected when the methanol catalyst is coupled with the copper mordenite catalyst. A lowering of this ratio indicates selectivity loss to CO as described previously. This indicates that the CO produced in the methanol decomposition step is not significantly

converted. Figure 5-13 presents the STY data for DME formation and methanol conversion with the Pd/CeO₂ catalyst. For both bed configurations it can be observed that the methanol conversion is also around 90%, the same as that for the Katalco catalyst. A similar trend is also observed with respect to DME formation in that the mixed bed configuration has a higher rate of DME formation when compared to the stacked bed and an induction period is observed for its production.

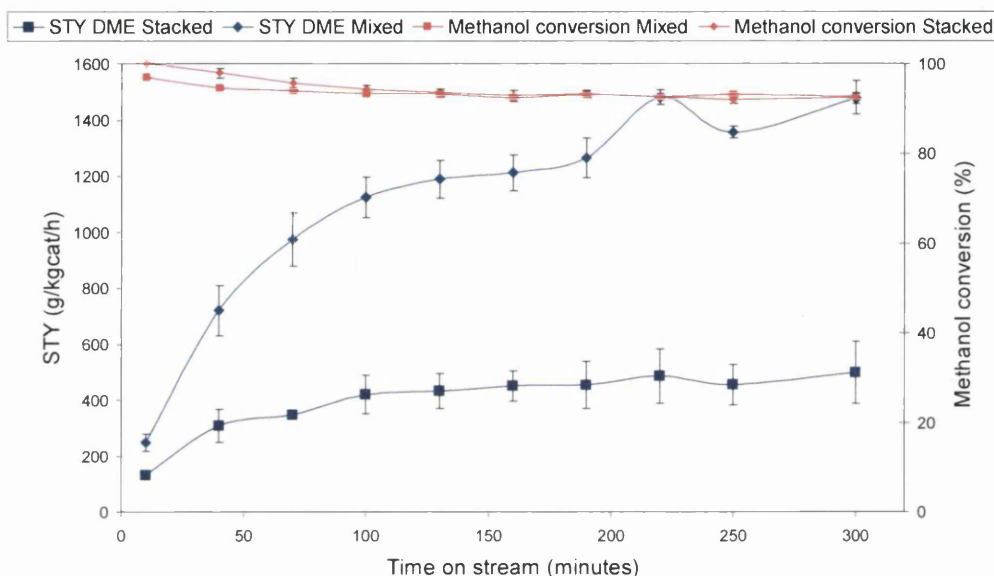


Figure 5-13: STY DME and methanol conversion for the Pd /CeO₂ catalyst

Figures 5-14 and 5-15 show the STY data for CO, H₂ and CH₄ for the mixed and stacked bed configurations respectively over the Pd /CeO₂ catalyst. CH₄ is produced in both configurations. Notably there is more synthesis gas produced when the palladium catalyst is in the stacked bed configuration with a steady state CO production rate of 3738 g/kgcat/h compared with 2336g/kgcat/h for the mixed bed configuration. There is also a higher rate of synthesis gas produced when comparing the palladium catalyst with the Katalco catalyst in both bed configurations. This is consistent with the palladium catalyst being a more active methanol decomposition catalyst. The STY CO/H₂ ratio is also not greatly reduced. The mean value for this ratio is 6.5 for the direct methanol decomposition as presented in Table 5-4, and it can be observed that the ratio mostly falls around this

value. This indicates that with both configurations, there is little evidence of a significant CO conversion.

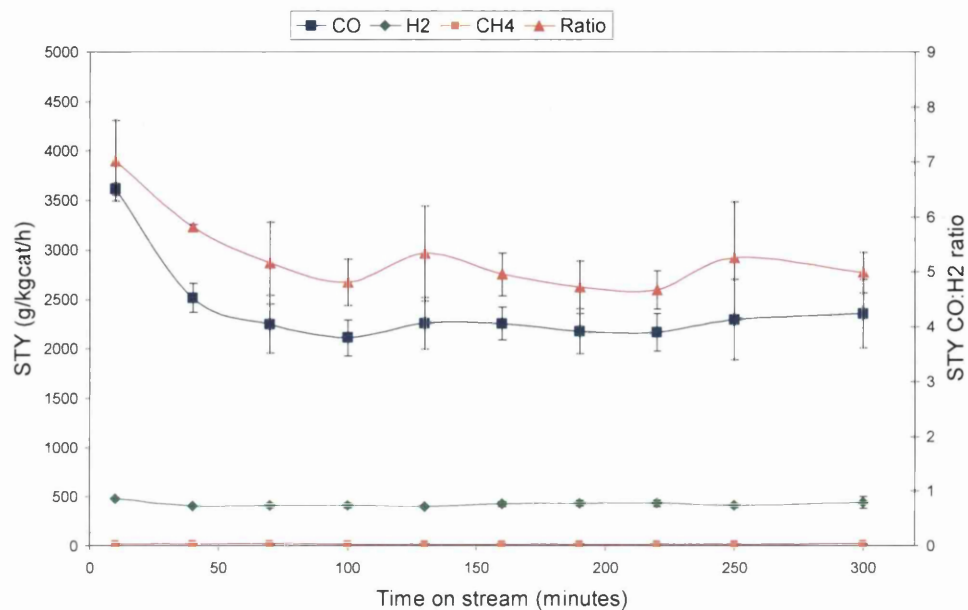


Figure 5-14: CO, H₂ and CH₄ STY data for the Palladium catalyst (mixed bed configuration)

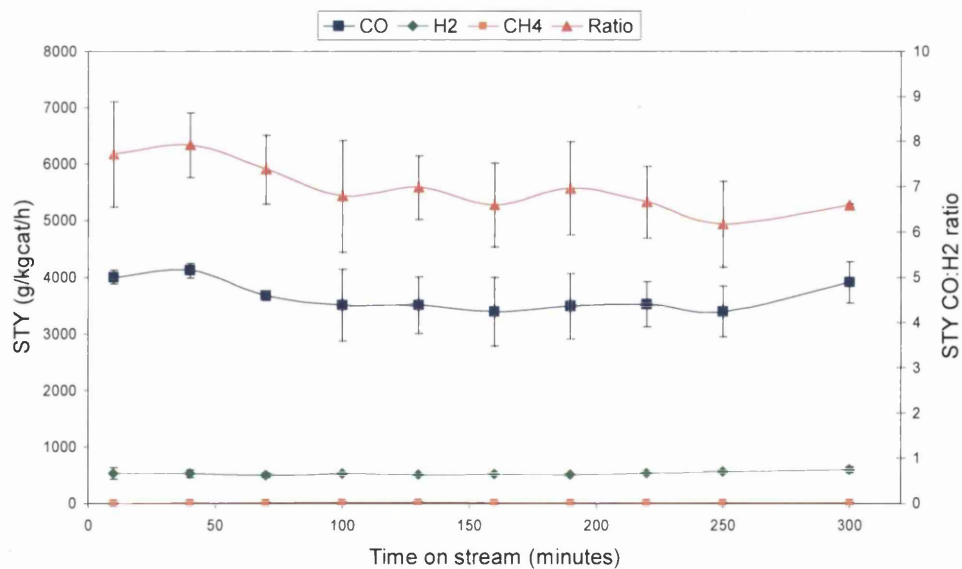


Figure 5-15: CO, H₂ and CH₄ STY data for the Palladium catalyst (stacked bed configuration)

In conjunction with the low CO conversions observed with all the gas plots and the acetyl data presented in Table 5-5, acetyl production is a minor product in the one-pot conversion of methanol over combined methanol decomposition and methanol carbonylation catalysts. The increased rate of acetic acid production over the stacked bed configuration is possibly due to the fact that this arrangement yields a higher rate of CO, whereas the mixed beds result in a lower production rate of CO and a higher conversion of methanol to form DME. The limiting factor for the low STY formation rates of acetic acid and methyl acetate are possibly a result of the limiting partial pressure of CO, in a H₂ rich feedstream. The maximum yield of acetic acid in Table 5-5 is 9.85 ± 0.45 g/kgcat/h for the Pd/CeO₂ catalyst in a stacked bed arrangement and the acetic acid STY value presented in Table 5-3 for the direct methanol carbonylation is similar at a value of 8g/kgcat/h for a feed CO/H₂ molar ratio of 0.5. This is the ideal ratio obtained when the synthesis gas is generated from methanol decomposition. This is further supported by the fact that more acetyls are produced with the Pd/CeO₂ catalyst compared with the Katalco catalyst, which is less selective to CO production with a lower CO/H₂ molar ratio.

5.4 Conversion of methanol with dual functional mordenite catalyst

The one-pot synthesis of acetic acid from methanol only has been demonstrated in the previous section by combining methanol dehydrogenation catalysts with a solid acid catalyst capable of methanol carbonylation activity. The benefits of such a system including the cheap capital costs of a simple reactor upon scale-up are profound compared to a system integrating two separate process steps. However a further advance would be the development of a single catalyst capable of synthesising acetic acid directly from methanol. Such a system would contain a catalyst of dual functionality. In theory, the active metals, capable of decomposing methanol at the given reaction conditions could be supported on the copper mordenite catalyst which could perform the methanol carbonylation. Such systems have been reported. In a study by Kanazirev *et al.* [142], the interaction of methanol over platinum supported on a range of zeolites and reaction conditions was studied to produce CO and CH₄. The activity and selectivity to the observed products were dependent on the reaction conditions and zeolite used. A given reaction pathway could be directed by selecting a given support and optimising the

reaction conditions. The platinum metal contained sites resulting in CO and CH₄ formation from methanol decomposition and methanation respectively. Both DME and a range of hydrocarbons were the observed products resulting from the acidic functionality of the zeolite supports. It was reported that the production of CO could be increased by increasing the platinum content in the catalysts. However the performance of the platinum was dependent on the type of zeolite used. It was observed that the less acidic supports were beneficial whilst the methanol decomposition activity decreased at the expense of DME and hydrocarbon products formed over the more acidic zeolites. For example, the yield to CO was 80% on platinum supported NaY at 400° C. At the same temperature over a more acidic offretite support, the yield of DME was 50%.

In the present study 5wt% palladium was impregnated onto the copper mordenite catalyst and exposed to methanol under the standard methanol carbonylation conditions. It can be observed from the XRD pattern presented in Figure 5-16, that the resulting material may contain a significant amorphous component. Although, the cause for this is most probably the presence of silica wool in the post reaction sample, which was used to separate the catalyst between the pre-and post bed silicon carbide material in the reactor.

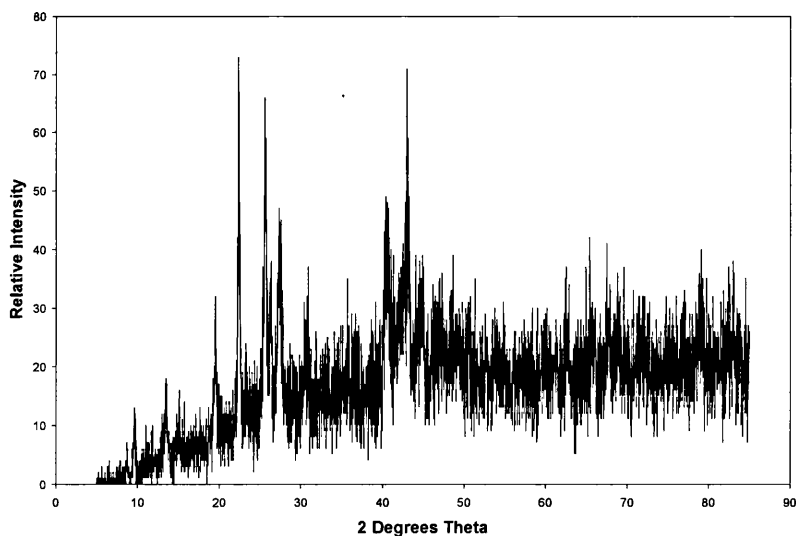


Figure 5-16: XRD pattern of spent palladium-copper mordenite catalyst

Figure 5-17 presents the methanol conversion and production rate data for DME. It can be observed that the methanol conversion drops to a steady state of 60%. DME production ¹⁵⁷

peaks at around 3738g/kgcat/h, and resides at 93g/kgcat/h at steady state. DME is however the major product due to methanol dehydration over the acidic mordenite support and the formation rate is comparable to that of the mixed bed systems presented in Figures 5-10 and 5-13.

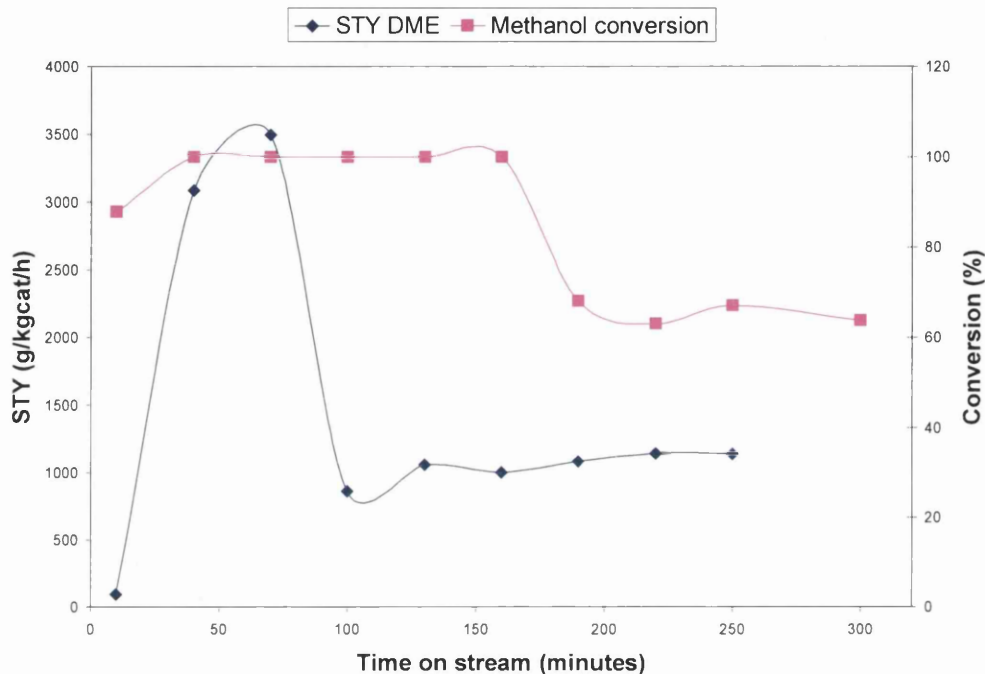


Figure 5-17: Methanol conversion and DME production over Pd-Cu-mordenite catalyst at 300°C

Figure 5-18 presents the STY data for products produced over the palladium-copper mordenite catalyst. Both CO and H₂ are produced indicating that methanol decomposition is occurring. However the production rate of CO is very low when comparing with the CO production rate over typical methanol decomposition catalysts indicating that mordenite is not a good support for palladium metal in methanol decomposition. For example, the palladium-copper mordenite catalyst has a steady state CO production rate of around 42g/kgcat/h whereas the Pd/CeO₂ catalyst presented in Figure5-14 has a steady state value of 2336g/kgcat/h. In addition to the synthesis gas produced, methane is also produced indicative of methanol interaction with the acidic mordenite. The methane appears to follow a deactivation profile within the first 200 minutes which coincides with the drop in methanol conversion at this time observed in Figure 5-17.

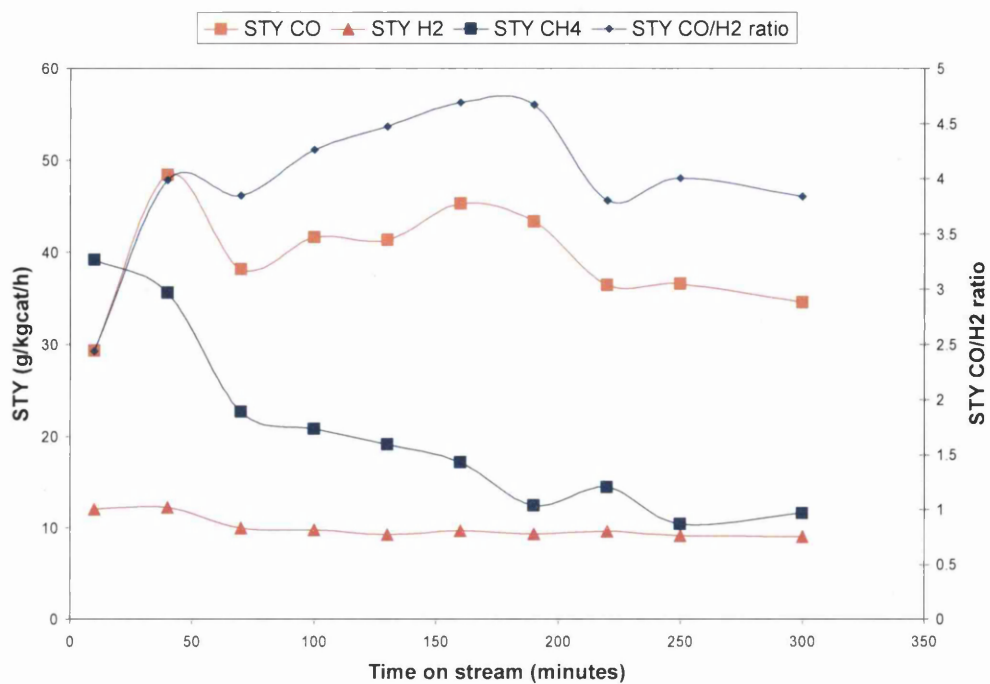


Figure 5-18: STY production of CO, H₂ and CH₄ over Pd-Cu-mordenite catalyst at 300°C

Figure 5-19 presents the STY data for observed on-line products for the methanol interaction with copper mordenite. H₂, CH₄ are the minor products whilst DME is the major product from methanol dehydration.

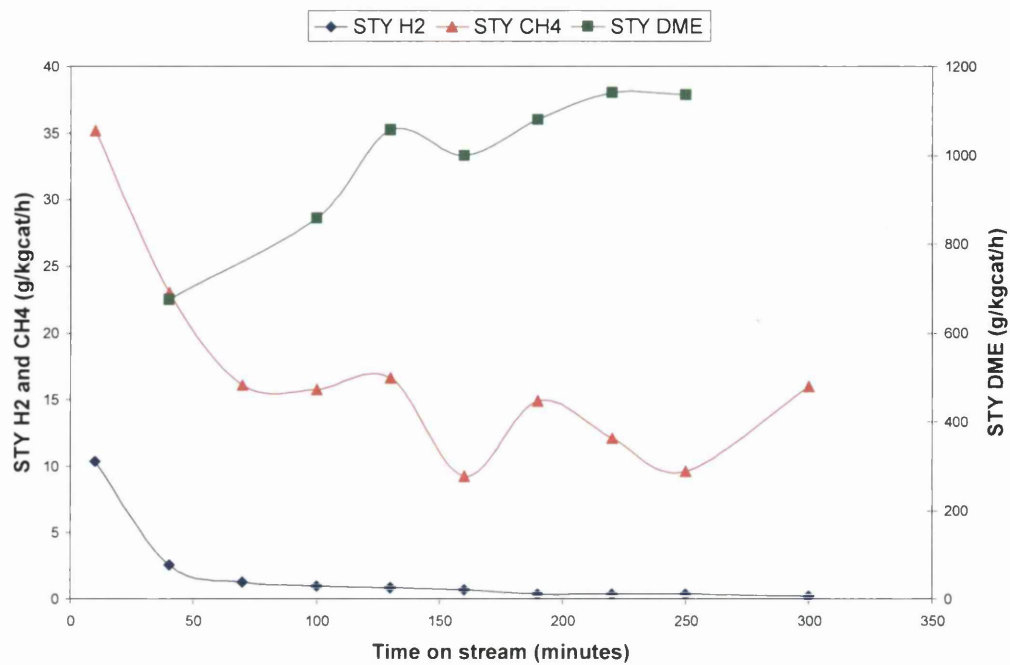


Figure 5-19: STY production for H₂ and CH₄ and DME for methanol reaction with copper mordenite at 300°C

Figure 5-20 presents data for an experiment where 5wt% MoO₃ was loaded onto the copper mordenite catalyst. It can be observed that most of the methanol is converted to DME over the mordenite acidic sites, which is consistent with the Pd-Cu-mordenite and Cu-mordenite. Trace amounts of CO, CH₄ and H₂ were also observed but not quantified.

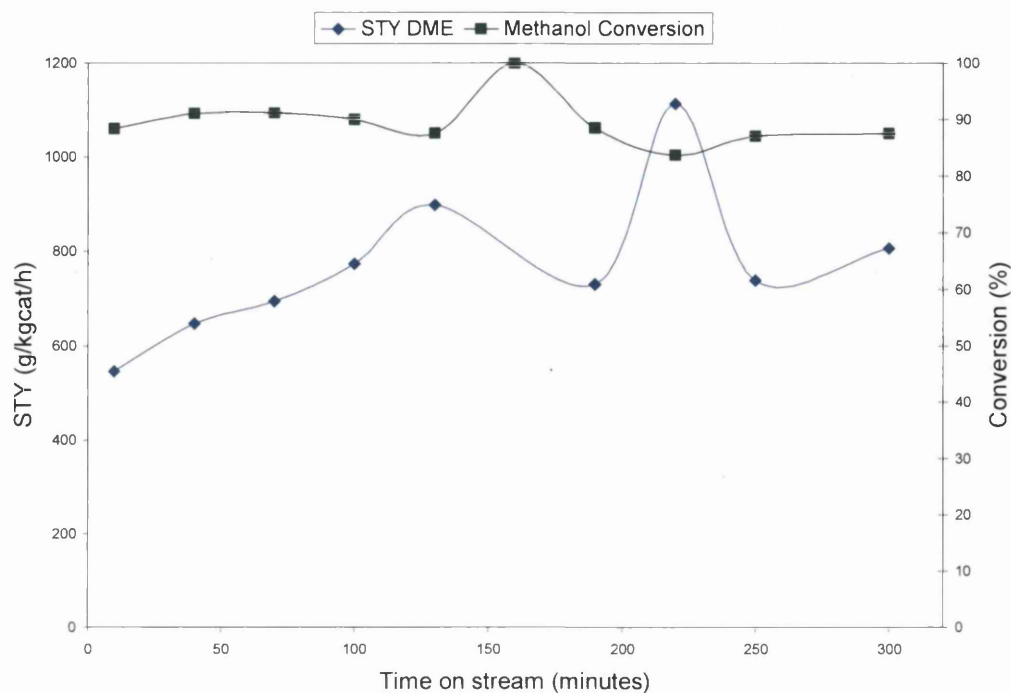


Figure 5-20: Methanol conversion and DME production over MoO₃-Cu-mordenite catalyst at 300°C

The yield of acetyls and the carbon content of the spent catalyst after five hours on stream are presented in Table 5-6.

Catalyst	STY Acetic acid (g/kgcat/h)	STY Methyl acetate (g/kgcat/h)	Carbon content (wt%)
Cu-mordenite	0.24	0.42	11.1
Pd-Cu-mordenite	0.41	0.23	11.5
MoO ₃ -Cu-mordenite	Trace	0.13	12.2

Table 5-6: Acetyl production and carbon content of Cu-Mor, MoO₃-Cu-mordenire and Pd-Cu-mordenite catalyst

It can be observed that acetic acid and methyl acetate are produced over all catalysts and there is no promotional effect on doping palladium and MoO₃ onto the copper mordenite. The yields are very low compared with that of the copper mordenite catalyst and methanol decomposition mixed systems presented in Table 5-5 where the maximum yield for acetic acid is 9.85g/kgcat/h. In addition the large post-reaction carbon content is consistent with methanol to gasoline based chemistry which occurs over the mordenite and has been commented on throughout this discussion.

The copper mordenite is a poor support for the palladium metal and MoO₃. As a result the production rate of CO is small and reaction pathways over the copper mordenite support are dominant including hydrocarbon production and methanol dehydration, as indicated by the high carbon content on the spent catalyst and DME formation rate. Although acetic acid is a detected product indicating that the catalyst is dual function, the activity is low.

5.5 Summary

In summary the one-pot synthesis of acetyls from methanol only feed using a methanol decomposition catalyst and copper mordenite catalyst is dependent on several factors. Although methanol carbonylation produces acetyls, many by-products are produced. The choice of methanol decomposition catalyst and reactor bed configuration influences the production of acetyls. Some findings are as follows:

- The direct carbonylation of methanol is influenced by the feed ratio of CO and H₂. Low ratios reduce the formation of acetyls.
- In the one-pot systems, both CH₄, DME, and carbon are observed, which are indicative of methanol reaction pathways over the copper mordenite.
- In the one-pot systems, synthesis gas is produced indicating that methanol decomposition occurs.
- There appears no loss of CO indicating that its rate of formation is greater than its rate of consumption.

- Stacked bed configurations yield more CO compared with mixed bed configurations which favour DME formation.
- Stacked bed configurations yield a higher rate of acetyls compared with the mixed beds.
- The one-pot synthesis of acetyls is increased when a more CO selective methanol decomposition catalyst is used.
- The interaction of methanol with copper mordenite yields trace amounts of acetyls
- Doping the copper mordenite with palladium and MoO₃ in an attempted dual functional catalyst does not result in a significant increase in acetyl formation.

6 Conclusions

Throughout this project, the experimental work undertaken has focused on several main objectives. The overall aim of the project was to investigate a methanol only route to acetic acid and methyl acetate via the combination of a methanol decomposition catalyst with a heterogeneous methanol carbonylation catalyst in the absence of a halide promoter. Firstly, the activity of standard methanol decomposition catalysts was investigated under directly comparable conditions in order to generate an activity profile for CO production. Several novel materials were also tested for methanol decomposition. Secondly, methanol carbonylation experiments were carried out over a copper mordenite catalyst, varying several process variables in order to study acetyl production at atmospheric pressure. Finally, selected methanol decomposition catalysts were combined with the copper mordenite catalyst to study a methanol only route to acetyls.

In summary, when comparing the activities of the standard methanol decomposition catalysts in the 250-300°C temperature range, several trends were observed. Palladium based catalysts are in general more active than copper based methanol synthesis catalysts. Methyl formate is an observed by-product observed over the latter. Raney nickel is active for methanol decomposition producing CH₄ as a by-product. An amorphous NiB material, formed by the reduction of nickel acetate by sodium borohydride is as active as the most best palladium catalyst. Several of the trends for the various classes of methanol decomposition catalysts tested are summarized below:

- A copper catalyst, where the formulation was based on a Katalco methanol synthesis catalyst containing 37.6 wt% Cu and 13.3wt% Zn was compared with an analogous catalyst containing 29.5wt% Cu and 32.0wt% Zn. Both catalysts produced methyl formate as a by-product, but the CO selectivity was increased by increasing reaction temperature. The most active Cu based catalyst was the Katalco catalyst. XRD analysis illustrated that this catalyst contained Cu metal and CuO phases whilst the other catalyst contained Cu metal and ZnO phases. The higher activity of the Katalco catalyst is possibly due to the higher copper content, the presence of Cu²⁺ in the reduced catalyst. In addition the Katalco catalyst also possessed a larger BET surface area of 51m²/g compared with 19m²/g for the other Cu catalyst. Whilst both catalysts deactivated with a reduction in methanol conversion observed, there was no evidence of the

CuZn alloy formation, reported to cause deactivation in these systems. Both spent catalysts demonstrated an increase in carbon content, as a result of coking.

- Two Pd catalysts, prepared by co-precipitation were tested in methanol decomposition. These catalysts had the formulation Pd(17wt%)/Ce_{0.8}Zr_{0.2}O₂ and the second Pd(3wt%)/CeO₂. Both catalysts were selective for CO formation at all temperatures and the CO was produced at comparable rates over both catalysts indicating that there was no relationship between Pd loading and catalyst activity. XRD analysis did not support the formation of solid solution formation with the ceria-zirconia mixed support, which is commonly reported in the literature.
- Three Pd catalysts supported on γ -Al₂O₃, formed by wet impregnation with Pd loadings of 1.5, 3 and 9 wt% were tested for methanol decomposition at 300°C. All three catalysts had a similar BET surface area and CO was produced selectively with no by-products detected. There was no metal loading relationship with respect to catalyst activity observed over this set of catalysts. These catalysts all contained coke after reaction and deactivation occurred over 5 hour reaction runs. DME, often reported to form from methanol dehydration over γ -Al₂O₃, was not detected.
- Both Raney Ni and an amorphous NiB alloy material are active for the decomposition of methanol. CH₄ is an observed by-product over both catalysts due to CO methanation whilst CO₂ is also observed over the Raney Ni catalyst at 300 °C. A characteristic reaction profile was observed with the Raney Ni catalyst at 300 °C whereby methanation activity dominates within the first 100 minutes on stream after which the methanol conversion drops and CO becomes the most abundant carbon containing product. Despite by-product formation, the NiB material produces CO at the highest rate for all of the tested methanol decomposition catalysts. Interestingly, although the Raney Ni catalyst contained coke, no carbon was observed in the spent NiB material.

Methanol decomposition experiments were also carried out over a series of molybdenum carbides and nitrides due to the volume of literature supporting similar behaviour to platinum group metals. The results are summarized as follows:

- Both pure phase β -Mo₂C and a mixed phase β -Mo₂C/MoO₂ material which was formed from the incomplete carburization of MoO₃, are active for methanol decomposition at 300 °C. CO and CH₄ are produced over the mixed phase carbide and pure phase carbide. However, in addition, CO₂ is the major carbon containing product formed over the pure phase carbide. Both materials showed comparable activity with a methanol conversion of 40%. As these materials were synthesised *in-situ* no BET surface areas were obtained for fresh catalysts but the spent carbides possessed comparable BET surface areas of 13 and 10m²/g for the pure and mixed phase carbides respectively.
- The surface areas of the synthesised nitride materials increased in the following order β -Mo₂N_{0.78} < δ -MoN < γ -Mo₂N and at a fixed reaction temperature of 300 °C the methanol conversion was shown to increase with increasing surface area and the general trends observed with the molybdenum nitride catalysts in methanol decomposition are now described:
- γ -Mo₂N is active for methanol decomposition at 250-300 °C. CO is not selectively produced and CH₄ and CO₂ are observed by-products. At 300°C, the maximum CO rate is 1190g/kgcat/h. At this temperature CH₄ and CO₂ are produced at 210 and 508 g/kgcat/h respectively.
- δ -MoN exhibited low activity in the temperature range 250-300°C. In a temperature programmed reaction regime the temperature was further increased to 400 °C in order to generate methanol conversions comparable to the other catalysts. At all temperatures, CO, CH₄ and CO₂ - the major product were detected and produced at rates of 1987, 561 and 1176 g/kgcat/h respectively.
- β -Mo₂N_{0.78} also exhibits low activity in methanol decomposition at a temperature range of 250 -300 °C and comparable methanol conversions are also obtained at 400°C using temperature programmed reaction. Although CH₄ is a detected by-product, produced with a rate of 103 g/kgcat/h, the CO selectivity is the largest

amongst the carbide and nitride materials and produced at a maximum rate of 2081 g/kgcat/h.

- All of the carbide and nitride materials deactivate. The spent catalysts have a reduced BET surface area compared with the fresh catalysts and coke is retained on the spent catalysts. XRD analysis indicates that the bulk structures of the carbide and nitride materials remain largely unaffected as there are no phase changes although in the case of the nitride materials, there is evidence of nitrogen loss from the bulk and coke formation as evidenced by elemental analysis.
- All of carbide and nitride materials studied exhibit behaviour which is analogous to the Ni based methanol decomposition catalysts as a similar product spectrum is observed with CH₄ and CO₂ by-products observed in addition to synthesis gas produced from methanol decomposition.

The second phase of the project concerned methanol carbonylation studies using a copper mordenite catalyst. Various reaction conditions were studied and characterization was performed on the spent mordenite catalyst. The findings are summarized below:

- Methanol carbonylation carried out at 300 °C and atmospheric pressure produces a characteristic product spectrum. Initially methanol to gasoline and methanol to olefin chemistry dominates and most of the carbon is deposited on the catalyst at this initial stage of the reaction. As a result, the micropores of the mordenite become completely blocked. Secondly, acetyls are produced whereby acetic acid is the major product and methyl acetate the minor product. In the final stage of the reaction acetyl selectivity declines and DME becomes the major product. Thermal gravimetric analysis of the spent copper mordenite catalyst yielded two weight loss features which did not correspond to the oxidation of carbon but the desorption of species which could not be determined.
- XRD analysis of the spent copper mordenite catalyst confirmed that the bulk structure and crystallinity of the mordenite was retained after reaction and in addition the Si/Al ratio indicates that no dealumination occurred from the presence of water generated in the reaction.

- The acetyl yield is increased by the presence of H₂ in the feedstream at low H₂ partial pressures. The maximum yield of acetyls is produced at an optimal CO:H₂ ratio of 4 and a further decrease in this ratio reduces the selectivity to acetyls although the increased concentration of H₂ lowers the carbon content on the spent catalyst. An increase in carbonylation temperature from 300 to 350 °C does not increase the acetyl yield but the coke content is increased. An increase in the methanol partial pressure results in an increase in DME yield.

The following points summarize the findings for the combined methanol decomposition and methanol carbonylation experiments using both the Katalco and Pd(3wt%)/CeO₂ methanol decomposition catalysts coupled with the methanol carbonylation catalyst:

- Synthesis gas is produced by the decomposition of methanol, although CO was not significantly converted in a subsequent methanol carbonylation step. CH₄, DME and CO₂ are observed on-line products indicating reaction pathways occurring over the copper mordenite catalyst. Carbon is also observed on the spent copper mordenite catalyst. Off-line analysis confirms the presence of both acetic acid and methyl acetate as minor products of the reaction. The low yields are consistent with the low CO:H₂ synthesis gas ratio generated from methanol decomposition.
- A higher yield of acetyls is produced when a palladium methanol decomposition catalyst is used compared with using a copper methanol decomposition catalyst. This is possibly due to the higher rate of CO production obtained from the synthesis gas in the palladium catalyst compared to the copper catalyst. Higher yields of acetyls are obtained when the catalysts are stacked whereas a mixed bed configuration leads to a reduction of acetyl formation and an increase in DME formation.

6.1 Future work

The results of this project demonstrate that in principle, acetic acid and methyl acetate can be synthesised directly from methanol. Throughout the stages of the project, several

areas of interest have become apparent. Firstly, in methanol decomposition it has been demonstrated that many alternative materials are active. It would be interesting to perform a more extensive investigation into these materials for synthesis gas production and elucidate structure-activity relationships. Testing could also be broadened to include a wider range of metal carbide and nitride materials.

Further work would also be required to fully understand the behaviour of the copper mordenite reaction profile as a function of catalyst deactivation and coking. It would also be of interest to study the nature of the acidity in the mordenite catalyst which may explain the changes in behaviour.

In addition, longer duration experiments could be performed on all systems. Particularly with the mixed bed systems where increasing the duration of stacked bed reactions could be performed to determine if the system is still activating.

7 Appendices

7.1 Methanol Decomposition

7.1.1 Methanol conversion

$$\text{Methanol conversion} = \frac{A - B}{A} \times 100$$

A = Methanol concentration to the reactor, B = Methanol concentration exiting the reactor

7.1.2 Space time yield calculations

Space time yield calculations for CO, H₂, CH₄ and CO₂. *GFM product* is the gram formula mass for the given product. *Catalyst* is the mass of catalyst loaded for the reaction run

$$STY = \frac{\text{TotalFlowIN}(ml / \text{min}) \times \text{mol\% product} \times 60 \times \text{GFMproduct}(g)}{24.04 \times \text{catalyst}(g)}$$

The molar % of each product is known from the GC peak areas with respect to gas calibrations described in the experimental section. The value 24.04 in the above equation is calculated from the ideal gas law and is the volume of gas in litres for one mole of a gas calculated at 20°C, assuming that the gas behave ideally.

7.1.3 Error values for duplicate reaction runs

The data points for methanol conversion plots and STY production plots containing error bars are the mean values obtained for duplicate measurements. The error is displayed as follows where (*value* = one of the two values used to calculate the mean value)

$$\text{MeanValue} \pm (\text{MeanValue} - \text{Value})$$

7.1.4 Error values for comparison tables

The Tables in Chapter 3 compare the average activities of methanol decomposition catalysts. The mean values obtained for methanol conversion and STY values are

calculated from every measurement obtained at each time interval during reaction runs. The error quoted is the Standard error (SE) which based on the standard deviation (SD) where N = the number of readings used to calculate the mean value

$$SE = \frac{SD}{\sqrt{N}}$$

$$SD = \sqrt{\frac{\sum (MeanValue - Value)^2}{N - 1}}$$

The significance of the standard error (SE) is that 68% of the values used to calculate the mean value will lie with the error range and 95% of the values lie within $2 \times SE$. For example if the standard error was displayed as 98 ± 5 , this would imply that 68% of the values used to calculate the mean value would be within the range 93-102, and 95% of the values used to calculate the mean would lie within the range 88-108.

7.1.5 Space time yield calculation for mixed bed methanol decomposition and carbonylation

The amount of acetic acid and methyl acetate produced is quantified by analysis of the knock out pot after a reaction run. The STY value obtained is therefore a total yield.

$$STY = \frac{Amount\ Product(g) / Mass\ of\ Carbonylation\ Catalyst(kg)}{Reaction\ Time(hours)}$$

The amount of product is calculated by using GC analysis and scaling up the number of moles obtained from the GC output (1 μ l injections) with the total volume obtained in the knock-out pot.

7.2 Methanol carbonylation

The analysis of the reaction products for methanol carbonylation is carried out for gas products which were obtained from gas sampling as described in the experimental section using GC analysis. Condensable products are analysed separately by GC analysis of the liquid mixture collected in the knock-out pot.

7.2.1 Analysis of gas phase products

The analysis of CH₄, C₂H₄, C₃H₆, C₄H₈, C₄H₁₀ and C₅ products is performed by sampling the effluent gas exit stream at regular intervals during methanol carbonylation. The STY values are calculated as a total yield. Typically the catalyst loading is 2.65g and the reaction run is 5 hours.

$$STY = 1000 \times \frac{Moles\ Product \times GFM}{Catalyst\ Mass(g) \times Total\ Hours}$$

The total number of moles of product is calculated as follows and is based on the entry flow where *Total Volume* is the total volume of reactant gas passed over the catalyst and *Volume % In Gas* is the volume or molar percentage of the given product.

$$Moles\ Product = Total\ Volume(l) \times \frac{Volume\ \%in\ Gas / 100}{22.4}$$

The *Volume % in Gas* is the average value obtained for the given product over a whole reaction run and is determined by using time averaging via the following equation

$$Volume\ \%in\ Gas = \frac{\sum (Average \times Time(\text{min}))}{Total\ Time(\text{min})}$$

In the above equation *Average* refers to the mean value obtained between a given reading and the value obtained in the previous reading. The *Time* factor is the time difference between these 2 readings.

7.2.2 Analysis of liquid phase products

The analysis of the condensable products is performed via GC analysis of the liquid obtained in a knock-out pot. These products in the present study are methanol, dimethylether (DME), ethanol, methyl formate (MF), acetaldehyde, acetone, propionic acid, acetic acid and methyl acetate (MA). The STY values were calculated using the same equation as the gas phase products. The difference is that the *Moles Product* factor is calculated on the basis of the weight percent for each product (*Wt % Product*) obtained from the GC analysis and the total weight of the liquid obtained in the effluent pot (*Total*

Weight Liquid).

$$\text{Moles Pr oduct} = \frac{\text{Wt\% Pr oduct}}{100} \times \frac{\text{TotalWeightLiquid(g)}}{\text{GFM}}$$

It should be noted that the STY values for DME are the sum of the STYs calculated from the knock out pot and those obtained from the gas phase, since a significant amount of DME is in the gas phase due to its high vapour pressure.

7.2.3 Methanol conversion

CO is not detected in the GC analysis for methanol carbonylation and hence the conversion is based on the amount of methanol as follows

$$\text{Methanol conversion} = \frac{A - B}{A} \times 100$$

A = Total number of moles methanol fed to the reactor, B = Total number of moles methanol exiting the reactor

The amount of moles of methanol out is known from what is obtained in the knock out pot and the number of moles of methanol in is known from the HPLC pump supplying the methanol which was accurately calibrated.

8 References

- [1] N. Yoneda, S. Kusano, M. Yasui, P. Pujado and S. Wilcher, *Appl. Catal. A: Gen.*, 2001, 221, 253
- [2] Michel Gubelmann-bonneau, US Patent 5840971, 1998
- [3] G. J. Sunley and D.J. Watson, *Catal. Today*, 2000, 58, 293
- [4] M. J. Howard, M. D. Jones, M. S. Roberts and S. A. Taylor, *Catal. Today*, 1993, 18, 325
- [5] A. Haynes, B. E. Mann, G. E. Morris and P. M. Maitlis, *J. Am. Chem. Soc.*, 1993, 115, 4093
- [6] Santi Kulprathipanja, US Patent 5962735, 1999
- [7] M. S. Jarrell and B. C. Gates, *J. Catal.*, 1975, 40, 255
- [8] A. S. Merenov and M. A. Abraham, *Catal. Today*, 1998, 40, 397
- [9] A. S. Merenov, A. Nelson and M. A. Abraham, *Catal Today*, 2000, 55, 91
- [10] L. Chateau, J. P. Hindermann, A. Kiennemann and E. Tempesti, *J. Mol. Catal. A: Chem.*, 1996, 107, 367
- [11] N. Takahashi, Y. Orikasa and T. Yashima, *J. Catal.*, 1979, 59, 61
- [12] T. Shikada, K. Fujimoto, M. Miyauchi and H. Tominaga, *Appl. Catal.*, 1983, 7, 361
- [13] F. Li, J. Huang, J. Zou, P. Pan and G. Yuan, *Appl. Catal. A: Gen.*, 2003, 251, 295
- [14] H. Jiang, Z. Liu, P. Pan and G. Yuan, *J. Mol. Catal. A: Chem.*, 1999, 148, 215
- [15] A. Calafat and J. Laine, *Catal. Lett.*, 1994, 28, 69
- [16] F. Peng and F. X. Bao, *Catal. Today*, 2004, 93-95, 451
- [17] R. W. Wegman, *J. Chem. Soc., Chem. Comm.*, 1994, 947
- [18] I. V. Kozhevnikov, S. Holmes and M. R. H. Siddiqui, *Appl. Catal. A: Gen.*, 2001, 214, 47
- [19] B. Ellis, M. J. Howard, R. W. Joyner, K. N. Reddy, M. B. Padley and W. J. Smith, *Stud. Sur. Sci. and Catal.*, 101, 1996, 771
- [20] P. Cheung, A. Bhan, G. J. Sunley and E. Iglesia, *Angew. Chem. Int. Ed.*, 2006, 45, 1617
- [21] P. Cheung, A. Bhan, G. J. Sunley, D. J. Law and E. Iglesia, *J. Catal.*, 2007, 245, 110
- [22] A. Bhan, A. D. Allian, G. J. Sunley, D. J. Law and E. Iglesia, *J. Am. Chem. Soc.*, 2007, 129, 4919
- [23] K. Ruth, R. Kieffer and R. Burch, *J. Catal.*, 1998, 175, 16
- [24] K. Ruth, R. Burch and R. Keiffer, *J. Catal.*, 1998, 175, 27
- [25] Michael F Lemanski., US Patent 5304678, 1994
- [26] A. P. E. York, T. Xiao and M.L.H. Green, *Topics in Catal.*, 2003, 22 (3-4), 345
- [27] J. Nakamura, Y. Choi and T. Fujitani, *Topics in Catal.*, 2003, 22 (3-4), 277

- [28] John. B. Hansen, US Patent 5189203, 1993
- [29] Joseph. C. Carlin, US Patent 1961736, 1934
- [30] M. Ojeda, S. Rojas, F. J. G. Garcia, M. L. Granados, P. Terreros and J. L. G. Fierro, *Catal. Comm.*, 2004, 5, 703
- [31] *Progress in C1 Chemistry in Japan*, 1, Elsevier, 1989, 281
- [32] H. Luo, P. Lin, S. Xie, H. Zhou, C. Xu, S. Huang, L. Lin, D. Laing, P. Yin and Q. Xin, *J. Mol. Catal. A: Chem.*, 1997, 122, 115
- [33] K. X. Wang, H. F. Xu, W. S. Li and X. P. Zhou, *J. Mol. Catal. A: Chem.*, 2005, 225, 65
- [34] M. Lin and A. Sen, *Nature*, 1994, 368, 613
- [35] E. M. Wilcox, G. W. Roberts and J. Spivey, *Catal. Today*, 2003, 88, 83
- [36] W. Wuang, K. Xie, J. P. Wang, Z. Gao, L. Yin and Q. Zhu, *J. Catal.*, 2001, 201, 11
- [37] 118. Y. Ding, W. Huang and Y. Wang, *Fuel. Processing. Technol.* 2007, 88, 319
- [38] S. Shinoda and T. Yamakawa, *J. Chem. Soc., Chem. Comm.*, 1990, 1511
- [39] T. Yamakawa, P. Tsai and S. Shinoda, *Appl. Catal. A: Gen.*, 1992, 92, L1
- [40] X. Huang, N. W. Cant, M.S. Wainwright and L. Ma, *Chem. and Proc.*; 2005, 44(3), 393
- [41] T. Ohnishi, T. Yamakawa and S. Shinoda, *Appl. Catal. A: Gen.*, 2002, 231, 27
- [42] A. K. Avci, Z. I. Onsan and D. L. Trimm, *Topics in Catal.*, 22(3-4), 359
- [43] T. Inui, H. Matsuda, H. Okaniwa and A. Miyamoto, *Appl. Catal.*, 1990, 58, 155
- [44] M. Stocker, *Micropor. Mesopor. Mat.*, 1999, 29, 3
- [45] F. Yaripour, F. Baghaei, I. Schmidt and J. Perregaard, *Catal. Comm.*, 2005, 6, 147
- [46] A. Y. Rozovskii and G. I. Lin, *Topics in Catal.*, 22(3-4), 137
- [47] A. Ruiz, *Appl. Catal*, 1991., 72, 119
- [48] Y. Xu, S. Kameoka, K. Kishida, M. Demura, A. Tsai and T. Hirano, *Intermetallics*, 2005, 13, 151
- [49] C. P. Thurgood, J. C. Amphlett, R. F. Mann and B. A. Peppley, *Topics in Catal.*, 2003, 22(3-4), 253
- [50] R. Perez, F. Marin and C. Castilla, *Appl. Catal. A: Gen.*, 2004, 275, 119
- [51] S. Imamura, T. Higashihara, Y. Saito, H. Aritana, H. Kanai, Y. Matsumura and N. Tsuda, *Catal. Today*, 1999, 50, 369
- [52] J. C. Brown and E. Gulari, *Catal. Comm.*, 2004, 5, 431
- [53] Y. Matsumura and N. Tode, *Phys. Chem. Chem. Phys.*, 2001, 3, 1284
- [54] Y. Matsumura, K. Tanaka, N. Tode, T. Yazawa and M. Haruta, *J. Mol. Catal. A: Chem.*, 2000, 152, 157
- [55] K. Nakagawa, T. Hashida, C. Kajita, N. Ikenaga, T. Kobayashi, M. N. Gamo, T. Suzuki and T. Ando, *Catal. Lett.*, 2002, 80 (3-4), 161
- [56] D. Paneva, T. Tsoncheva, E. Manova, I. Mitov and T. Ruskov, *Appl. Catal.*

A:Chem., 2004, 267, 67

- [57] S. Imamura, Y. Yamashita, R. Hamada, Y. Saito, Y. Nakao, N. Tsuda and C. Kaito, *J. Mol. Catal. A: Chem.*, 1998, 129 (2-3) 249
- [58] M. Kapoor and Y. Matsumura, *J. Mol. Catal. A: Chem.*, 2002, 178, 169
- [59] J.C.Brown and E. Gulari, *Catal. Comm.*, 2004, 5, 431
- [60] D. W. McKee, *Trans. Faraday. Soc.*, 1968, 64, 2200
- [61] A. Rozovskii and G. Lin, *Topics in Catal.*, 22 vol3-4, 137
- [62] I. A. Fischer and A. T. Bell, *J. Catal.*, 1999, 184, 357
- [63] Y. Xu, S. Kameoka, K. Kishida, M. Demura, A. Tsai and T. Hirano, *Intermetallics*, 2005, 13, 151
- [64] W. H. Cheng, C. Y. Shiau, T. H. Liu, H. L. Tung, J. F. Lu and C. C. Hsu, *Appl. Catal. A: Gen.*, 1998, 170, 215
- [65] W. Cheng, *Appl. Catal. A: Gen.*, 1995, 130, 13
- [66] T. Shishido, H. Sameshima and K. Takehira, *Topics in Catal.*, 2003, 22, 261
- [67] R. Shiozaki, T. Hayakawa, Y. Liu, T. Ishi, M. Kumagai, S. Hamakawa, K. Suzuki, T. Itoh, T. Shishido and K. Takehira, *Catal. Lett.*, 1999, 58, 131
- [68] Y. Liu, T. Thayakawa, T. Ishii, M. Kumagai, H. Yasuda, K. Suzuki, S. Hamakawa and K. Murata, *Appl. Catal. A: Gen.*, 2001, 210, 301
- [69] M. Kapoor, Y. Ichihashi, K. Kurada, W. Shen and Y. Matsumura, *Catal. Lett.*, 2003, 88, 83
- [70] Y. Liu, K. Suzuki, S. Hamakawa, T. Hayakawa, K. Murata, T. Ishii and M. Kumagai, *Catal. Lett.*, 2005, 66, 205
- [71] G. Mul and H. Hirschon, *Catal. Today*, 2001, 65, 69
- [72] W. Shen and Y. Matsumura, *J. Mol. Catal. A: Chem.*, 2000, 153, 165
- [73] M. P. Kappor, A. Raj and Y. Matsumura, *Micropor Mesopor. Mat.*, 2001, 44-45, 565
- [74] P. Kapoor, Y. Ichihashi, K. Kuroaka and Y. Matsumura, *J. Mol. Catal. A: Chem.*, 2003, 198, 303
- [75] C. Yang, J. Ren and Y. Sun, *Catal. Comm.*, 2001, 2, 353
- [76] Y. Choi and H. G. Strenger, *Appl. Catal. B: Env.*, 2002, 38, 259
- [77] J. Xi, Z. Wang and G. Lu, *Appl. Catal. A: Gen.*, 2002, 225, 77
- [78] W. Cheng, *Appl. Catal. B: Env.*, 1995, 7, 127
- [79] S. D. Jackson, D. S. Anderson, G. J. Kelly, T. Lear, D. Lennon and S. R. Watson, *Topics in Catal.*, 2003, 22(3-4), 173
- [80] M. V. Twigg and M. S. Spencer, *Topics in Catal.*, 2003, 22 (3-4), 191
- [81] W. Cheng, C. Shiau, T. H. Liu, H. L. Tung, H. H. Chen, J. Lu and C. C. Hsu, *Appl. Catal. B: Env.*, 1998, 18, 63
- [82] W. Cheng, *Mater. Chem. and Phy.*, 1995, 41, 36
- [83] M. S. Spencer, *Catal. Lett.*, 2000, 66, 255
- [84] J. Li and T. Inui, *Appl. Catal. A: Gen.*, 1996, 137, 105

- [85] G. D. Short, US Patent number 4,788,175, 1988
- [86] International zeolite association, database of zeolite structures
- [87] Y. Usami, K. Kagawa, M. Kawazoa, Y. Matsumura, H. Sakurai and M. Haruta, *Appl. Catal. A: Gen.*, 1998,171, 123
- [88] K. Sun, W. Lu, M. Wang and X. Xu, *Appl. Catal. A: Gen.*, 2004,268, 107
- [89] Y. Matsumura, M. Okumura, Y. Usami. K. Kagawa, H. Yamashita, M. Anpo and M. Haruta, *Catal. Lett.*, 1997, 44, 189
- [90] W. Shen and Y. Matsumura, *Phys. Chem. Chem. Phys.*, 2000, 2, 1519
- [91] C. Contescu, C. Sivaraj and J. A. Schwarz, *Appl. Catal.*, 74, 1991, 95
- [92] J. Vakros, C. Kordulis and A. Lycourghiotis, *Chem. Comm.*, 2002, 1980
- [93] M. Contescu and M. I. Vass, *Appl. Catal*, 1987, 33, 259
- [94] Y.Fu and T. Hong, *Thermochimica Acta*, 2005, 434, 22
- [95] Y. Matsumura, N. Tode, T. Yazawa and M. Haruta, *J. Mol. Catal. A:Chem.*,1995, 99, 183
- [96] I. Yasumori, T. Nakamura and E. Miyazaki, *Bull. Chem. Soc. Jpn.*, 1967, 40, 1372
- [97] Y. Matsumura, K. Kagawa, Y. Usami, M. Kawaoe, H. Sakurai and M. Haruta, *Chem. Comm.*, 1997, 657
- [98] J. Geng, D. A. Jefferson and B. F. G. Johnson, *Chem. Comm.*, 2007, 969
- [99] Z. Wu, M. Zhang, W. Li, S. Mu and K. Tao, *J. mol Catal. A: Chem.*, 2007, 273, 277
- [100] R. D. Kelley, G. A. Candela, T. E. Madey, D. E. Newbury and R. R. Schehl, *J. Catal.*, 1983, 80, 235
- [101] S. Hilaire, X. Wang, T. Luo, R. J. Gorte and J. Wagner, *Appl. Catal. A: Gen.*, 2004, 258, 271
- [102] S. Takenaka, T. Shimizu and K. Otsuka, *International. J. of Hydro. Energy*, 2004, 29, 1065
- [103] J. R. R. Nielsen, K. Pedersen and J. Sehested, *Appl. Catal. A: Gen.*, 2007
- [104] P. M. Patterson, T. K. Das and B. H. Davis, *Appl. Catal. A: Gen.*, 2003, 251, 449
- [105] M. Xiang, D. Li, H. Qi, W. Li, B. Zhong and Y. Sun, *Fuel*, 2007, 86, 1298
- [106] A. Consuegra, P. M. Patterson and M. A. Keane, *Appl. Catal. B:Env.*, 2006, 65, 227
- [107] H. He, H. X. Dai, K. Y. Ngan and C. T. Au, *Catal. Lett.*, 2001, 71 (3-4)
- [108] R. Kojima and K. Aika, *Appl. Catal A: Gen.*, 2001, 219, 141
- [109] H. Imamura, T. Nuruya, T. Kawasaki, T. Teranishi and Y. Sakata, *Catal. Lett.*, 2004, 96, 185
- [110] Z. Wu, Z. Hao, P. Ying, C. Li and Q. Xin. *J. Phy. Chem. B*, 2000, 104, 12275
- [111] E. Miyazaki, I. Kojima and M. Orita, *J. Chem. Soc., Chem. Comm.*, 1985, 108
- [112] R. Barthos and F. Solymosi, *J. Catal.*, 2007, 249, 289
- [113] T. Oyama, *The chemistry of transition metal carbides and nitrides*, Blackie

Academic and Profesional, ISBN 07514 03652 1996

- [114] M.E Eberhart and J. M. MacLaren, The chemistry of transition metal carbides and nitrides, Blackie Academic and Profesional, ISBN 07514 03652, 1996
- [115] T. Xiao, A. P. E. York, K. S. Coleman, J. B. Claridge, J. Sloan, J. Charnock and M. L. H. Green, *J. Mater. Chem.*, 2001, 11, 3094
- [116] A. Hanif, T. Xiao, A. P. E. York, J. Sloan and M. L. H. Green, *Chem. Mat*, 2002, 14, 1009
- [117] J.S.J. Hargreaves and D. McKay, *Catalysis*, Vol 19, 2006, 84
- [118] R. Marchand, X. Gouin, F. Tessier and Y. Laurent, The chemistry of transition metal carbides and nitrides, Blackie Academic and Profesional, ISBN 07514 03652 1996, 252
- [119] E. Lalik, W. I. F. David, P. Barnes and J. F. C. Turner, *J. Phys. Chem. B*, 2001, 9153
- [120] R. Barthos, T. Bansagi, T. S. Zakar and F. Solymosi, *J. Catal*, 2007, 247, 368
- [121] G. S. Ranhotra, A. T. Bell and J. A. Reimer, *J. Catal*, 1987, 108, 40
- [122] G. Kim, Y. Lee, D. Kim, S. Oh, S. Chang and Y. Kim, *J. Alloys. and Comp.*, 2007, 454, 327
- [123] R. Marchand, F. Tessier and F. DiSalvo, *J. Matter. Chem.*, 1999, 9, 297
- [124] International zeolite association, database of zeolite structures
- [125] J. H. Zhang, Y. Q. Yang, J. M. Shen and J. A. Wang, *J. Mol. Catal. A: Chem.*, 2005, 237, 182
- [126] P. Dejaifve, A. Auroux, P. C. Gravelle and J. C. Vedrine, *J. Catal.*, 1981, 70, 123
- [127] C. A. Henriques, A. M. Bentes, P. Magnoux, M. Guisnet and J. L. F. Monteiro, *Appl. Catal. A: Gen.*, 1998, 166, 301
- [128] C. Lee, K. Han and B. Ha, *Micropor Mater.*, 1997, 11, 227
- [129] S. J. Gregg and K. S. W. Sing, *Adsorption, Surface area and Porosity*, Academic Press, London, 1982
- [130] W. Liu, Y. Xu, S. T Wong, L. Wang, J. Qiu and N. Yang, *J. Mol. Catal. A: Chem.*, 1997, 120, 257
- [131] T. Chen, K. Houthoofd and P. J. Grobet, *Micropor. Mesopor. Mat.*, 2005, 86, 31
- [132] N. Viswanadham and M. Kumar, *Micropor. Mesopor. Mat.*, 2006, 92, 31
- [133] J. Bandiera and C. Naccache, *Appl. Catal.* 1991, 69, 139
- [134] R. Carvajal, P. Chu and J.H.J Lunsford, *J. Catal.*, 1990, 125, 123
- [135] J. T. Miller, P. D. Hopkins, B. L. Meyeer, G. J. Ray, R. T. Roginski, G. W. Zajac and N. H. Rosenbaum, *J. Catal.*, 1992, 138, 115
- [136] P. Ciambelli and P. Corbo, *Thermochimica Acta*, 1988, 137, 51
- [137] M. Boveri, C. Alvarez, M. Laborde and E. Sastre, *Catal. Today*, 2006, 114, 217
- [138] J. M. Fougerit, N. S. Gnep and M. Guisnet, *Micropor. Mesopor. Mater.*, 1999, 29, 79
- [139] T. R. Souza, S. Brito and H. Andrade, *Appl. Catal. A: Gen.*, 1999, 178, 7

- [140] F.S. Ramos, A. M. Farias, L. E. E. P. Borges, J. L. Monteiro, M. A. Fraga, E. F. Aguiar and L. E. Appel, *Catal. Today*, 2005, 101, 39
- [141] T. Matsumoto, T. N. Shiguchi, H. Kanai, K. Utari, Y. Matsumura and S. Imamura, *Appl. Catal. A: Gen.*, 2004, 276, 267
- [142] V. Kanazirev and T. Tsoncheva, *Zeolites*, 1989, 9, 516
- [143] M. Stocker, *Micropor. And. Mesopor. Matt.* 82, 2005, 82, 257
- [144] B. Wichterlova, Z. Sobalik and A. Vondrova, *Catal. Today*, 1996, 29, 149
- [145] J. Dedecek, Z. Sobalik, Z. Tvaruzkova, D. Kaucky and B. Wichterlova, *J. Phy. Chem*, 1995, 99, 16327
- [146] *Physical and mechanistic organic chemistry*, RAY Jones, Cambridge University Press, 2nd Edition, ISBN 0521278864, Page 29
- [147] A. Y. Gannin, L. Kienle, G. V. Vajenine, *J. of. Solid. State. Chem*, 2006, 179, 2339
- [148] *Physical and mechanistic organic chemistry*, RAY Jones, Cambridge University Press, 2nd Edition, ISBN 0521278864, Page 287
- [149] *Physical and mechanistic organic chemistry*, RAY Jones, Cambridge University Press, 2nd Edition, ISBN 0521278864, Page 285
- [150] Y. Lwin, W. Ramli, A. Mohamed, and Z. Yaakab, *International. Journal. Of. Hydrogen. Energy*, 2000, 25, 47
- [151] P. Bodart, J. Nagy, G. Debras, Z. Gabelica and P. Jacobs, *J. Phy. Chem*, 1986, 90, 5183

